CURRENT PERSPECTIVES IN NATURAL SCIENCES AND MATHEMATICS

DOĞA BİLİMLERİ VE MATEMATİKTE GÜNCEL PERSPEKTİFLER

Editor
Prof. Dr. Mehmet YILMAZ

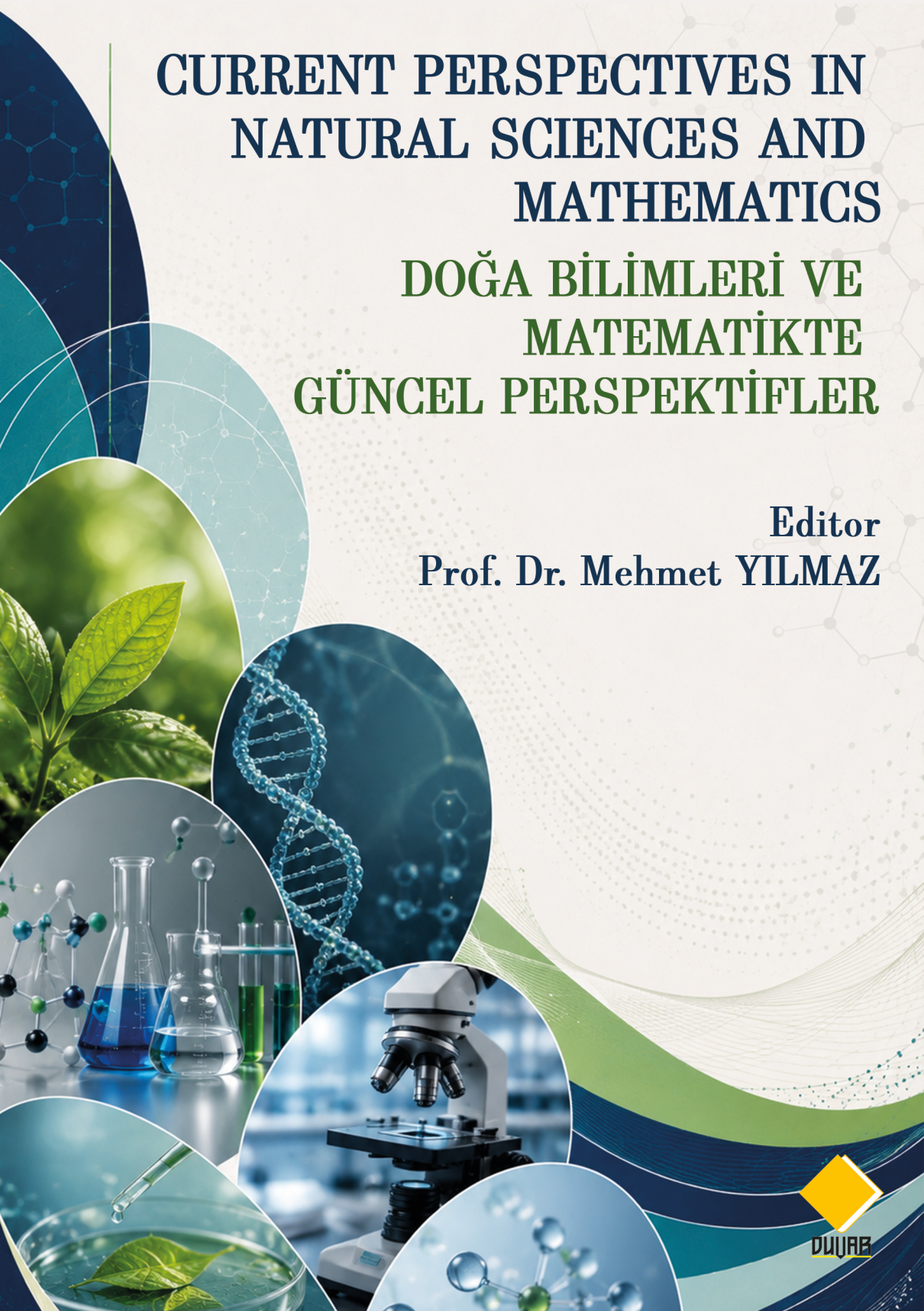

DUJAB

CURRENT PERSPECTIVES IN NATURAL SCIENCES AND MATHEMATICS

DOĞA BİLİMLERİ VE MATEMATİKTE GÜNCEL PERSPEKTİFLER

Editor

Prof. Dr. Mehmet YILMAZ

CURRENT PERSPECTIVES IN NATURAL SCIENCES AND MATHEMATICS
DOĞA BİLİMLERİ VE MATEMATİKTE GÜNCEL PERSPEKTİFLER
Editor
Prof. Dr. Mehmet YILMAZ

General Director: Berkan Balpetek
Cover and Page Design: Duvar Design
Printing : July-2026
Publisher Certificate No: 49837
E-ISBN:978-625-8936-37-7

853 Sokak No:13 P.10 Kemeraltı-Konak/İzmir
Tel: 0 232 484 88 68
www.duvaryayinlari.com
duvarkitabevi@gmail.com

TABLE OF CONTENTS

Chapter 1

The 100th recorded species of the genus *Zercon* (Acari: Zerconidae) from Türkiye: *Zercon mirayae* sp. nov.

Mehmet KARACA[1], Raşit URHAN[2]

Abstract

A new species of the genus *Zercon* C. L. Koch, 1836 (Acari: Mesostigmata: Zerconidae), *Zercon mirayae* sp. nov., is described from Trabzon Province, northeastern Türkiye, based on adult and immature specimens. The new species is characterized by the absence of podonotal seta *s1*, completely smooth idiosomal setae, and smooth dorsal shields without ornamentation. It is compared with the morphologically similar species *Z. arcuatus*, *Z. bulgaricus*, and *Z. perforatulus*, and the diagnostic morphological differences are discussed. A comparison with Turkish specimens previously identified as *Z. perforatulus* indicates that these specimens were likely misidentified and may actually represent *Zercon mirayae* sp. nov. The description of this new species increases the number of *Zercon* species known from Türkiye to 100 and further highlights the remarkable diversity of Turkish Zerconidae.

Key words: Mesostigmata, taxonomy, new species, soil mites, Turkish acarofauna

[1] Prof. Dr., Pamukkale University, Denizli Vocational School of Technical Sciences, Department of Electronic and Automation, 20160, Denizli, Türkiye. karacamehmet@pau.edu.tr; ORCID No: 0000-0002-3249-4215
[2] Prof. Dr., Pamukkale University, Faculty of Science, Department of Biology, 20070, Denizli, Türkiye. rurhan@pau.edu.tr; ORCID No: 0000-0002-6548-7927

INTRODUCTION

Mites of the family Zerconidae Canestrini, 1891 are small soil-dwelling mesostigmatic mites that constitute an important component of the zooedaphon in temperate regions of the Northern Hemisphere. They occur predominantly in leaf litter, decomposing organic matter, soil, and moss, although a few species have also been recorded from caves as well as bird and mammal nests (Jandík & Fend'a 2026). Most zerconid mites are predatory, feeding on nematodes, small arthropods, and other microarthropods, thereby contributing to the regulation of soil microfaunal communities and the maintenance of ecological balance (Karg 1993; Mašán & Fend'a 2004). Owing to their abundance, habitat specificity, and sensitivity to environmental conditions, zerconid mites are regarded as important components of soil biodiversity and have considerable potential for ecological and biogeographical studies.

The genus *Zercon* C. L. Koch, 1836 is the type genus of the family Zerconidae and, with 307 described species worldwide (Jandík & Fend'a 2026), is its most species-rich genus. Together with the genus *Prozercon* Sellnick, 1943, it is one of only two zerconid mite genera currently known from Türkiye and is represented by 99 species in the country (Karaca & Urhan 2025; Urhan & Karaca 2025; Urhan et al., 2026). However, systematic and ecological studies on Turkish zerconid mites are continuing throughout the country, and the number of recorded species is expected to increase considerably in the coming years. During the examination of zerconid mite specimens collected in 2018 from Trabzon Province in northeastern Türkiye (Figure 1), a previously unknown species of *Zercon* was discovered and is described in this study.

Figure 1: Aerial view of the habitat at Büyük Harman Plateau, Trabzon Province (Url-1) (red arrow indicates the locality of the new species was collected)

MATERIALS AND METHODS

Soil, leaf litter, and moss materials were sampled from forest habitats located on the Büyük Harman Plateau, Trabzon Province). Geographic coordinates and altitude of the sampling site were determined using the Altimeter GPS & Barometer application (Url-2). All collected material was transferred to the PAU (Acarology Laboratory, Department of Biology, Faculty of Science, Pamukkale University, Denizli, Türkiye). Standard methods were used for the extraction of zerconid mites, the examination and measurement of various idiosomal structures, and the preparation of illustrations (Urhan & Karaca 2025). The chaetotactic and poroidotactic nomenclature follows the terminology proposed by Sikora (2014). All measurements of idiosomal structures and setae, as well as the scale bars shown in the figures, are presented in micrometers (μm).

RESULTS

Family **Zerconidae** Canestrini, 1891
Genus ***Zercon*** C. L. Koch, 1836
Type species: ***Zercon triangularis*** C. L. Koch, 1836

For a detailed diagnosis of the genus, see Urhan & Karaca (2023).

***Zercon mirayae* sp. nov.** (Figures 2-7)

Type Material. Holotype: female: Trabzon Province, Hayrat County, Büyük Harman Plateau, near Geçitli Village, 40°45.441'N 40°23.996'E, 1980 m a.s.l.; 15.05.2018; in litter, soil and moss (unspecified) samples under Oriental beech=*Fagus orientalis* (Fagaceae), bramble=*Rubus* sp. (Rosaceae) and common rhododendron=*Rhododendron ponticum* (Ericaceae). Paratypes: 72 ♀, 3 ♂, 17 deutonymphs, 8 protonymphs: same data as holotype. Leg. M. Tataroğlu & Y. Katılmış. All material deposited in the PAU.

Diagnosis. On podonotum, all setae smooth, seta *s1* absent. On opisthonotum, all setae smooth. Gland pore *gdS2* located between setae *S2* and *S3*, closer to S3, *gdZ3* located between setae *Z3* and *Z4, closer to Z4*. Dorsal cavities as transversely arcuate, weakly developed and distinct. Podonotum and opisthonotum entirely smooth, without tile-like patterns, reticulation, punctation, or any other sculptural ornamentation.

Description. Female (Figures 2-3). İdiosomal length 432, width 326 in holotype (excluding gnathosoma). Measurements in paratypes: 407-438 × 314-332 (n=10).

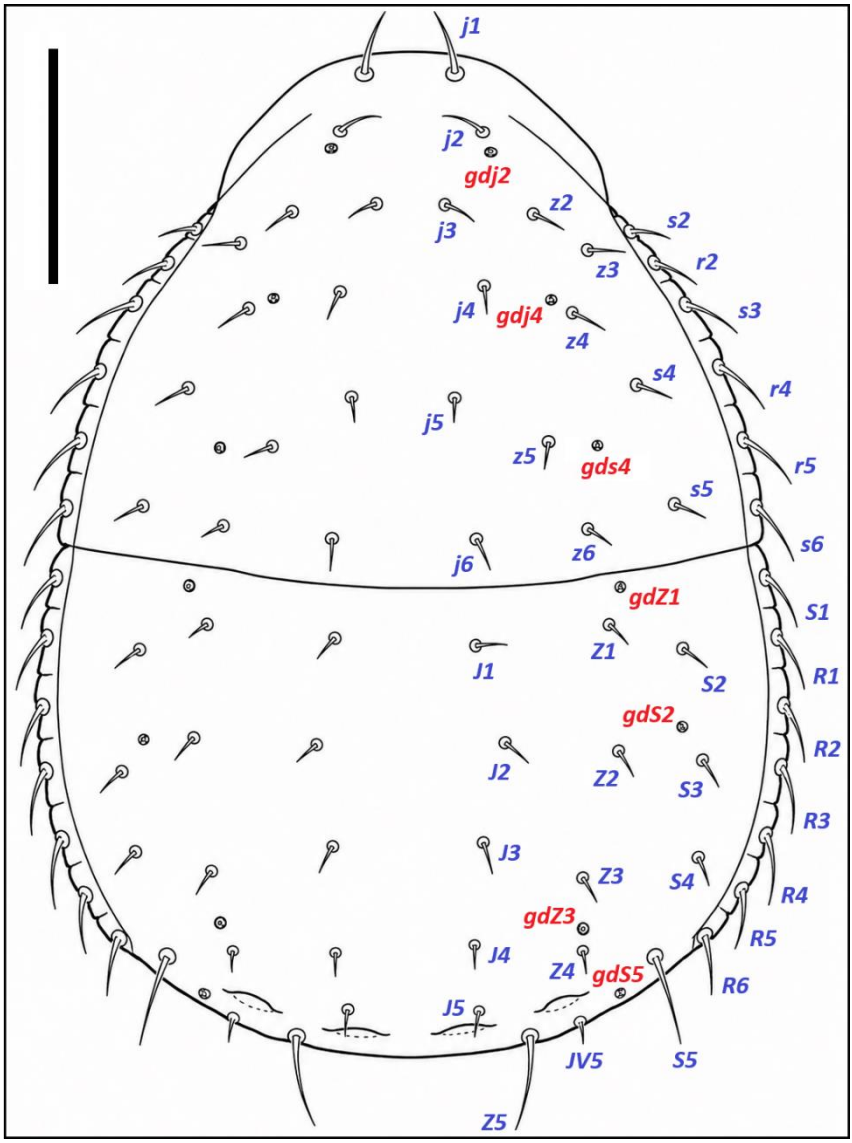

Figure 2: Female of *Zercon mirayae* sp. nov., dorsum (scale bar = 100 µm).

Dorsal side (Figure 2). Nineteen pairs of setae on podonotal shield, including *j1–6*, *z2–6*, *s2–6*, *r2* and *r4–5*. Seta *s1* absent. Insertions of setae *r1* and *r3* inserted ventrally on peritrematal shields. All podonotal setae similar in shape, all of them smooth and needle-like. Marginal setae *s3*, *s6* and *r4–5* slightly longer than the others. None of setae *j6*, *z6* and *s5* reaching posterior margin of podonotal shield. The podonotal shield lacks ornamentation. Twenty-one pairs of setae present on opisthonotal shield, including *J1–5*, *Z1–5*, *S1–5* and *R1–6*. All opisthonotal setae similar in shape, all of them smooth and needle-like. Marginal setae (*S1* and *R1–6*), *Z5* and *S5* longer than the others. None of opisthonotal setae reaching insertions of

next setae in the related rows. Only setae *Z5* and *S5* reaching beyond margin of opisthonotum, remaining opisthonotal setae not reaching margin of opisthonotum. Distances between setae *Z5–Z5* 88-96, *Z5–JV5* 23-28, respectively. The opisthonotal shield lacks ornamentation.

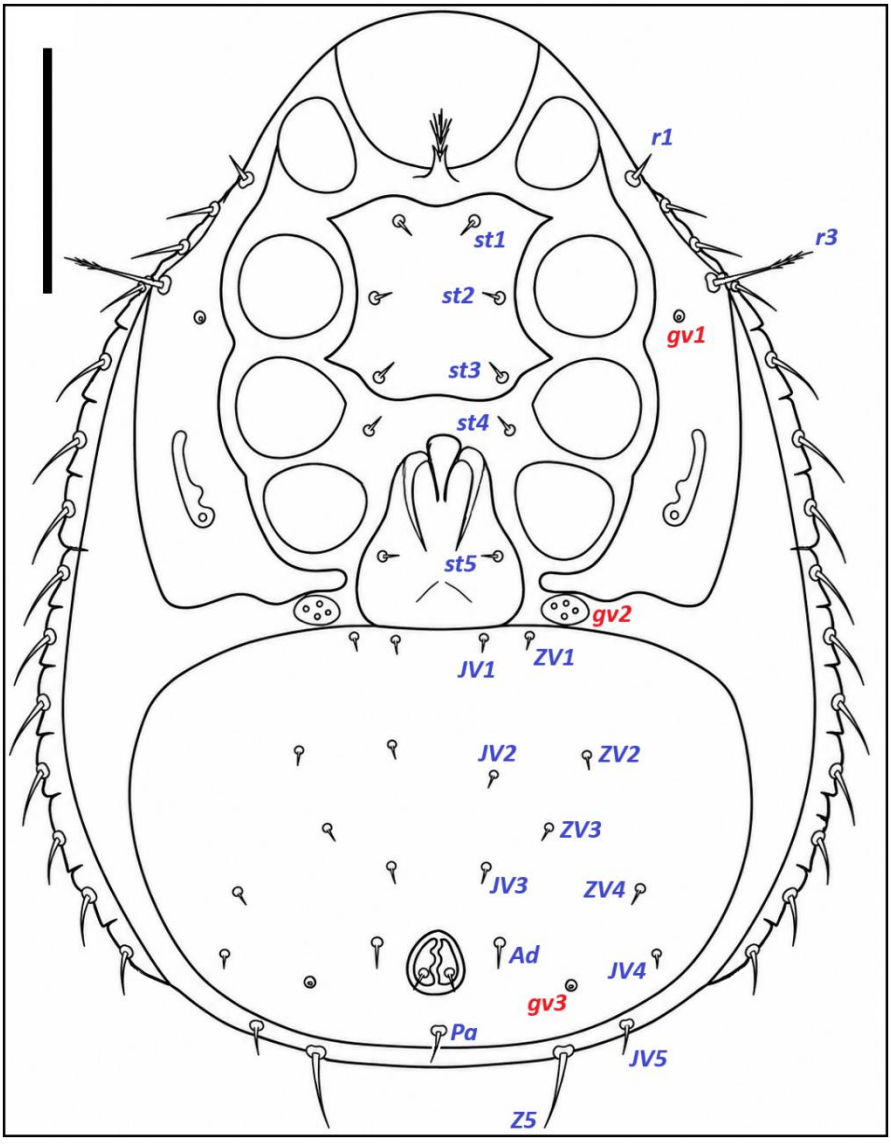

Figure 3: Female of *Zercon mirayae* sp. nov., venter (scale bar = 100 μm).

Pores (Figure 2). All gland pores are generally in the same size. Gland pores *gdj2* situated among setae *j2* and *z2*, closer to *z2*, *gdj4* situated among setae *j4* and *z4*, closer to *z4*, *gds4* situated among setae *z6* and *s4*, *gdZ1* situated anterior to the base of seta *Z1*, *gdS2* situated among setae *S2* and *S3*, closer to S3, *gdZ3* situated

among setae *Z3* and *Z4*, closer to *Z4*, *gdS5* situated among setae *S5* and *JV5*. Dorsal cavities as transversely arcuate, with smooth anterior margins, equal in size and shape, axes parallel to that of the body.

Ventral side (Figure 3). The ventral ornamentation, poroidotaxy, and chaetotaxy are consistent with those of the genus *Zercon*. The posterolateral ends of the peritrematal shield extend to the level of seta *S1*. Seta *r1* short, smooth and needle-like, *r3* elongated and finely barbed without hyaline endings on peritrematal shield. The peritreme is inversely comma-shaped. Gland pore *gv1* is located anterior to the peritreme, *gv2* at the junction of the peritrematal, epigynal, and ventrianal shields with four opening valves, and *gv3* between setae *Ad* and *JV5*. All sternal setae (*st1–3*), epigynal seta *st5*, and seta *st4* located on the soft cuticle between the sternal and epigynal shields are short, smooth, and needle-like. The anterior margin of the ventrianal shield bears two pairs of setae, *JV1* and *ZV1*. All ventrianal setae (*JV1–4*, *ZV1–4*, *Ad*) are short, smooth and needle-like. The postanal seta (*Pa*) is single and similar in length to the other setae on the ventrianal shield. Seta *JV5* is smooth and needle-like, resembling the marginal setae of the opisthonotum but distinctly shorter. The ventrianal shield is entirely smooth.

The lengths and ranges of opisthonotal setae in the *J*, *Z*, and *S* rows of female, male, deutonymph and protonymph specimens are presented in Table 1.

Male (Figures 4-5). Length and width of idiosoma 327-357 × 242-274 (n=3). The shape of idiosomal setae, locations of idiosomal gland pores and ornamentation of dorsal (Figure 4) and ventral (Figure 5) shields similar to those of females. Adgenital shield (gland pore *gv2*) with three opening valves Distances between setae *Z5* and *Z5* 76-80, between *Z5* and *JV5* 20-26.

Table 1: Lengths of and longitudinal distances between the insertions of opisthonotal setae in *Zercon mirayae* sp. nov. (Symbols and abbreviations: ♀: female, ♂: male, DN: deutonymph, PN: protonymph)

Setae	♀♀	♂♂	DN	PN	Setae	♀♀	♂♂	DN	PN	Setae	♀♀	♂♂	DN	PN
J1	7-14	7-11	5-8	3-5	***Z1***	8-14	7-10	3-11	4-5	***S1***	24-29	12-14	15-19	8-11
J1–J2	42-54	28-34	28-42	25-29	***Z1–Z2***	49-56	36-43	33-52	32-38	***S1–S2***	38-45	22-28	21-25	23-28
J2	6-10	10-12	5-11	3-5	***Z2***	8-15	7-12	5-7	4-5	***S2***	12-15	8-11	8-13	17-33
J2–J3	39-47	28-35	27-35	20-28	***Z2–Z3***	55-59	33-37	27-35	22-30	***S2–S3***	45-50	28-35	28-41	28-35
J3	8-17	7-13	3-5	3-4	***Z3***	8-14	7-12	3-6	3-4	***S3***	12-15	9-13	8-11	26-34
J3–J4	37-45	24-31	22-29	28-31	***Z3–Z4***	29-38	24-36	26-30	26-36	***S3–S4***	46-50	32-35	29-34	25-29
J4	7-13	7-11	3-5	2-4	***Z4***	9-14	5-8	3-5	3-4	***S4***	14-17	9-11	8-11	32-38
J4–J5	26-32	19-22	19-29	20-25	***Z4–Z5***	38-44	32-38	21-26	22-28	***S4–S5***	43-48	29-41	29-36	27-33
J5	10-12	5-8	3-5	2-3	***Z5***	32-38	31-35	37-56	52-56	***S5***	31-36	28-42	45-50	50-53

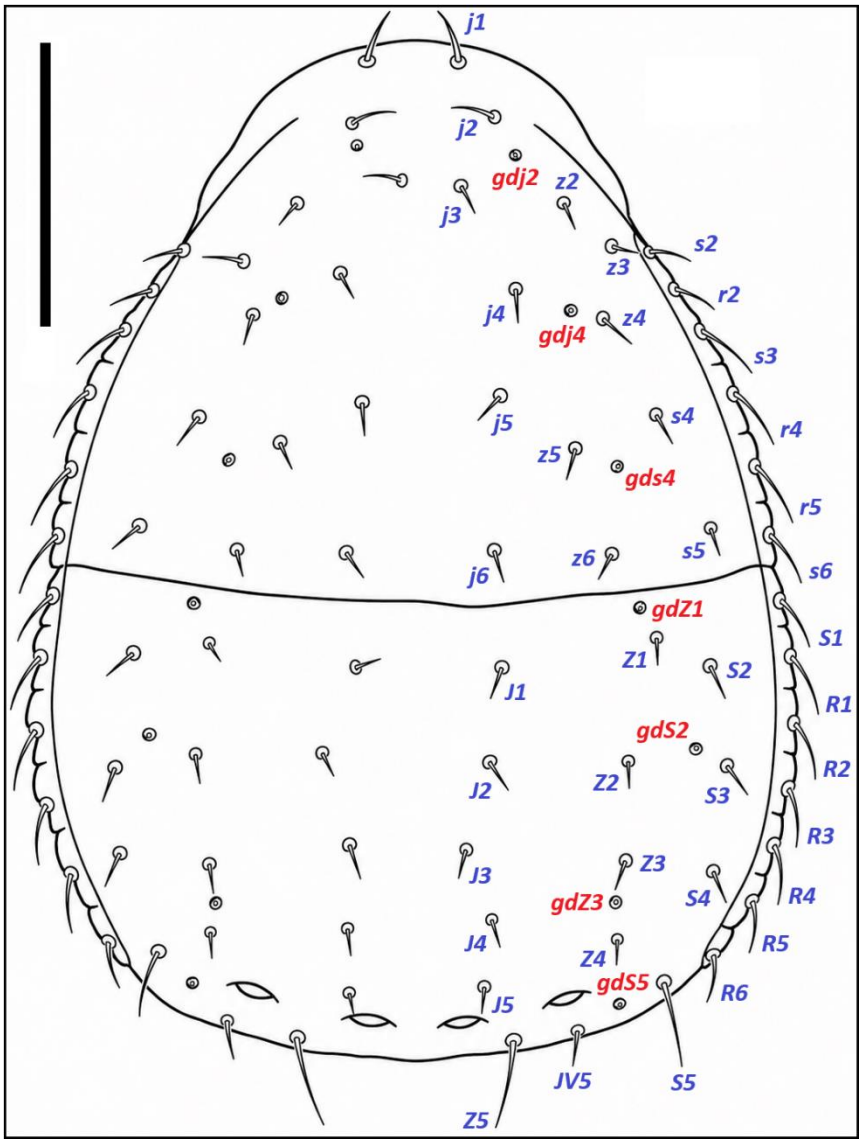

Figure 4: Male of *Zercon mirayae* sp. nov., dorsum (scale bar = 100 µm).

Deutonymph (Figure 6). Length and width of idiosoma 307-364 × 217-289 (n=10).

All podonotal setae smooth and needle-like. Seta *s1* absent. Setae *j1* and *s3* longer than the others. None of podonotal setae reaching margin of posterior part of podonotum. The podonotal shield is smooth, without ornamentation. All opisthonotal setae smooth and needle-like. None of opisthonotal setae reaching insertions of next setae in the related rows. Setae *Z5* and *S5* longer than the others, reaching beyond margin of opisthonotum, remaining opisthonotal setae not reaching margin of opisthonotum. Distances between setae *Z5* and *Z5* 72-98, *Z5*

and *JV5* 22-26. The opisthonotal shield is smooth, without ornamentation. Gland pores *gdj2* situated among setae *j2* and *z2*, closer to *j2*, *gdj4* situated among setae *j4* and *z4*, *gds4* situated among setae *z5* and *s5*, closer to *z5*, *gdZ1* situated anterior to the base of seta *Z1*, *gdS2* situated among setae *S2* and *S3*, *gdZ3* situated among setae *Z3* and *Z4*, closer to *Z3*, *gdS5* situated anterior to the base of seta *JV5*. Dorsal cavities as transversely arcuate, equal in size and weakly sclerotised.

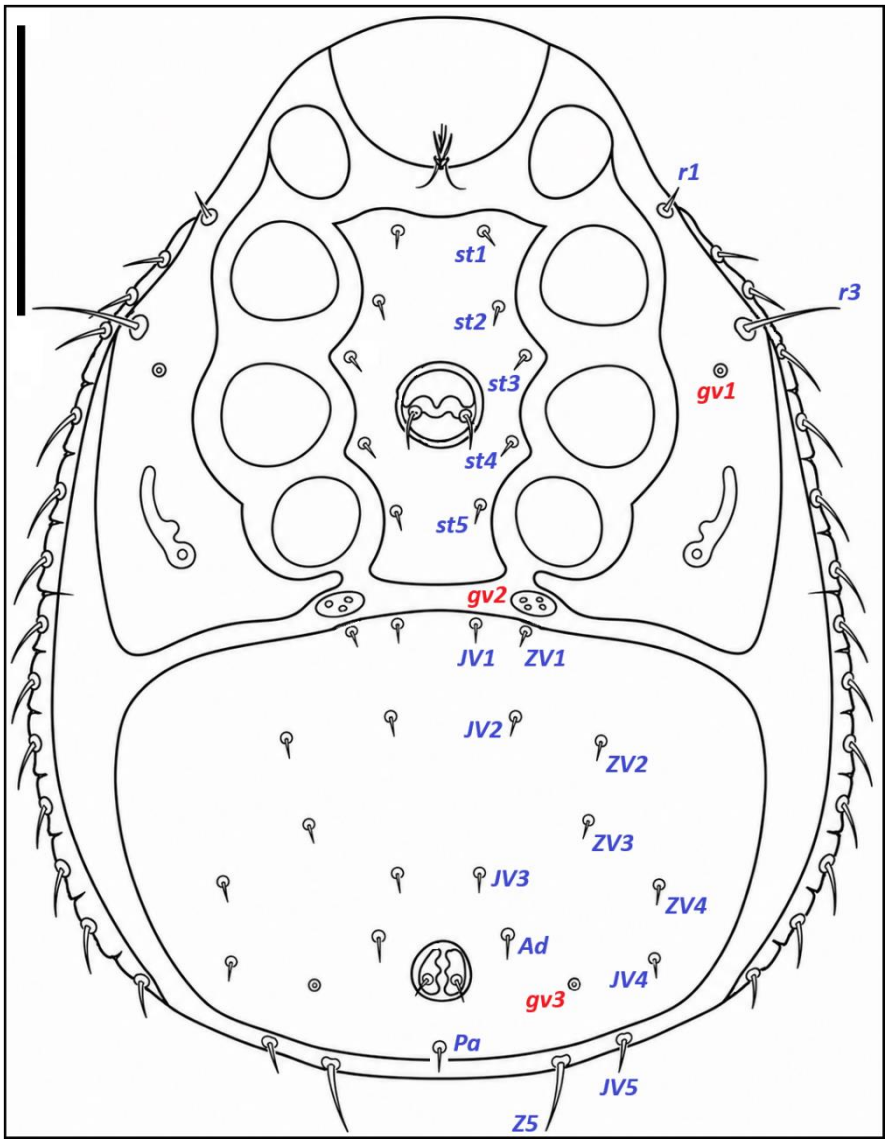

Figure 5: Male of *Zercon mirayae* sp. nov., venter (scale bar = 100 µm).

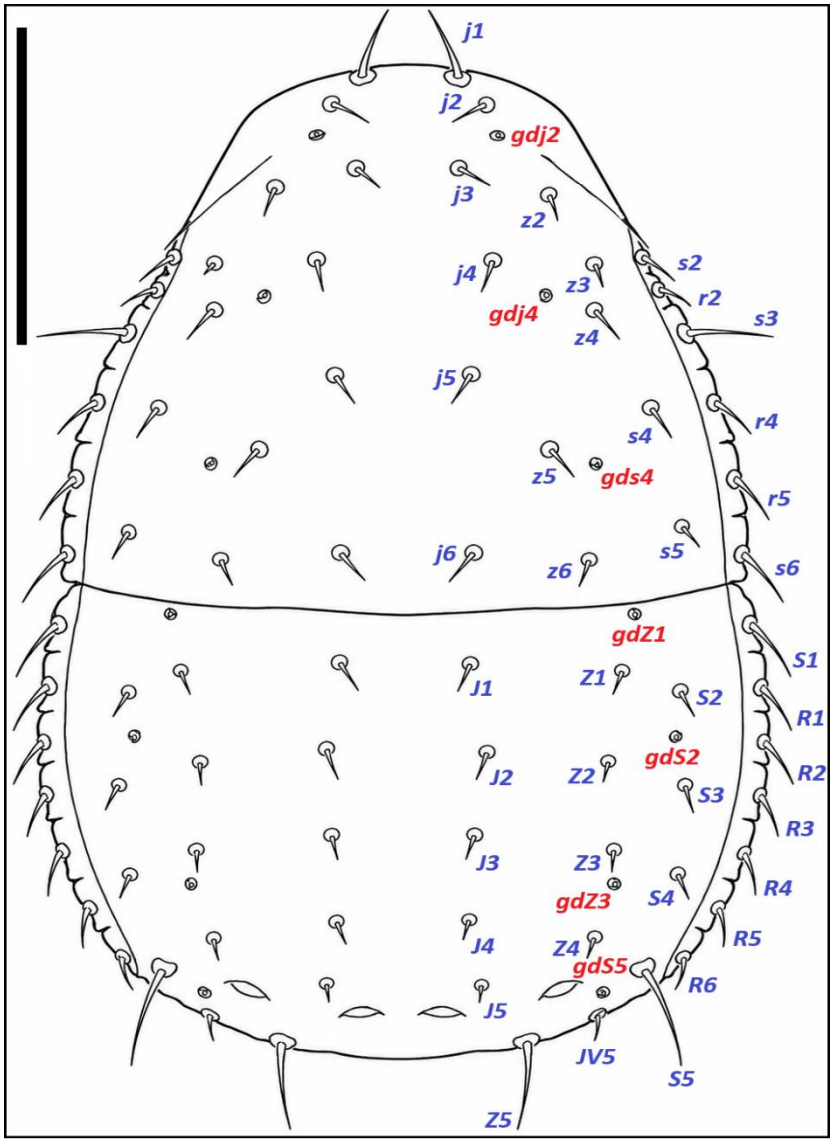

Figure 6: Deutonymph of *Zercon mirayae* sp. nov., dorsum (scale bar = 100 μm).

Protonymph (Figure 7). Length and width of idiosoma 282-298 × 190-212 (n=8).

All podonotal setae smooth and needle-like. Setae *z2* and *s3* longer than the others. Some podonotal setae (*z3*, *z6*, *s2*, *r4–5*) and gland pore *gds4* invisible. Only seta *s5* reaching margin or beyond of posterior part of podonotum. The podonotal shield is smooth, without ornamentation. All opisthonotal setae smooth and needle-like. None of opisthonotal setae reaching insertions of next setae in the related rows. Setae *Z5* and *S2–5* longer than the others. In contrary of female, male and deutonymph specimens, setae *S2–5* reaching beyond margin of opisthonotum. Only

seta *R1* visible in marginal row. Distances between setae *Z5* and *Z5* 79–83, *Z5* and *JV5* 21–24. The opisthonotal shield is smooth, without ornamentation. Gland pores *gdj2* situated among setae *j2* and *j3*, closer to *j2*, *gdj4* situated among setae *j4* and *z4*, closer to *z4*, *gds4* invisible, *gdZ1* situated anterolaterally to the base of seta *Z1*, *gdS2* invisible, *gdZ3* situated among setae *Z3* and *Z4*, *gdS5* situated anterior to the base of seta *JV5*. Dorsal cavities as transversely arcuate, equal in size and weakly sclerotised.

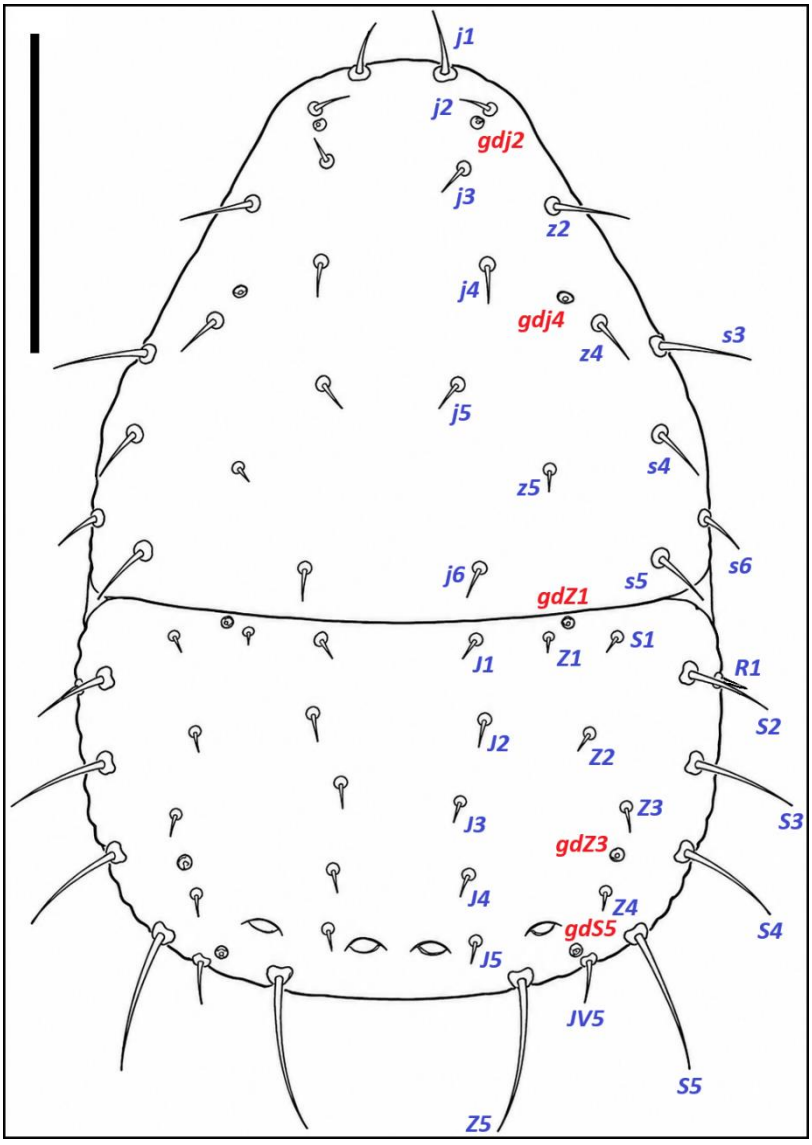

Figure 7: Protonymph of *Zercon mirayae* sp. nov., dorsum (scale bar = 100 μm).

Differential diagnosis. The morphological characters of *Zercon mirayae* sp. nov. are similar to *Z. arcuatus*, *Z. bulgaricus*, and *Z. perforatulus*. The distinguishing features of these species are summarized in Table 2. Two of these species (*Z. arcuatus* and *Z. perforatulus*) have a complete set of podonotal setae, whereas the other two species (*Z. bulgaricus* and *Z. mirayae*) lack seta *s1*. However, none of these species lacks any setae in the related rows of the opisthonotum. All species listed in Table 2, including the new species, share the following morphological features: All podonotal and opisthonotal setae smooth (except the finely barbed seta *j1* in *Z. arcuatus* and the narrowly lanceolate or spatulate setae *Z4–5* and *S5* in *Z. perforatulus*). None of the podonotal setae *j6*, *z6*, and *s5* reaches the posterior margin of the podonotal shield or extends beyond it. None of the opisthonotal setae *J1–2*, *Z1–2*, and *S2–3* reaches the base of the following seta in the same row. In all of these species, seta *JV5* smooth on the posterior part of opisthonotum. All species have dorsal cavities that are equal in size and appearance (except *Z. bulgaricus*, in which the outer pair is about 2-4 times larger than the inner pair), and their axes are parallel to the longitudinal axis of the body. In addition, all of these species have four setae in the anterior margin of the ventrianal shield.

Etymology. The specific epithet "*mirayae"* is dedicated to Miray Karaca, the daughter of the first author.

Habitat. All specimens were collected from forest habitats. Zerconid mites were extracted from litter, soil, and moss samples collected Oriental beech (*Fagus orientalis*, Fagaceae), bramble (*Rubus* sp., Rosaceae), and common rhododendron (*Rhododendron ponticum*, Ericaceae).

DISCUSSION AND CONCLUSIONS

The presence of completely smooth idiosomal setae has been documented in several *Zercon* species (Karaca & Urhan 2016), including *Z. bulgaricus*, *Z. cabylus*, and *Z. filiformis*. In addition to these species, *Z. mirayae* sp. nov., described in the present study, also possesses completely smooth idiosomal setae, with none bearing finely barbs or a hyaline sheaths. This feature represents a distinctive morphological character shared by all of the above-mentioned *Zercon* species.

On the other hand, *Z. mirayae* sp. nov., described in the present study, exhibits a remarkable morphological resemblance to the specimens identified as *Zercon perforatulus* by Urhan and Ayyıldız (1996), which were reported from Artvin Province as a new record for the Turkish acarofauna. However, the specimens illustrated by Urhan and Ayyıldız (1996) do not correspond to the original description and illustrations of *Z. perforatulus* published by Sellnick (1958).

Examination of Sellnick's original figures clearly shows that the idiosoma of Z. perforatulus is broadly oval, whereas the specimens reported from Artvin do not exhibit the characteristic oval outline of the original species. Furthermore, the idiosoma of *Z. perforatulus* is irregularly punctate in Sellnick's original description, whereas the Artvin specimens have a generally smooth idiosoma lacking the characteristic punctate ornamentation. These two conspicuous morphological differences strongly suggest that the specimens reported by Urhan and Ayyıldız (1996) were most likely misidentified. Considering the geographical proximity between Trabzon Province, where the type specimens examined in the present study were collected, and Artvin Province, where the morphologically similar specimens reported by Urhan and Ayyıldız (1996) were collected, *Z. mirayae* sp. nov. is likely to be distributed over a relatively wide area in the eastern Black Sea region of Türkiye.

Table 2: Comparison of the distinguishing morphological features of *Zercon mirayae* sp. nov. and related species of the genus *Zercon*. Data compiled from Berlese (1904), Trägårdh (1931), and Balogh (1961).

	Z. mirayae sp. nov.	***Z. arcuatus*** Trägårdh, 1931	***Z. bulgaricus*** Balogh, 1961	***Z. perforatulus*** Berlese, 1904
Podonotal seta *j1*	smooth	finely barbed	smooth	smooth
Podonotal seta *s1*	absent	present	absent	present
Podonotal shield ornamentation	smooth	reticulate only medially	smooth	mainly punctate pattern
Opisthonotal setae *Z4–5* and *S5*	smooth	narrowly lanceolate or spatulate	smooth	smooth
Opisthonotal setae *J3–4*, *Z3–4* and *S3–4*	not reaching insertions of next seta	not reaching insertions of next seta	reaching insertions of next seta	not reaching insertions of next seta
Opisthonotal seta *J5*	not reaching the margin of opisthonotum	reaching the margin of opisthonotum	reaching beyond the margin of opisthonotum	not reaching the margin of opisthonotum
Opisthonotal seta *Z4*	not reaching the margin of opisthonotum	reaching beyond the margin of opisthonotum	reaching beyond the margin of opisthonotum	not reaching the margin of opisthonotum
Opisthonotal seta *S3*	not reaching the margin of opisthonotum	reaching the margin of opisthonotum	reaching the margin of opisthonotum	not reaching the margin of opisthonotum
Opisthonotal seta *S4*	not reaching the margin of opisthonotum	reaching beyond the margin of opisthonotum	reaching beyond the margin of opisthonotum	reaching the margin of opisthonotum
Opisthonotal pore *gdS2*	between setae *S2* and *S3*	between setae *S1* and *S2*	between setae *Z1* and *Z2*	not stated
Opisthonotal pore *gdZ3*	between setae *Z3* and *Z4*	between setae *Z3* and *Z4*	between setae *J4* and *Z4*	between setae *Z3* and *Z4*
Dorsal cavities shape	transversely arcuate	saddle-like	saddle-like	transversely arcuate
Opisthonotal shield ornamentation	smooth	reticulate-punctate pattern	smooth	mainly punctate pattern

Türkiye is characterized by remarkable environmental heterogeneity, encompassing diverse topographical formations, a wide range of climatic regimes, and highly variable vegetation types. These conditions create numerous ecological niches that provide suitable habitats for soil-dwelling mites, including members of the family Zerconidae. As a result, the country supports a rich and diverse acarofauna. Despite this considerable ecological potential, large parts of Türkiye have not yet been investigated comprehensively, and the acarological diversity of many regions remains poorly documented.

Future taxonomic surveys focusing on the family Zerconidae are therefore expected to reveal additional species, particularly in regions that have received relatively little attention, such as the Mediterranean, Eastern Anatolia, Southeastern Anatolia, Black Sea, and Central Anatolia. Continued sampling in these areas, together with detailed morphological and integrative taxonomic studies, will certainly contribute to the discovery and description of numerous new taxa. Accordingly, the known diversity of the Turkish Zerconidae fauna is likely to increase significantly as further investigations are conducted. These observations emphasize the importance of expanding systematic acarological research throughout the country and demonstrate that comprehensive faunistic and taxonomic studies will provide valuable insights into the true biodiversity of Türkiye.

ACKNOWLEDGEMENTS

We sincerely thank Musa Tataroğlu (Ph.D., Assistant Professor) and Yusuf Katılmış (Ph.D., Professor), specialists in Cynipidae (Hymenoptera: Cynipoidea) at Pamukkale University, for their valuable assistance in collecting Zerconidae specimens from Trabzon Province.

FUNDING

No financial support was received for this study.

DISCLOSURE STATEMENT

The authors declare that they have no competing interests.

REFERENCES

Balogh, J., 1961. *Zercon bulgaricus* spec. nov. (Mesostigmata, Acari). *Folia Entomologica Hungarica*, 14, 433-435.

Berlese, A., 1904. Acari Nuovi. *Redia*, 1, 235-280.

Jandík, M., Fend'a, P., 2026. Catalogue of family Zerconidae (Acari: Mesostigmata) with a key to genera. *Zootaxa*, 5841 (1), 1-131.

Karaca, M., Urhan, R., 2025. First report of *Zercon triangularis* C. L. Koch, 1836 (Acari: Zerconidae) from Türkiye. 5th International Paris Applied Science Congress, Paris, France, 20-22 December, p. 498-507.

Karg, W., 1993. Acari (Acarina) Milben. Parasitiformes (Anactinochaeta). Cohors Gamasina Leach, Raubmilben. 2. Auflage. Die Tierwelt Deutschlands, 59, 1-523.

Mašán, P., Fend'a, P., 2004. *Zerconid mites of Slovakia (Acari, Mesostigmata, Zerconidae)*. Institute of Zoology, Slovak Academy of Sciences, Bratislava, 238 pp.

Sellnick, M., 1958. Die Familie Zerconidae Berlese. *Acta Zoologica Academiae Scientiarum Hungaricae*, 3, 313-368.

Sikora, B., 2014. Mites of the family Zerconidae (Acari: Mesostigmata) of the Nearctic Region. *Annales Zoologici (Warszawa),* 64 (2), 131-250.

Trägårdh, I., 1931. Terrestrial Acarina. *The Zoology of the Faroes*, Copenhagen, 49, 1-69.

Urhan, M., Katılmış, Y., Karaca, M., 2026. Two new mite species of *Zercon* (Acari: Zerconidae) from Türkiye. *Zoology in the Middle East*, 72 (1), 97-107.

Urhan, R., Ayyıldız, N., 1996. Four new species of the genus *Zercon* C. L. Koch 1836 (Acari, Mesostigmata, Zerconidae) to the Turkish fauna (in Turkish). *Turkish Journal of Zoology*, 20 (Suppl), 293-302.

Urhan, R., Karaca, M., 2023. Species diversity of the mite family Zerconidae (Acari: Mesostigmata) in İzmir province. In: *Multifaceted Academic Perspective: Basic Sciences and Engineering Research*, 1st ed.; Demirer, A. (Ed.); SRA Academic Publishing, Klaipeda, Lithuania, Chapter 1, pp. 1-26; 978-625-6750-09-1.

Urhan, R., Karaca, M., 2025. A new species of zerconid mites (Acari: Zerconidae) from northeastern Türkiye: *Zercon rizeensis* sp. nov. In: *Advances in Biological and Environmental Research: From Molecules to Ecosystems*, 1st ed.; Akyıldız, G.K. (Ed.); SRA Academic Publishing, Klaipeda, Lithuania, Chapter 7, pp. 87-100; 978-625-6750-41-8.

Url-1: https://earth.google.com/web/ (Erişim Tarihi: 17/07/2026)

Url-2: https://apps.apple.com/us/app/altimeter-gps-barometer/id572227849 (Erişim Tarihi: 17/07/2026)

Chapter 2

On the Wheel Graph Constructed from a Monogenic Semigroup Graph

Seda OĞUZ ÜNAL[1]

1. Introduction

Let $\mathrm{G} = (\mathrm{V}, \mathrm{E})$ be a simple graph with vertex set $V(G) = \{v_1, v_2, \dots, v_n\}$ and edge set

$E(G) = \{e_1, e_2, \dots, e_m\}$. The degree of a vertex $v \in V(G)$ is denoted by $d(v)$. If two vertices u and v are adjacent, the corresponding edge is represented by uv. The distance between two vertices u and v, denoted by $d(u, v)$, is defined as the length of a shortest path connecting them. For standard terminology and notation, we refer the reader to West [1].

A finite multiplicative monogenic semigroup with zero is defined as

$$S_M = \{0, x, x^2, x^3, \dots, x^n\}$$

Based on the concept of zero-divisor graphs, Das et al. introduced the monogenic semigroup graph $\Gamma(S_M)$. The vertex set of $\Gamma(S_M)$ consists of all nonzero elements of S_M. Two distinct vertices x^i and x^j, where $1 \leq i, j \leq n$, are adjacent if and only if $i + j > n$.

Since its introduction by Das et al. [2], monogenic semigroup graphs have become an active research topic in algebraic graph theory. Several graph-theoretical and topological properties of these graphs have been investigated in the literature. Akgüneş, Das and Çevik [3] studied various topological indices associated with monogenic semigroup graphs and demonstrated their connections with chemical graph theory. In subsequent years, numerous degree-based graph invariants were determined for this graph family. In particular, the Sombor index was investigated in [4], while the Banhatti–Sombor index was studied in [5]. The Nirmala index was computed in [6], and several other vertex degree based indices were examined in [7]. These studies reveal that monogenic semigroup graphs

[1] Sivas Cumhuriyet University Faculty of Education, Department of Mathematics and Science Education 58140 Sivas, Türkiye
ORCID: 0000-0003-1338-1466
E-mail: sdaoguz@gmail.com

constitute a rich class of algebraically defined graphs whose structural and topological characteristics deserve further investigation.

The origin of monogenic semigroup graphs lies in the theory of zero-divisor graphs. Zero-divisor graphs were first introduced for commutative rings by Beck [8] and were subsequently extended to both commutative and noncommutative rings [9]. Later, DeMeyer and coauthors generalized these ideas to semigroups [10, 11], leading to a rich interaction between algebraic structures and graph theory. Monogenic semigroup graphs constitute one of the most important graph classes arising from this interaction. Another well-known graph family is the wheel graph. A wheel graph is obtained by joining a new central vertex to every vertex of a cycle [12]. Owing to their simple structure and numerous applications, wheel graphs have been extensively investigated in graph theory. Various graph parameters and topological indices of wheel graphs have been studied, making them a natural candidate for further structural investigations.

Motivated by the significance of both monogenic semigroup graphs and wheel graphs, we introduce and study a new graph structure obtained by adjoining a central vertex to every vertex of a monogenic semigroup graph. We call this graph the wheel graph constructed from a monogenic semigroup graph and denote it by $W(\Gamma(S_M))$. The purpose of this chapter is to investigate several classical graph parameters of $W(\Gamma(S_M))$, including the maximum degree, minimum degree, radius, diameter, girth, clique number, chromatic number, and domination number.

The chapter is organized as follows. In Section 2, we present the necessary definitions and preliminary results. Section 3 introduces the wheel graph constructed from a monogenic semigroup graph and establishes its basic structural properties. Section 4 is devoted to determining the maximum degree, minimum degree, radius, diameter, girth, clique number, chromatic number, and domination number of $W(\Gamma(S_M))$. Finally, concluding remarks and possible directions for future research are discussed.

2. Preliminaries

In this section, we recall the basic definitions and notation that will be used throughout this chapter. We also introduce the wheel graph constructed from a monogenic semigroup graph, which serves as the main object of our study.

Definition 2.1

Let $S_M = \{0, x, x^2, \cdots, x^n\}$ be a finite multiplicative monogenic semigroup with zero. The monogenic semigroup graph associated with (S_M), denoted by $\Gamma(S_M)$, is defined as the graph whose vertex set is

$$V\big(\Gamma(S_M)\big) = \{x, x^2, \cdots, x^n\}$$

and two distinct vertices x^i and x^j are adjacent if and only if $i + j > n$.
Unless otherwise stated, $\Gamma(S_M)$ will denote the monogenic semigroup graph throughout this chapter.

Definition 2.2

A wheel graph W_n is a graph obtained by joining a single central vertex to every vertex of the cycle graph C_n. Motivated by this classical construction, we define the wheel graph constructed from a monogenic semigroup graph in Definition 2.3. Equivalently, $W_n = K_1 + C_n$ where " + " denotes the graph join operation. The additional vertex is called the hub (or center) of the wheel graph.

Definition 2.3

Let $\Gamma(S_M)$ be a monogenic semigroup graph with vertex set $V\big(\Gamma(S_M)\big) = \{x, x^2, \cdots, x^n\}$. The wheel graph constructed from $\Gamma(S_M)$, denoted by $W(\Gamma(S_M))$, is obtained by adding a new vertex c and joining c to every vertex of $\Gamma(S_M)$. Hence,

$V\left(W\big(\Gamma(S_M)\big)\right) = V(\Gamma(S_M)) \cup \{c\}$ and $E\left(W\big(\Gamma(S_M)\big)\right) = E\big(\Gamma(S_M)\big) \cup \{cx^i \big| 1 \le i \le n\}$

The vertex c is called the center of $W(\Gamma(S_M))$.

Remark 2.1

Since the center vertex c is adjacent to every vertex of $\Gamma(S_M)$, several graph parameters of $W(\Gamma(S_M))$ are expected to differ significantly from those of $\Gamma(S_M)$. In particular, the radius, diameter, domination number, and degree sequence are directly influenced by the introduction of the center vertex.

3. Construction of the Wheel Graph from a Monogenic Semigroup Graph

This section is dedicated to the formal construction and structural breakdown of a novel graph family emerged by expanding a monogenic semigroup graph via a wheel-like initialization. Specifically, we generate this configuration by adding a unique external center vertex and establishing an adjacency toward every pre-existing vertex within the semigroup graph boundary. This architectural integration fundamentally alters the density and connectivity profiles of the underlying algebraic framework. The resulting join operation serves as a

controlled environment to observe how classical graph parameters adapt when an algebraically restricted adjacency network is coupled with a universal center.

By Definition 2.3, the graph $W(\Gamma(S_M))$ is obtained by adjoining a center vertex c to every vertex of $\Gamma(S_M)$. We now present some basic structural properties of this construction. Consequently, the graph $W(\Gamma(S_M))$ contains exactly one additional vertex compared to $\Gamma(S_M)$. This implies that:

$$\left|V\left(\left(W(\Gamma(S_M))\right)\right)\right| = n + 1.$$

Since the center vertex \$c\$ is adjacent to every vertex of $\Gamma(S_M)$, exactly n new edges are added to the system. Therefore, we obtain:

$$\left|E\left(\left(W(\Gamma(S_M))\right)\right)\right| = \left|E(\Gamma(S_M))\right| + n.$$

Furthermore, the degree of the center vertex is exactly the order of the underlying graph:

$$d(c) = n.$$

For every vertex $v \in V(\Gamma(S_M))$ one additional adjacency is created through the connection with the center vertex. Hence, the new degree configuration becomes:

$$d_{W(G)}(v) = d_{\Gamma}(v) + 1.$$

These observations will play a fundamental role in determining the exact structural parameters of $W(\Gamma(S_M))$ in the subsequent sections.

Example 3.1

Consider the monogenic semigroup graph $\Gamma(S_M)$ corresponding to

$$S_M = \{0, x, x^2, x^3, x^4, x^5, x^6\}.$$

The wheel graph $W(\Gamma(S_M))$ is obtained by introducing a new vertex c and joining it to each vertex of $\Gamma(S_M)$. In this case, $\left|V\left(\left(W(\Gamma(S_M))\right)\right)\right| = 7$ while

the number of edges increases by six compared to $\Gamma(S_M)$. The center vertex c has degree six and is adjacent to every other vertex of the graph.

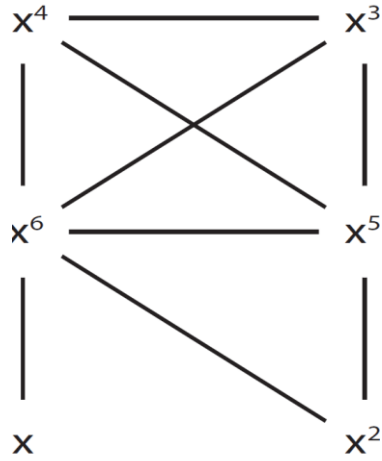

Figure 3.1: The monogenic semigroup graph $\Gamma(S_M)$ for $n = 6$.

4. Structural Parameters of the Wheel Graph Constructed from a Monogenic Semigroup Graph

In this section, we systematically determine and rigorously analyze several classical graph parameters of the graph $W(\Gamma(S_M))$, which constitute the core analytical findings of this chapter. To provide a comprehensive topological profile of this newly introduced hybrid structure, our investigation is partitioned into four fundamental structural domains. First, we examine degree-based parameters to evaluate local connectivity transitions. Second, we compute distance-based parameters, such as radius and diameter, to quantify the geometric compactness of the system. Third, we delve into cycle and coloring invariants, including girth, clique number, and chromatic number, to establish the boundaries of structural density and monochromatic partitioning. Finally, we determine the domination-related characteristics of the network. By evaluating these diverse invariants, we explicitly map how the algebraic boundaries of the underlying monogenic semigroup interact with a globally dominant central hub.

4.1 Degree-Based Parameters

The degree distribution of monogenic semigroup graphs exhibits a characteristic asymmetric structure, where the vertex x^n attains the highest degree while the remaining vertices possess varying levels of connectivity determined by the adjacency condition $i + j > n$. When a new central vertex is

introduced to construct the wheel graph $W(\Gamma(S_M))$, this heterogeneous degree structure undergoes a significant centralization process. In particular, the center vertex becomes adjacent to all vertices of $\Gamma(S_M)$, thereby increasing every existing degree by one and creating a highly connected hub that substantially influences the degree-based characteristics of the resulting graph.

The first results concern the maximum and minimum degrees of $W(\Gamma(S_M))$.

Theorem 4.1

Let $G = \Gamma(S_M)$ be the monogenic semigroup graph and let $W(G)$ be the wheel graph constructed from G. Then $\Delta(W(G)) = n$.

Proof

Let c denote the center vertex of $W(G)$. Since c is adjacent to every vertex of G, we have

$d(c) = |V(G)| = n$. Furthermore, it is known that the vertex x^n has maximum degree in G, namely

$$d_G(x^n) = n - 1$$

Since the construction of $W(G)$ adds the center vertex as a new neighbor of every vertex of G, we obtain

$$d_{W(G)}(x^n) = d_G(x^n) + 1 = (n-1) + 1 = n.$$

For any other vertex $v \in V(G)$,

$$d_G(v) \leq n - 2$$

and therefore $d_{W(G)}(v) = d_G(v) + 1 \leq n - 1$.

Hence no vertex of $W(G)$ has degree exceeding n. Consequently,

$$\Delta(W(G)) = n.$$

This completes the proof.

Theorem 4.2 (Minimum Degree) Let $G = \Gamma(S_M)$ be the monogenic semigroup graph and let $W(G)$ be the wheel graph constructed from G. Then $\delta(W(G)) = 2$.

Proof Let c denote the center vertex of $W(G)$. By construction, the degree of the center vertex is

$$d_{W(G)}(c) = n.$$

For every vertex $x^i \in V(G)$, the introduction of the center vertex increases its degree by exactly one:

$$d_{W(G)}(x^i) = d_G(x^i) + 1.$$

As established by Das et al. [2], the minimum degree of the monogenic semigroup graph G is attained at the vertex x, giving $\delta(G) = d_G(x) = 1$. Therefore, for the vertex x, we have

$$d_{W(G)}(x) = d_G(x) + 1 = 1 + 1 = 2.$$

Since the minimum degree of the graph is the minimum among all vertex degrees, it follows that $\delta(W(G)) \leq 2$.

On the other hand, for every vertex $x^i \in V(G)$, we have $d_{G(x^i)} \geq 1$. Consequently, $d_{W(G)}(x^i) = d_G(x^i) + 1 \geq 2$.

Moreover, the center vertex c has degree n. Thus, no vertex of $W(G)$ has a degree less than 2, which implies $\delta(W(G)) \geq 2$.

Combining the inequalities $\delta(W(G)) \leq 2$ and $\delta(W(G)) \geq 2$, we conclude that

$\delta(W(G)) = 2$. This completes the proof.

This result indicates that regardless of the order n of the monogenic semigroup, the minimum degree of the constructed wheel graph remains invariant at 2. In contrast to standard wheel graphs W_n where peripheral vertices maintain a degree of 3, the algebraic boundary conditions of $\Gamma(S_M)$ generate a unique structural constraint that forces the minimum degree to drop to 2.

4.2 Distance-Based Parameters

In this subsection, we shift our attention to the distance-based parameters of the constructed graph system, which reflect its geometric compactness and internal connectivity. Specifically, we determine the exact values of the radius and diameter of $W(\Gamma(S_M))$. By analyzing these metrics, we illustrate how the introduction of a universal center vertex c minimizes the eccentricity across all

algebraic configurations, effectively compressing the metric layout of the underlying monogenic semigroup graph to its theoretical minimum.

Theorem 4.3 (Radius)

Let $G = \Gamma(S_M)$ be the monogenic semigroup graph and let $W(G)$ be the wheel graph constructed from G. Then $rad\big(W(G)\big) = 1$

Proof

Let c denote the center vertex of $W(G)$. By construction, c is adjacent to every vertex of G. Hence,

$$d(c, v) = 1$$

for every vertex

$$v \in V(W(G))\backslash\{\mathrm{c}\}$$

Therefore, the eccentricity of the center vertex is $e(c) = 1$.

Since the radius of a graph is defined as the minimum eccentricity among all vertices, we obtain

$$\mathrm{rad}\big(W(G)\big) = \min_{v \in V\left(W(G)\right)} e(v) \leq e(c) = 1.$$

On the other hand, the radius of a nontrivial graph cannot be less than 1. Thus, $rad(W(G) \geq 1$.

Combining the above inequalities yields

$$rad(W(G)) = 1.$$

This completes the proof.

Theorem 4.4

Let $W(\Gamma(S_M))$ be the wheel graph constructed from the monogenic semigroup graph $\Gamma(S_M)$. Then $diamW\big(\Gamma(S_M)\big) = 2$.

Proof

Let $u, v \in V(W\big(\Gamma(S_M)\big))$. By construction, $W\big(\Gamma(S_M)\big)$ contains a center vertex c which is adjacent to every vertex of $\Gamma(S_M)$.

If one of the vertices is c, say u= $u = c$, then $d(u, v) = 1$. Now assume that $u, v \in V(\Gamma(S_M))$. If u and v are adjacent in $\Gamma(S_M)$, then they remain adjacent in $W(\Gamma(S_M))$, and hence $d(u, v) = 1$.

Suppose that u and v are not adjacent. Since the center vertex c is adjacent to both u and v, there exists a path $u - c - v$ of length two. Therefore, $d(u, v) \leq 2$.

Consequently, every pair of vertices in $W(\Gamma(S_M))$ is at distance at most two, implying that

$$diam(W(\Gamma(S_M)) \leq 2.$$

On the other hand, $\Gamma(S_M)$ is not a complete graph. Hence, there exist two vertices $u, v \in V(\Gamma(S_M))$ that are not adjacent. For such vertices,

$$d(u, v) \neq 1.$$

Since the path $u - c - v$ has length two, we obtain $d(u, v) = 2$.

Therefore,

$$diam(W(\Gamma(S_M)) \geq 2.$$

Combining the inequalities

$diam(W(\Gamma(S_M)) \leq 2$ and $diam(W(\Gamma(S_M)) \geq 2$.

we conclude that

$$diam(W\big(\Gamma(S_M)\big) = 2.$$

This completes the proof.

4.3 Cycle and Coloring Parameters

In this subsection, we delve into the cycle-related and coloring parameters of the constructed graph family, specifically examining its girth, clique number, and chromatic number. In structural graph theory, these invariants are deeply intertwined; the clique number provides a lower bound for the chromatic number, while the girth determines the local structural density and the presence of minimal cycles. By analyzing these parameters for $W(\Gamma(S_M)$, we explore how the algebraic boundary constraints of the underlying monogenic semigroup interact with a universal hub, ultimately demonstrating how this combination influences the chromatic stability and leads to a weakly perfect graph configuration.

Theorem 4.5 (Girth)

Let $G = \Gamma(S_M)$ be the monogenic semigroup graph and let $W(G)$ be the wheel graph constructed from G. Then $girth\big(W(G)\big) = 3$.

Proof

Let c denote the center vertex of $W(G)$. By construction, c is adjacent to every vertex of G.

Since x^n and x^{n-1} are adjacent in G, we have

$$x^n x^{n-1} \in E(G).$$

Moreover,

$$cx^n \in E(W(G))$$

and

$$cx^{n-1} \in E(W(G)).$$

Therefore, the vertices c, x^n, x^{n-1} form a cycle of length three:

$$c - x^n - x^{n-1} - c.$$

Hence,

$$girth(W(G)) \leq 3.$$

On the other hand, every cycle in a simple graph has length at least three. Thus,

$$girth(W(G)) \geq 3.$$

Combining these inequalities, we obtain

$$girth\big(W(G)\big) = 3.$$

This completes the proof.

Theorem 4.6 (Clique Number)

Let $G = \Gamma(S_M)$ be the monogenic semigroup graph and let $W(G)$ be the wheel graph constructed from G. Then $\mathrm{w}(W\big(\Gamma(S_M)\big) = \left\lceil \frac{n}{2} \right\rceil + 1$.

Proof

Consider the set

$$A = \left\{ x^{\left\lfloor \frac{n}{2} \right\rfloor + 1}, x^{\left\lfloor \frac{n}{2} \right\rfloor + 2}, \cdots, x^n \right\}.$$

For any two vertices $x^i, x^j \in A$, we have $i, j > \frac{n}{2}$.

Hence, $i + j > n$, which implies that x^i and x^j are adjacent in G. Therefore, A forms a clique in G. The number of vertices in A is

$$|A| = n - \left\lfloor \frac{n}{2} \right\rfloor = \left\lceil \frac{n}{2} \right\rceil.$$

Thus,

$$\mathrm{w}(G) = \left\lceil \frac{n}{2} \right\rceil.$$

Now consider the wheel graph $W(G)$. Let c denote its center vertex. By construction, c is adjacent to every vertex of G. Consequently, $A \cup \{c\}$

is a clique in $W(G)$ of size

$$\left\lceil \frac{n}{2} \right\rceil + 1$$

Hence,

$$\mathrm{w}(W(G)) \geq \left\lceil \frac{n}{2} \right\rceil + 1.$$

On the other hand, every clique in $W(G)$ contains at most one additional vertex beyond a clique of G, namely the center vertex c. Since $\mathrm{w}(G) = \left\lceil \frac{n}{2} \right\rceil$, no clique in $W(G)$ can have more than $\left\lceil \frac{n}{2} \right\rceil + 1$ vertices.

Therefore,

$$\mathrm{w}(W(G)) = \left\lceil \frac{n}{2} \right\rceil + 1.$$

This completes the proof.

Theorem 4.7 (Chromatic Number)

Let $G = \Gamma(S_M)$ be the monogenic semigroup graph and let $W(G)$ be the wheel graph constructed from G. Then $\chi\big(W(G)\big) = \left\lceil \frac{n}{2} \right\rceil + 1$.

Proof

By Theorem 4.6,

$$\mathrm{w}(W(G)) = \left\lceil \frac{n}{2} \right\rceil + 1.$$

Since the chromatic number of a graph is always at least its clique number, we obtain

$$\chi\big(W(G)\big) \geq \left\lceil \frac{n}{2} \right\rceil + 1.$$

Now consider the clique $A = \left\{ x^{\left\lfloor \frac{n}{2} \right\rfloor + 1}, x^{\left\lfloor \frac{n}{2} \right\rfloor + 2}, \cdots, x^{n} \right\}$.

This clique contains $\left\lceil \frac{n}{2} \right\rceil$ vertices. Assign distinct colors

$$1, 2, \cdots, \left\lceil \frac{n}{2} \right\rceil$$

to the vertices of A.

Let c be the center vertex of $W(G)$. Since c is adjacent to every vertex of G, it cannot receive any of the colors assigned to the vertices of A. Therefore, assign a new color to c.

Hence, $\left\lceil \frac{n}{2} \right\rceil + 1$ colors are sufficient to color the vertices of $A \cup \{c\}$.

To explicitly show that $\left\lceil \frac{n}{2} \right\rceil + 1$ colors are sufficient, we define a proper vertex coloring function $f: V(W(G)) \to \left\{1, 2, \cdots, \left\lceil \frac{n}{2} \right\rceil + 1\right\}$ as follows:

1. For the center vertex, we assign a unique color: $f(c) = \left\lceil \frac{n}{2} \right\rceil + 1$
2. For the vertices in the maximum clique $A = \left\{ x^{\left\lfloor \frac{n}{2} \right\rfloor + 1}, \cdots, x^{n} \right\}$, we assign distinct colors: $f\big(x^{n-k}\big) = k + 1$ for $0 \leq k < \left\lceil \frac{n}{2} \right\rceil$.
3. For the remaining vertices x^i where $1 \leq i \leq \left\lfloor \frac{n}{2} \right\rfloor$, we can set $f\big(x^i\big) = 1$.

To verify that this coloring is proper, notice that the only vertex with color $\left\lceil \frac{n}{2} \right\rceil + 1$ is c, which causes no conflicts. For any two vertices x^i, x^j with $1 \leq i, j \leq \left\lfloor \frac{n}{2} \right\rfloor$, they both receive color 1, but they are not adjacent since $i + j \leq n$. Furthermore, a vertex x^i (where $1 \leq i \leq \left\lfloor \frac{n}{2} \right\rfloor$ is adjacent to a vertex $x^j \in A$ if and only if $i + j > n$. If they are adjacent, since $f\big(x^i\big) = 1$ and $f\big(x^j\big) > 1$ (as color 1 is strictly reserved for the independent set or a non-adjacent boundary vertex), no two adjacent vertices receive the same color. Thus, f is a proper coloring, which implies:

$$\chi\big(W(G)\big) \leq \left\lceil \frac{n}{2} \right\rceil + 1.$$

Combining the inequalities $\chi\big(W(G)\big) \geq \left\lceil \frac{n}{2} \right\rceil + 1$ and $\chi\big(W(G)\big) \leq \left\lceil \frac{n}{2} \right\rceil + 1$, we conclude that

$$\chi\big(W(G)\big) = \left\lceil \frac{n}{2} \right\rceil + 1.$$

This completes the proof.

The identical nature of the clique number and the chromatic number confirms that $W\big(\Gamma(S_M)\big)$ belongs to the class of weakly perfect graphs. This symmetric expansion demonstrates that the addition of a universal center vertex preserves the chromatic structural tightly bound to its maximum clique size.

4.4 Domination Parameter

In this final subsection of our structural analysis, we investigate the domination-related characteristics of the constructed graph system. In structural graph theory and network optimization, the domination number is a fundamental parameter used to determine the minimum number of strategic positions required to monitor, control, or efficiently allocate resources across the entire vertex set. By evaluating this parameter for $W\big(\Gamma(S_M)\big)$, we explore the immediate consequence of coupling an algebraically constrained adjacency layout with a universal hub. Our findings explicitly demonstrate how the presence of a single globally connected center vertex collapses the domination requirements of the network to its absolute theoretical minimum, transforming a distributed structure into an optimally centralized system.

Theorem 4.8 (Domination Number)

Let $G = \Gamma(S_M)$ be the monogenic semigroup graph and let $W(G)$ be the wheel graph constructed from G. Then $\gamma\big(W(G)\big) = 1$.

Proof

Let c denote the center vertex of $W(G)$. By construction, c is adjacent to every vertex of G. Hence, every vertex of $V(W(G))\backslash\{c\}$ is adjacent to c.

Therefore, the singleton set

$$D = \{c\}$$

is a dominating set of $W(G)$. Consequently, $\gamma(W(G) \leq 1$.

Since the domination number of a nonempty graph is at least one, we have

$$\gamma\big(W(G)\big) \geq 1.$$

Combining these inequalities yields

$$\gamma\big(W(G)\big) = 1.$$

This completes the proof.

5. Concluding Remarks and Open Problems

The present chapter establishes several fundamental structural parameters of W(Γ(S_M)), including its degree-based, distance-based, chromatic, and domination properties. These results provide a solid foundation for future investigations concerning topological indices, spectral properties, metric parameters, and graph operations associated with this algebraically defined graph family.

Based on the results obtained in this chapter, the following open problems and research directions naturally arise:

Problem 1 Determine degree-based topological indices of $W\big(\Gamma(S_M)\big)$, including the Zagreb indices, Reverse Zagreb indices, Sombor index, Banhatti–Sombor index, Nirmala index, and other related invariants.

Problem 2 Investigate the spectral properties of $W\big(\Gamma(S_M)\big)$, including its adjacency spectrum, Laplacian spectrum, and signless Laplacian spectrum.

Problem 3 Determine metric-based parameters of $W\big(\Gamma(S_M)\big)$, such as the metric dimension, strong metric dimension, and resolving domination number.

Problem 4 Study graph operations associated with $W\big(\Gamma(S_M)\big)$, including its line graph, complement graph, subdivision graph, and total graph.

Problem 5 Generalize the present construction by replacing the single center vertex with more general graph structures or operations, and investigate the resulting structural and topological properties.

References

[1] West, D.B.: *Introduction to Graph Theory*. Prentice Hall, Upper Saddle River (1996).

[2] Das, K. C., Akgüneş, N., Çevik, A. S.: *On a graph of monogenic semigroup*. J. Inequal. Appl. 2013:44 (2013).

[3] Akgüneş, N., Das, K. C., Çevik, A. S.: *Topological indices on a graph of monogenic semigroups*. In: *Topics in Chemical Graph Theory*, Math. Chem. Monographs (2014).

[4] Oğuz Ünal, S.: *An application of Sombor index over a special class of semigroup graph*. J. Math. Article ID 3273117 (2021).

[5] Oğuz Ünal, S.: *Banhatti–Sombor index over a graph of a special class of semigroup*. Konuralp J. Math. 10, 40–43 (2022).

[6] Oğuz Ünal, S.: *Nirmala index over a graph of monogenic semigroups*. Bull. Int. Math. Virtual Inst. 12(1), 119–124 (2022).

[7] Oğuz Ünal, S.: *On vertex degree based indices of monogenic semigroup graphs*. Ikon. J. Math. 4(2), 12–20 (2022).

[8] Beck, I.: Coloring of commutative rings. J. Algebra 116(1), 208–226 (1988).

[9] Anderson, D.F., Livingston, P.S.: The zero-divisor graph of a commutative ring. J. Algebra 217(2), 434–447 (1999).

[10] DeMeyer, F., McKenzie, T., Schneider, K.: The zero-divisor graph of a commutative semigroup. Semigroup Forum 65(2), 206–214 (2002).

[11] DeMeyer, F., DeMeyer, L.: Zero divisor graphs of semigroups. J. Algebra 283(1), 190–198 (2005).

[12] Bondy, J.A., Murty, U.S.R.: Graph Theory. Graduate Texts in Mathematics, Springer, London (2008).

Chapter 3

In Silico Targeting of Sting Pathway: Application of Molecular Docking and Molecular Dynamics Simulations in Drug Discovery

Selma AKDENİZ[1], Nazmiye SABANCI[2]

1. Introduction

The innate immune system constitutes the first line of defense against infectious agents and cellular damage and functions through pattern recognition receptors (PRRs), which enable the rapid detection of foreign or abnormal molecular structures (Hooftman et al., 2026). Molecular and structural biology studies conducted in recent years have demonstrated that the cGAS–STING (cyclic GMP-AMP synthase–Stimulator of Interferon Genes) signaling pathway plays a central role in the detection of cytoplasmic double-stranded DNA (dsDNA) (Hooftman et al., 2026; Sun et al., 2013). In addition to regulating host defense against viral and bacterial infections, this pathway is critically involved in the pathogenesis of cancer, autoimmune diseases, chronic inflammation, neurodegenerative disorders, and cardiovascular diseases (Hooftman et al., 2026). Accordingly, STING is currently regarded as one of the most important molecular targets in both fundamental biomedical research and drug development.

STING is a transmembrane adaptor protein located in the endoplasmic reticulum membrane and is activated not directly by cytoplasmic DNA, but through 2′3′-cGAMP synthesized by the DNA sensor cGAS (Ishikawa & Barber, 2008). Recognition by cGAS of foreign DNA or DNA released from damaged cells into the cytoplasm leads to the synthesis of cGAMP, which binds to STING and induces a marked conformational change in the protein (Sun et al., 2013). Activated STING is subsequently translocated to the Golgi apparatus, where it activates several signaling proteins, particularly TANK-binding kinase 1 (TBK1) and interferon regulatory factor 3 (IRF3) (Ishikawa & Barber, 2008; Tanaka & Chen, 2012). This process stimulates the expression of type I interferons and numerous proinflammatory cytokines, thereby initiating an effective antiviral or

[1] PhD Student, Siirt University, Science Institute, Chemistry Department, Siirt,
ORCID: 0009-0007-6865-8203
[2] Assoc. Prof., Siirt University, Faculty of Arts and Science, Chemistry Department, Siirt,
ORCID: 0000-0002-0733-1692

antitumor immune response. STING activation is also involved in the regulation of NF-κB signaling, autophagy, cellular senescence, apoptosis, and various forms of programmed cell death (Barber, 2015). Therefore, this pathway performs multiple functions not only in the initiation of immune responses but also in the maintenance of cellular homeostasis (Hooftman et al., 2026).

Recent studies have shown that controlled activation of the STING signaling pathway at physiological levels provides protection against infections, whereas excessive or chronic activation may contribute to the development of systemic lupus erythematosus (SLE), STING-associated vasculopathy with onset in infancy (SAVI), rheumatoid arthritis, and various inflammatory disorders (Barber, 2015). Similarly, suppression of STING signaling in many tumor cells is considered an important mechanism of immune evasion, while excessive STING activation in certain cancer types may support tumor progression by promoting chronic inflammation. This bidirectional biological effect has accelerated efforts to develop both STING agonists and STING inhibitors as therapeutic agents (Barber, 2015; Hooftman et al., 2026). At present, numerous STING agonists and inhibitors acting through different mechanisms are being evaluated in preclinical studies, while several candidate molecules have progressed to clinical investigation.

The development of new drugs is generally a lengthy, costly, and low-success process. In conventional drug discovery, bringing a single molecule into clinical use often requires more than 10-15 years and investments amounting to billions of dollars. In contrast, computer-aided drug design (CADD) methods provide considerable advantages in terms of both time and cost by allowing potential drug candidates to be evaluated before experimental testing. In particular, the high-resolution determination of three-dimensional protein structures, advances in artificial intelligence-assisted protein modeling, and the increasing availability of high-performance computing systems have made structure-based drug design an indispensable component of modern pharmaceutical research.

One of the most widely used computational methods in structure-based drug design is molecular docking analysis. Molecular docking is an optimization-based approach used to predict the orientation and binding energy with which small-molecule ligands may occupy the active site of a target protein. Docking analyses enable thousands or even millions of candidate compounds to be screened within a relatively short period, allowing molecules with high predicted binding affinity to be identified and prioritized for experimental investigation. However, docking methods commonly treat the protein structure as rigid and only partially represent the dynamic characteristics of the biological environment. Consequently, docking results should be interpreted together with

complementary computational approaches capable of evaluating receptor flexibility and interaction stability.

Molecular dynamics (MD) simulations complement molecular docking by describing the time-dependent behavior of protein–ligand complexes, enabling assessment of structural stability and interaction persistence. Together with binding free-energy calculations, MD simulations substantially improve the reliability of docking predictions and have become an integral component of modern STING drug discovery (Hussain et al., 2022; Shang et al., 2019).

In recent years, intensive research on STING-targeted drug development has focused on natural products, synthetic small molecules, cyclic dinucleotides (CDNs), non-CDN agonists, and selective inhibitors (Wang et al., 2026; Kong et al., 2022; Wu et al., 2025). A substantial proportion of these studies are supported by multistep in silico approaches that combine molecular docking, molecular dynamics simulations, and free-energy calculations with experimental biochemical methods (Sood, & Kulharia, 2024; Hou et al., 2025; Özkurt, 2026). These integrated strategies enable the binding mechanisms of candidate molecules to be characterized in greater detail and facilitate the identification of the most promising compounds before experimental validation. Considering the rapid advances in computational biology and bioinformatics, in silico methods are expected to play an increasingly decisive role in the discovery of next-generation therapeutic agents targeting the STING pathway.

2. Structural Biology of STING as a Drug Target

2.1. Structural Organization of STING

Stimulator of interferon genes (STING), encoded by the TMEM173 gene, is an endoplasmic-reticulum-resident transmembrane protein that functions as a central signaling scaffold in cytosolic nucleic-acid sensing. Human STING is a 379-amino-acid protein organized into an N-terminal four-pass transmembrane domain, a connector region, a cytosolic ligand-binding domain, and a flexible C-terminal tail (Figure 1). This integrated architecture enables ligand recognition in the cytosol to be coupled with intracellular trafficking, oligomerization, and recruitment of downstream signaling proteins (Ishikawa & Barber, 2008; Ergun & Li, 2020; Decout et al., 2021; Zhang et al., 2022). Figure 1, illustrates the overall architecture of the STING homodimer, highlighting the N-terminal transmembrane domain (TMD), the connector region, the cytosolic ligand-binding domain (LBD), and the ligand-binding cavity located at the dimer interface. The endoplasmic reticulum (ER) membrane is shown schematically to indicate the membrane orientation of the receptor. The C-terminal tail (CTT),

which is largely unresolved in the cryo-EM structure because of its intrinsic flexibility, is indicated separately.

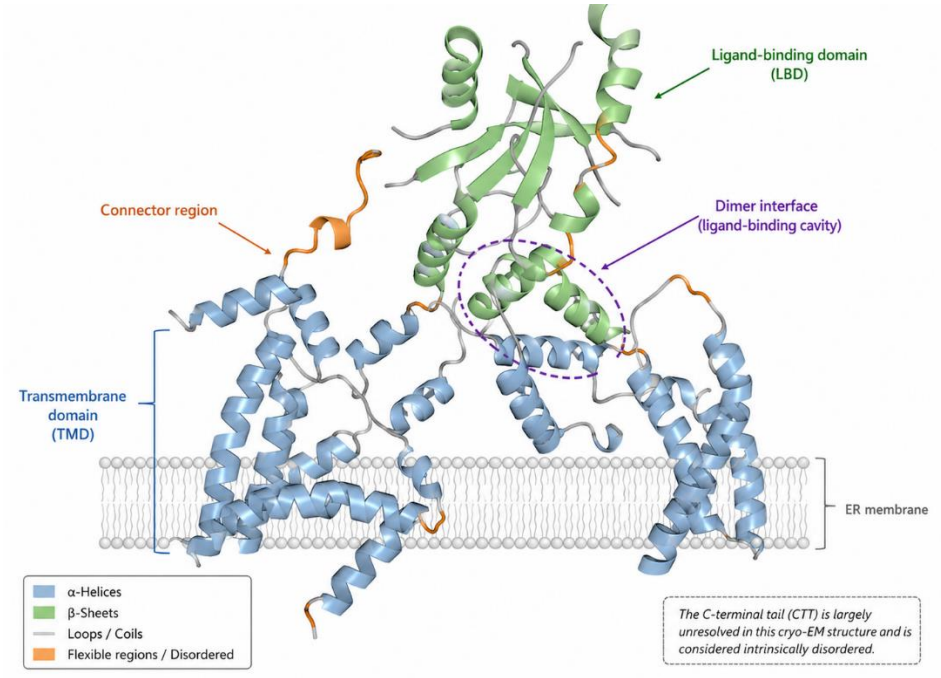

Figure 1. Structural organization of full-length human STING based on the cryo-EM structure

STING exists predominantly as a preassembled, domain-swapped homodimer rather than undergoing ligand-induced dimerization. The transmembrane helices form a stable membrane-embedded base that supports the cytosolic ligand-binding domains, giving the dimer its characteristic butterfly-shaped architecture (Decout et al., 2021). A connector region situated between the transmembrane and ligand-binding domains provides structural communication between these components, and alterations at this interface can substantially affect receptor activation. The integrity of both the dimer interface and interdomain contacts is therefore essential for maintaining the inactive receptor configuration and transmitting ligand-induced structural changes (Shang et al., 2019; Coderch et al., 2023).

The cytosolic ligand-binding domain contains the canonical cyclic-dinucleotide-binding pocket at the interface of the two protomers. This pocket recognizes the endogenous second messenger 2′3′-cyclic GMP-AMP, bacterial cyclic dinucleotides, and numerous synthetic agonists and antagonists (Gao et al., 2013). Ligand recognition is mediated by a combination of hydrogen bonds,

electrostatic interactions, aromatic stacking, hydrophobic contacts, and coordinated water molecules. The ligand-binding pocket accommodates endogenous cyclic dinucleotides together with numerous synthetic agonists and antagonists through hydrogen-bonding, electrostatic, hydrophobic, aromatic, and water-mediated interactions (Gao et al., 2013; Hong et al., 2021). Because STING adopts multiple experimentally observed conformations, selection of an appropriate structural model is an important consideration for structure-based drug discovery (Coderch et al., 2023).

The flexible C-terminal tail extends beyond the folded ligand-binding domain and provides the principal docking platform for downstream signaling components, particularly TANK-binding kinase 1. In inactive STING, this region is conformationally restrained or poorly ordered; ligand-induced structural rearrangements facilitate its release and functional exposure. Because of its intrinsic flexibility, the C-terminal tail has frequently been unresolved in crystallographic structures, whereas cryo-electron microscopy and complementary biochemical studies have provided greater insight into its relationship with receptor oligomerization and signal propagation (Shang et al., 2019; Ergun & Li, 2020).

Structural studies have also shown that the classical cyclic-dinucleotide pocket is not the only pharmacologically accessible region of STING. Small-molecule agonists may bind to a cryptic pocket within the transmembrane domain, while molecular-glue-like compounds can occupy an interface between the transmembrane domains of neighboring STING dimers and promote higher-order assembly (Li et al., 2024). These findings expand STING from a single-pocket receptor into a multidomain drug target with several potentially ligandable sites and conformational states (Lu et al., 2022). Lu et al. demonstrated activation through a transmembrane pocket, whereas Li et al. showed that NVS-STG2 binds between neighboring transmembrane-domain dimers and promotes oligomerization through a molecular-glue-like mechanism.

Collectively, STING functions as an integrated multidomain receptor in which the transmembrane domain, connector region, ligand-binding domain, and flexible C-terminal tail cooperate to support ligand recognition and intracellular signal transduction. The structural transitions associated with receptor activation are discussed in the following section.

2.2. Conformational Activation of STING

Conformational activation of STING is a dynamic process that transforms the receptor from an inactive dimer into a signaling-competent oligomer following ligand recognition. Activation is primarily initiated by binding of the endogenous

cyclic dinucleotide 2′3′-cyclic GMP–AMP (2′3′-cGAMP), produced by cyclic GMP–AMP synthase (cGAS) in response to cytosolic DNA, although bacterial cyclic dinucleotides and several synthetic agonists can also activate the receptor (Gao et al., 2013; Zhao et al., 2019). Structural studies have shown that ligand binding induces coordinated conformational changes within the preassembled STING dimer, including inward rotation of the ligand-binding domains, formation of a four-stranded β-sheet lid over the ligand-binding pocket, and remodeling of the connector region linking the transmembrane and cytosolic domains. In full-length STING, these changes are accompanied by an approximately 180° rotation of the ligand-binding domain relative to the transmembrane domain, generating a structural configuration that enables receptor activation and higher-order assembly (Li et al., 2023; Gharpure et al., 2025).

These conformational rearrangements promote oligomerization into tetramers and larger supramolecular assemblies that serve as signaling platforms. Although individual STING dimers are capable of binding TANK-binding kinase 1 (TBK1), efficient phosphorylation of STING and interferon regulatory factor 3 (IRF3) requires higher-order oligomerization, which brings adjacent signaling complexes into the appropriate spatial arrangement for trans-phosphorylation and downstream signaling (Zhang et al., 2022; Dempsey et al., 2019). Activated STING subsequently traffics from the endoplasmic reticulum to the Golgi apparatus, where assembly of the STING–TBK1–IRF3 signaling complex initiates type I interferon production together with NF-κB-mediated inflammatory responses (Hornung et al., 2014; Hopfner & Hornung, 2020). Collectively, these findings demonstrate that receptor activation is governed not by a single structural transition but by a coordinated sequence of ligand recognition, conformational rearrangement, oligomerization, intracellular trafficking, and signalosome assembly.

Recent structural studies have further refined this classical activation model by demonstrating that STING can be activated through multiple conformational pathways (Xie et al., 2022; Gharpure et al., 2025; Han et al., 2026). While nucleotide agonists such as 2′3′-cGAMP typically induce the canonical closed ligand-binding domain conformation, several non-nucleotide agonists are capable of activating STING through alternative structural mechanisms. Compounds such as diABZI can promote receptor activation without complete closure of the ligand-binding domain, whereas other agonists induce signaling through remodeling of the transmembrane domain or stabilization of inter-dimer interfaces rather than the canonical cyclic-dinucleotide-binding pocket (Xie et al., 2022; Gharpure et al., 2025; Han et al., 2026). These discoveries indicate that

STING activation is structurally more diverse than previously recognized and that multiple conformational states can converge on the same functional outcome of receptor oligomerization and signaling competence. This structural plasticity has clear implications for structure-based drug discovery, because different agonist classes engage different pockets and stabilize different active assemblies (Lu et al. 2022).

2.3. Structural Basis of STING Modulation

Recent structural studies have substantially expanded the understanding of STING as a therapeutic target by demonstrating that receptor modulation is not restricted to the canonical cyclic dinucleotide (CDN)-binding pocket. In addition to the cytosolic ligand-binding domain, alternative ligandable sites have been identified within the transmembrane domain and at inter-dimer interfaces, providing multiple opportunities for pharmacological intervention. Small-molecule agonists can activate STING through distinct allosteric mechanisms, including stabilization of transmembrane conformations or promotion of higher-order oligomerization independently of the classical CDN-binding mode (Lu et al., 2022). Representative compounds such as C53 and NVS-STG2 illustrate that structurally diverse ligands can engage different regions of the receptor while converging on the same functional outcome of productive STING activation. These discoveries demonstrate that STING contains multiple pharmacologically accessible binding sites, providing new opportunities for rational agonist and antagonist design.

The recognition of multiple binding sites and conformational states has important implications for rational drug discovery. Ligand affinity and pharmacological activity are further influenced by species-specific sequence differences and naturally occurring human STING polymorphisms, making the selection of an appropriate structural model a critical step in computational studies (Kong et al., 2022). Consequently, successful structure-based drug design increasingly relies on approaches that account for receptor flexibility rather than assuming a single static protein conformation (Ferreira et al., 2015). Ensemble docking, molecular dynamics simulations, and binding free-energy calculations have therefore become essential tools for identifying biologically relevant binding modes, characterizing allosteric mechanisms, and optimizing both agonists and antagonists (Tehrani et al., 2022; Basciu et al., 2025). Together, these advances establish the structural foundation for modern in silico strategies targeting the STING pathway.

3. Computational Strategies for STING Drug Discovery

3.1. Preparation of STING Structural Models and Ligands

The success of structure-based drug discovery depends fundamentally on the quality of the protein and ligand models used throughout the computational workflow. Before molecular docking or molecular dynamics (MD) simulations are performed, both the receptor and ligand must be carefully prepared to ensure chemically and structurally meaningful representations. Proper system preparation includes assignment of bond orders, addition of hydrogen atoms, optimization of hydrogen-bonding networks, determination of protonation and tautomeric states, completion of missing residues or side chains, and restrained energy minimization. These procedures substantially improve docking accuracy and virtual screening performance, whereas inadequate preparation may introduce systematic errors that propagate through subsequent computational analyses (Sastry et al., 2013; Schrödinger, 2021). Likewise, ligand preparation requires generation of reliable three-dimensional conformations, stereochemical verification, ionization-state prediction, and conformational sampling prior to docking. Because ligand flexibility strongly influences binding predictions, high-quality conformer generation has become an essential component of modern virtual screening workflows (Hawkins et al., 2010). Increasingly, receptor flexibility is also incorporated through ensemble-based strategies that employ multiple experimentally determined or computationally generated conformations instead of relying on a single static structure, thereby improving the identification of biologically relevant binding modes (Amaro et al., 2018).

For STING, protein preparation requires additional considerations owing to the receptor's exceptional conformational plasticity and membrane-associated architecture. Multiple high-resolution X-ray and cryo-EM structures are now available, representing apo and holo states, open and closed ligand-binding domains, transmembrane-bound conformations, and complexes with endogenous cyclic dinucleotides, synthetic agonists, antagonists, and downstream signaling proteins (Gao et al., 2013; Shang et al., 2019). Consequently, receptor selection should be driven by the biological objective of the study rather than by structural resolution alone. For example, investigations of canonical cyclic dinucleotide recognition generally benefit from ligand-bound closed conformations, whereas studies targeting recently identified allosteric transmembrane pockets require full-length cryo-EM structures that preserve these binding sites (Lu et al., 2022). Accordingly, receptor selection should be guided by the biological objective of the study and the availability of experimentally resolved conformational states. Therefore, careful selection of the receptor structure, together with appropriate protein and ligand preparation, provides the structural foundation for reliable

docking, molecular dynamics simulations, and subsequent free-energy calculations in STING-targeted drug discovery. The overall computational workflow employed in structure-based STING drug discovery is summarized in Figure 2. The workflow summarizes the principal stages of computer-aided drug design (CADD) applied to STING, including structural model selection, protein and ligand preparation, virtual screening, molecular docking, molecular dynamics simulations, binding free-energy calculations, and lead optimization followed by experimental validation.

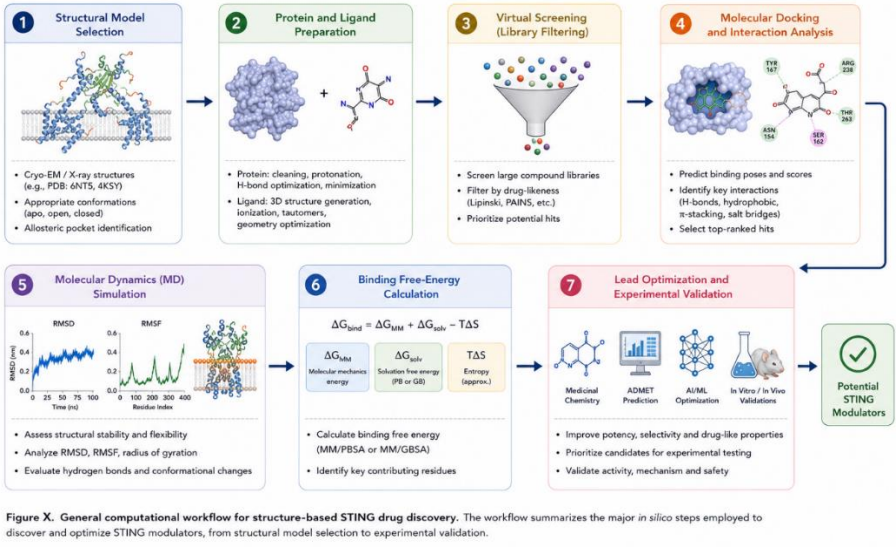

Figure 2. General computational workflow for structure-based STING drug discovery

3.2. Molecular Docking Strategies for STING Modulator Discovery

Molecular docking has become one of the fundamental computational techniques for discovering and optimizing small-molecule modulators targeting the stimulator of interferon genes (STING). The rapid increase in experimentally resolved STING structures, particularly those obtained by X-ray crystallography and cryo-electron microscopy (cryo-EM), has markedly improved the reliability of structure-based drug discovery by enabling the accurate prediction of ligand-binding modes and receptor–ligand interactions. Rather than functioning solely as a virtual screening tool, molecular docking is now routinely integrated with structural biology, medicinal chemistry, molecular dynamics (MD) simulations, and free-energy calculations to accelerate the identification and optimization of both agonists and antagonists. Recent cryo-EM studies have further revealed

multiple conformational states of STING, providing valuable structural templates for receptor selection and rational ligand design (Bai & Zhang, 2024).

A major milestone in STING-targeted drug discovery was achieved by Ramanjulu et al. (2018), who reported the first systemically active non-cyclic dinucleotide (non-CDN) STING agonist through an integrated strategy combining high-throughput screening, X-ray crystallography, and structure-guided medicinal chemistry. Initial screening identified amidobenzimidazole (ABZI) compounds capable of binding the canonical cGAMP-binding pocket, while crystallographic analysis demonstrated that two ABZI molecules simultaneously occupied the STING homodimer interface. Structural information obtained from these complexes enabled the rational linking of two ABZI molecules, leading to the development of diABZI with substantially enhanced affinity and biological activity. Importantly, this work demonstrated that structural information could directly guide lead optimization rather than merely validate computational predictions, establishing one of the earliest and most influential examples of structure-guided drug design for STING (Duvall et al., 2023).

The increasing availability of structural information subsequently enabled large-scale structure-based virtual screening approaches aimed at expanding the chemical diversity of STING modulators. Using receptor-based virtual screening, Hou et al. (2020) identified triazoloquinoxaline derivatives as a novel class of non-CDN STING agonists. Experimental validation demonstrated that the lead compound activated the STING–TBK1–IRF3 signaling cascade, increased the expression of IFN-β, CXCL10, and IL-6, and exhibited biological activity comparable to endogenous cGAMP in cellular assays. This study clearly illustrated how molecular docking can efficiently explore large chemical libraries to identify entirely new chemical scaffolds with immunostimulatory activity before extensive medicinal chemistry optimization (Hou et al., 2020).

Following hit identification, molecular docking has become an indispensable component of structure-guided lead optimization. An excellent example is provided by Duvall et al. (2023), who optimized a non-CDN STING agonist platform for antibody–drug conjugate (ADC) applications through an iterative workflow integrating crystallographic information, molecular modeling, medicinal chemistry, and biological evaluation. Co-crystal structures identified key interactions within the STING ligand-binding pocket and revealed opportunities for scaffold modification, including optimization of benzimidazole derivatives, heterocyclic substituents, linker chemistry, and scaffold hydrophilicity. Successive rounds of structure-guided optimization ultimately generated highly potent agonists with improved pharmacokinetic properties,

demonstrating that molecular docking is equally valuable during hit-to-lead optimization as during initial virtual screening.

Recent structural studies have further broadened the application of molecular docking by revealing previously unrecognized ligand-binding conformations and regulatory mechanisms. Cryo-EM analyses have demonstrated that STING activation involves large-scale conformational rearrangements, including rotation of the ligand-binding domain, higher-order oligomerization, and recruitment of TBK1. These structural discoveries have enabled computational studies to move beyond the traditional closed conformation of STING by incorporating multiple receptor states into docking protocols. Consequently, ensemble docking and conformation-dependent virtual screening have become increasingly important strategies for identifying ligands capable of selectively stabilizing distinct functional states of the receptor (Bai & Zhang, 2024).

The role of molecular docking has also evolved within broader computer-aided drug discovery (CADD) frameworks. Instead of relying exclusively on docking scores, contemporary studies combine machine learning, virtual screening, ADMET prediction, molecular docking, molecular dynamics simulations, and experimental validation into integrated discovery pipelines. A representative example is provided by Zhao et al. (2026), who developed a machine learning-driven workflow to prioritize potential STING inhibitors from multiple traditional Chinese medicine databases. More than 1,500 candidate compounds were progressively filtered using predictive models, docking analyses, ADMET evaluation, and molecular dynamics simulations before biological validation identified Cassiaside and Plantaginin as promising STING inhibitory compounds. This multidimensional strategy illustrates how docking now functions as one component within an integrated computational framework rather than as a stand-alone prediction method (Zhao et al., 2026).

Besides agonist discovery, molecular docking has become equally important for elucidating the binding mechanisms of STING antagonists. Recent computational investigations of the covalent inhibitor H-151 demonstrated that, in addition to its established interaction with the palmitoylation region, the compound can adopt a stable non-covalent binding mode within the canonical cGAMP-binding pocket. By integrating molecular docking, Gaussian accelerated molecular dynamics, MM-GBSA free-energy calculations, and interaction fingerprint analyses, the study identified residues such as Tyr261, Thr263, and Ala262 as major contributors to ligand stabilization. These findings highlight the capacity of docking-guided simulations to identify alternative pharmacophores and previously unrecognized inhibitory mechanisms that may facilitate the

rational design of next-generation non-covalent STING antagonists (Özkurt, 2026).

Collectively, these studies demonstrate that molecular docking has evolved from a simple binding-pose prediction technique into a central component of modern STING drug discovery. It now supports virtual screening, structure-guided medicinal chemistry, scaffold optimization, mechanistic interpretation of ligand recognition, and prioritization of compounds for experimental validation. Nevertheless, because docking provides only a static representation of receptor–ligand interactions, its predictions require further validation through molecular dynamics simulations and binding free-energy analyses, which offer a more comprehensive description of conformational flexibility, interaction stability, and binding energetics. Accordingly, these complementary computational approaches constitute the next stage of contemporary STING-targeted computer-aided drug discovery and are discussed in the following section.

3.3. Molecular Dynamics Simulations in STING Drug Discovery

Molecular dynamics (MD) simulations have become an indispensable component of STING-targeted drug discovery by providing mechanistic insights that extend far beyond the static receptor–ligand complexes predicted by molecular docking. Because STING activation involves extensive conformational rearrangements, including ligand-binding domain closure, allosteric communication between structural elements, oligomerization, and recruitment of TBK1, the dynamic behavior of the receptor cannot be adequately described using static structural models alone (Li et al., 2023). Consequently, MD simulations are now routinely integrated with docking, cryo-electron microscopy (cryo-EM), and free-energy calculations to investigate ligand stability, receptor flexibility, interaction networks, and activation mechanisms at atomic resolution. As highlighted in recent reviews, these computational approaches have become essential for understanding both canonical and non-canonical mechanisms of STING modulation and for guiding the rational development of agonists and antagonists.

Recent studies clearly illustrate the expanding role of MD simulations in the discovery and optimization of novel STING agonists. Li et al. (2023) demonstrated through 1000 ns MD simulations that agonist binding induces coordinated movements of helices α5–α7 together with loop 6, loop 8, and the C-terminal tail, thereby promoting stable STING–TBK1 interactions. Their free-energy perturbation analyses further identified the α5 region as a critical determinant of agonist efficacy, providing a structural basis for the rational optimization of non-nucleotide agonists such as SR-717. More recently, Liu et al.

(2026) combined multilevel virtual screening, medicinal chemistry, and MD simulations to identify the allosteric agonist LA24, demonstrating that persistent hydrogen bonds with G114 and Y106 together with π–π interactions involving H50 stabilize ligand binding within the transmembrane allosteric pocket. Similarly, Hou et al. (2025) employed molecular dynamics simulations to optimize a new class of 3-(fluoro-imidazolyl)pyridazine derivatives, showing that appropriate spatial orientation and dynamic stabilization of the ligand–STING complex were critical determinants of agonistic activity, ultimately leading to the identification of compound A4, which exhibited superior antitumor efficacy compared with SR-717. These studies collectively demonstrate that MD simulations have evolved from a post-docking validation tool into a key driver of structure-guided lead optimization and mechanistic understanding.

Beyond agonist optimization, MD simulations have substantially advanced the understanding of ligand recognition, species specificity, and receptor dynamics in STING biology. Wang et al. (2024) demonstrated that cyclic adenosine–inosine monophosphate analogues adopt stable U-shaped conformations within the canonical ligand-binding pocket, promoting the transition from the inactive open state to the active closed conformation through persistent interactions with residues such as Tyr167, Arg238, Thr263, and Thr267. Likewise, Gates et al. revealed that explicit-solvent MD simulations could explain the species-selective activity of DMXAA by identifying the critical contributions of mutations G230I and S162A/Q266I and, importantly, by demonstrating the essential role of bridge water molecules in stabilizing STING–ligand complexes and modulating local electrostatic environments (Gates et al., 2024). Furthermore, recent structure-based virtual screening studies have successfully integrated MD simulations with binding free-energy calculations to identify novel STING modulators, including natural CdnP inhibitors, underscoring the increasing role of dynamic simulations in hit validation and lead prioritization. Collectively, these findings establish MD simulations as a cornerstone of contemporary STING drug discovery, enabling a comprehensive understanding of receptor activation, conformational plasticity, and ligand recognition that is unattainable through static structural approaches alone.

4. Current Progress, Challenges, and Future Perspectives

Over the past decade, remarkable progress has been achieved in the development of STING-targeted therapeutics through the integration of structural biology and computational drug discovery. Advances in X-ray crystallography and cryo-electron microscopy have provided detailed insights into the conformational dynamics of STING, enabling the identification of key ligand-

binding regions and activation mechanisms. These structural data have significantly improved the accuracy of molecular docking, virtual screening, and molecular dynamics (MD) simulations, facilitating the rational design and optimization of novel STING agonists and antagonists. As a result, several promising small-molecule agonists, including amidobenzimidazole (ABZI)-based derivatives, diABZI, MSA-2, and SR-717, have been successfully developed and demonstrated potent immunostimulatory activity in preclinical studies (Ramanjulu et al., 2018; Shang et al., 2019; Ergun & Li, 2020; Li et al., 2023). These advances clearly demonstrate that computational approaches have evolved from supportive tools into essential components of modern STING-directed drug discovery.

Despite these remarkable advances, several scientific and computational challenges continue to limit the efficient development of STING-targeted therapeutics. One of the major obstacles is the pronounced conformational plasticity of STING, which undergoes substantial structural rearrangements during activation. As a result, static protein structures obtained from X-ray crystallography or cryo-electron microscopy may not fully represent the dynamic conformational ensemble involved in ligand recognition. In addition, significant sequence variations among human STING haplotypes and the well-documented differences between human and murine STING complicate the translation of preclinical findings into clinical applications. The species-specific activity of early agonists such as DMXAA clearly illustrates this challenge and has encouraged the development of new compounds capable of activating multiple human STING variants. Furthermore, although molecular docking has become an indispensable screening tool, accurately predicting ligand affinity remains difficult because conventional scoring functions often fail to capture induced-fit effects, long-range electrostatic interactions, and the energetic contribution of ordered water molecules. Recent computational studies have demonstrated that explicit-solvent molecular dynamics simulations and free-energy calculations substantially improve the reliability of binding predictions, emphasizing the need for integrated computational workflows rather than relying on docking alone (Gates et al., 2024; Li et al., 2023). These challenges indicate that future progress will depend on combining high-resolution structural data with advanced simulation techniques and experimental validation to improve both prediction accuracy and clinical translatability.

Future advances in STING-targeted drug discovery will increasingly rely on the integration of computational and experimental approaches rather than on the application of individual techniques. The growing availability of high-resolution structural data, together with improvements in molecular docking, molecular

dynamics simulations, and binding free-energy calculations, is expected to facilitate the identification of more selective and pharmacologically optimized STING modulators. At the same time, advances in artificial intelligence and machine learning are transforming structure-based drug design by accelerating virtual screening, predicting ligand–protein interactions, and guiding lead optimization. These emerging technologies, combined with medicinal chemistry and experimental validation, are expected to reduce the time and cost of drug development while improving the probability of clinical success. Future studies should also focus on designing compounds with broad activity against human STING variants, improved oral bioavailability, reduced systemic toxicity, and enhanced tissue selectivity. Such multidisciplinary strategies will play a pivotal role in translating computational discoveries into clinically effective therapeutics for cancer, infectious diseases, and immune-mediated disorders.

5. Concluding Remarks

Advances in structural biology and computational methodologies have transformed STING-targeted drug discovery from an empirical process into a rational, structure-guided discipline. As discussed throughout this chapter, the integration of molecular docking, molecular dynamics simulations, pharmacophore modeling, and virtual screening has significantly improved the identification and optimization of novel STING modulators while reducing the time and cost associated with early-stage drug discovery. At the same time, continuous improvements in high-resolution structural characterization and computational algorithms have enhanced our understanding of STING activation mechanisms and ligand recognition, providing valuable guidance for the design of more potent and selective therapeutic agents. Despite these advances, important challenges remain, including the dynamic nature of STING, interspecies differences, genetic polymorphisms, and the need to improve the pharmacokinetic and safety profiles of candidate molecules. Addressing these challenges will require close collaboration between computational scientists, structural biologists, medicinal chemists, and experimental researchers. Looking forward, the integration of next-generation computational technologies with experimental validation is expected to accelerate the discovery of clinically effective STING-targeted therapeutics. Such multidisciplinary approaches will not only facilitate the development of improved cancer immunotherapies but also expand the therapeutic potential of STING modulation in antiviral therapies, vaccine adjuvant design, and the treatment of immune-mediated diseases.

REFERENCES

Amaro, R. E., Baudry, J., Chodera, J., Demir, Ö., McCammon, J. A., Miao, Y., & Smith, J. C. (2018). Ensemble Docking in Drug Discovery. *Biophysical Journal*, 114(10), 2271–2278. https://doi.org/10.1016/j.bpj.2018.02.038

Bai, X. chen, & Zhang, X. (2024). Applications of cryo-EM in drug development for STING. *Current Opinion in Structural Biology*, 84, 102767. https://doi.org/10.1016/j.sbi.2023.102767

Barber, G. N. (2015). STING: infection, inflammation and cancer. *Nature Reviews Immunology*, *15*(12), 760–770. https://doi.org/10.1038/nri3921

Basciu, A., Athar, M., Kurt, H., Neville, C., Malloci, G., Muredda, F. C., Bosin, A., Ruggerone, P., Bonvin, A. M. J. J., & Vargiu, A. V. (2025). Toward the Prediction of Binding Events in Very Flexible, Allosteric, Multidomain Proteins. *Journal of Chemical Information and Modeling*, 65(4), 2052–2065. https://doi.org/10.1021/acs.jcim.4c01810

Coderch, C., Arranz-Herrero, J., Nistal-Villan, E., de Pascual-Teresa, B., & Rius-Rocabert, S. (2023). The Many Ways to Deal with STING. *International Journal of Molecular Sciences*, 24(10), 9032. https://doi.org/10.3390/ijms24109032

Decout, A., Katz, J. D., Venkatraman, S., & Ablasser, A. (2021). The cGAS–STING pathway as a therapeutic target in inflammatory diseases. *Nature Reviews Immunology* 21 (9), 548–569). https://doi.org/10.1038/s41577-021-00524-z

Dempsey, L. A. (2019). STING-ing insights. *Nature Immunology*, 20(4), 377. https://doi.org/10.1038/s41590-019-0370-9

Duvall, J. R., Thomas, J. D., Bukhalid, R. A., Catcott, K. C., Bentley, K. W., Collins, S. D., Eitas, T., Jones, B. D., Kelleher, E. W., Lancaster, K., Protopopova, M., Ray, S. S., Ter-Ovanesyan, E., Xu, L., Yang, L., Zurita, J., Damelin, M., Toader, D., & Lowinger, T. B. (2023). Discovery and Optimization of a STING Agonist Platform for Application in Antibody Drug Conjugates. *Journal of Medicinal Chemistry*, 66(15), 10715–10733. https://doi.org/10.1021/acs.jmedchem.3c00907

Ergun, S. L., & Li, L. (2020). Structural Insights into STING Signaling. *Trends in Cell Biology*, 30(5), 399–407. https://doi.org/10.1016/J.TCB.2020.01.010

Ferreira, L. G., Dos Santos, R. N., Oliva, G., & Andricopulo, A. D. (2015). Molecular Docking and Structure-Based Drug Design Strategies. *Molecules*, 20(7), 13384-13421. https://doi.org/10.3390/molecules200713384

Gao, P., Ascano, M., Zillinger, T., Wang, W., Dai, P., Serganov, A. A., Gaffney, B. L., Shuman, S., Jones, R. A., Deng, L., Hartmann, G., Barchet, W., Tuschl, T., & Patel, D. J. (2013). Structure-function analysis of STING activation by c[G(2′,5′) pA(3′,5′)p] and targeting by antiviral DMXAA. *Cell*, 154(4), 748–762. https://doi.org/10.1016/j.cell.2013.07.023

Gates, H., Payne, R. T., Pfeifer, H., Le, L., Crivelli, S., & Watanabe, M. (2024). Roles of water molecules in STING activation: A computational perspective. *ChemRxiv*. https://doi.org/10.26434/chemrxiv-2024-7k67q

Gharpure, A., Sulpizio, A., Loeffler, J. R., Fernández-Quintero, M. L., Tran, A. S., Lairson, L. L., & Ward, A. B. (2025). Distinct oligomeric assemblies of STING induced by non-nucleotide agonists. *Nature Communications*, 16(1), 3440-. https://doi.org/10.1038/s41467-025-58641-5

Han, J., Zhang, S., Hou, Y., Wang, Y., Zhang, Z., Yang, J., Xu, Y., Peng, Z., Yin, H., Chen, K., Liu, X., & Zhang, C. (2026). A chemical agonist and the Golgi-resident lipid PI4P activate STING by inducing transmembrane helix rearrangement. *Immunity*, 59(1), 34-47.e9. https://doi.org/10.1016/j.immuni.2025.11.004

Hawkins, P. C. D., Skillman, A. G., Warren, G. L., Ellingson, B. A., & Stahl, M. T. (2010). Conformer generation with OMEGA: Algorithm and validation using high quality structures from the protein databank and cambridge structural database. *Journal of Chemical Information and Modeling*, 50(4), 572–584. https://doi.org/10.1021/ci100031x

Hong, Z., Mei, J., Li, C., Bai, G., Maimaiti, M., Hu, H., Yu, W., Sun, L., Zhang, L., Cheng, D., Liao, Y., Li, S., You, Y., Sun, H., Huang, J., Liu, X., Lieberman, J., & Wang, C. (2021). STING inhibitors target the cyclic dinucleotide binding pocket. *Proceedings of the National Academy of Sciences of the United States of America*, 118(24), e2105465118. https://doi.org/10.1073/pnas.2105465118

Hooftman, A., Keller, A., Ablasser, A. (2026). The cGAS-STING pathway: Mechanism and medical implications. *Cell*, 189(13), 3849–3870. https://doi.org/10.1016/j.cell.2026.06.001

Hopfner, K. P., & Hornung, V. (2020). Molecular mechanisms and cellular functions of cGAS–STING signalling. *Nature Reviews Molecular Cell Biology*, 21(9), 501–521. https://doi.org/10.1038/s41580-020-0244-x

Hornung, V., Hartmann, R., Ablasser, A., & Hopfner, K. P. (2014). OAS proteins and cGAS: Unifying concepts in sensing and responding to cytosolic nucleic acids. *Nature Reviews Immunology*, 14(8), 521–528. https://doi.org/10.1038/nri3719

Hou, H., Yang, R., Liu, X., Wu, X., Zhang, S., Chen, K., & Zheng, M. (2020). Discovery of triazoloquinoxaline as novel STING agonists via structure-based virtual screening. *Bioorganic Chemistry*, *100*, 103958. https://doi.org/10.1016/j.bioorg.2020.103958

Hou, S., Chang, J., Xing, C., Ye, Z., Li, W., Zhang, Y., Zheng, Z., Xiao, J., & Li, S. (2025). Design, Synthesis, and Biological Evaluation of Selective STING Synergists That Enhance cGAMP-STING Pathway Activation without Inherent Agonist Activity. *Journal of Medicinal Chemistry*, 68(9), 9407–9430. https://doi.org/10.1021/ACS.JMEDCHEM.4C03131/SUPPL_FILE/JM4C03131_SI_003.PDF

Hussain, B., Xie, Y., Jabeen, U., Lu, D., Yang, B., Wu, C., & Shang, G. (2022). Activation of STING Based on Its Structural Features. *Frontiers in Immunology*, 13, 808607. https://doi.org/10.3389/fimmu.2022.808607

Ishikawa, H., & Barber, G. N. (2008). STING is an endoplasmic reticulum adaptor that facilitates innate immune signaling. *Nature*, 455(7213), 674–678. https://doi.org/10.1038/nature07317

Kong, X., Zuo, H., Huang, H. Da, Zhang, Q., Chen, J., He, C., & Hu, Y. (2022). STING as an emerging therapeutic target for drug discovery: Perspectives from the global patent landscape. *Journal of Advanced Research*, 44, 119. https://doi.org/10.1016/J.JARE.2022.05.006

Li, R., Chen, L., He, X., Cao, D., Zhang, Z., Jiang, H., Chen, K., & Cheng, X. (2023). Loops Mediate Agonist-Induced Activation of the Stimulator of Interferon Genes Protein. Journal of Chemical Information and Modeling, 63(23), 7373–7381. https://doi.org/10.1021/acs.jcim.3c00984

Li, J., Canham, S. M., Wu, H., Henault, M., Chen, L., Liu, G., Chen, Y., Yu, G., Miller, H. R., Hornak, V., Brittain, S. M., Michaud, G. A., Tutter, A., Broom, W., Digan, M. E., McWhirter, S. M., Sivick, K. E., Pham, H. T., Chen, C. H., … Feng, Y. (2024). Activation of human STING by a molecular glue-like compound. *Nature Chemical Biology*, 20(3), 365–372. https://doi.org/10.1038/s41589-023-01434-y

Liu, Y., Wu, J., Gao, N., Zheng, L., Zhang, W., Zhao, F., Meng, B., Liu, X., Liu, L., Zhao, H., & Kang, D. (2026). Discovery and optimization of 2,3-dihydroindole derivatives as STING receptor allosteric agonists. *Bioorganic & Medicinal Chemistry Letters*, 132, 130508. https://doi.org/10.1016/j.bmcl.2025.130508

Lu, D., Shang, G., Li, J., Lu, Y., Bai, X. chen, & Zhang, X. (2022). Activation of STING by targeting a pocket in the transmembrane domain. *Nature*, 604(7906), 557–562. https://doi.org/10.1038/s41586-022-04559-7

Özkurt, Ç. (2026). Non-covalent engagement of the cGAMP-binding pocket by STING inhibitor H-151: Characterization by molecular docking, Gaussian accelerated molecular dynamics, and MM-GBSA free energy analysis. *Computational Biology and Chemistry*, 124, 109164. https://doi.org/10.1016/J.COMPBIOLCHEM.2026.109164

Ramanjulu, J. M., Pesiridis, G. S., Yang, J., Concha, N., Singhaus, R., Zhang, S. Y., Tran, J. L., Moore, P., Lehmann, S., Eberl, H. C., Muelbaier, M., Schneck, J. L., Clemens, J., Adam, M., Mehlmann, J., Romano, J., Morales, A., Kang, J., Leister, L., … Bertin, J. (2018). Design of amidobenzimidazole STING receptor agonists with systemic activity. *Nature*, 564(7736), 439–443. https://doi.org/10.1038/s41586-018-0705-y

Sastry, G.M., Adzhigirey, M., Day, T., Annabhimoju, R., & Sherman, W. (2013). Protein and ligand preparation: Parameters, protocols, and influence on virtual screening enrichments. *Journal of Computer-Aided Molecular Design*, 27(3), 221–234. https://doi.org/10.1007/s10822-013-9644-8

Schrödinger Release 2021-3: Protein Preparation Wizard. (2021). Schrödinger, LLC, New York, NY.

Shang, G., Zhang, C., Chen, Z. J., Bai, X. C., & Zhang, X. (2019). Cryo-EM structures of STING reveal its mechanism of activation by cyclic GMP-AMP. *Nature*, 567 (7748), 389–393. https://doi.org/10.1038/s41586-019-0998-5

Sood, A., & Kulharia, M. (2024). Inhibition of IRF3-STING axis interaction in silicosis using natural compounds: an in-silico study using molecular docking, ADMET, molecular dynamics and MMPBSA approach. *In Silico Pharmacology*, 13(1). https://doi.org/10.1007/S40203-024-00290-5

Sun, L., Wu, J., Du, F., Chen, X., & Chen, Z. J. (2013). Cyclic GMP-AMP Synthase Is a Cytosolic DNA Sensor That Activates the Type I Interferon Pathway. *Science*, 339 (6121), 786–791. https://doi.org/10.1126/science.1232458

Tanaka, Y., & Chen, Z. J. (2012). STING specifies IRF3 phosphorylation by TBK1 in the cytosolic DNA signaling pathway. *Science Signaling*, 5(214), ra20. https://doi.org/10.1126/scisignal.2002521

Tehrani, Z. A., Rulíšek, L., & Černý, J. (2022). Molecular dynamics simulations provide structural insight into binding of cyclic dinucleotides to human STING protein. *Journal of Biomolecular Structure and Dynamics*, 40(20), 10250–10264. https://doi.org/10.1080/07391102.2021.1942213

Wang, M., Fan, B., Lu, W., Ryde, U., Chang, Y., Han, D., Lu, J., Liu, T., Gao, Q., Chen, C., & Xu, Y. (2024). Unraveling the Binding Mode of Cyclic Adenosine–Inosine Monophosphate (cAIMP) to STING through

Molecular Dynamics Simulations. *Molecules*, 29(11), 2650. https://doi.org/10.3390/molecules29112650

Wang, L., Nafees, M., Fei, H., Hanif, M., & Yang, P. (2026). Recent progress in cGAS–STING agonist design and mechanisms of cancer immune modulation. *RSC Chemical Biology*. Advance online publication. https://doi.org/10.1039/D6CB00005C

Wu, K., Xu, Y., Liu, P., Chen, K., & Zhao, Y. (2025). STING inhibitors and degraders: Potential therapeutic agents in inflammatory diseases. *European Journal of Medicinal Chemistry*, 291, 117632. https://doi.org/10.1016/j.ejmech.2025.117632

Xie, Z., Wang, Z., Fan, F., Zhou, J., Hu, Z., Wang, Q., Wang, X., Zeng, Q., Zhang, Y., Qiu, J., Zhou, X., Xu, H., Bai, H., Zhan, Z., Ding, J., Zhang, H., Duan, W., Yu, X., & Geng, M. (2022). Structural insights into a shared mechanism of human STING activation by a potent agonist and an autoimmune disease-associated mutation. *Cell Discovery*, 8(1), 133-. https://doi.org/10.1038/s41421-022-00481-4

Zhang, Z., Zhou, H., Ouyang, X., Dong, Y., Sarapultsev, A., Luo, S., & Hu, D. (2022). Multifaceted functions of STING in human health and disease: from molecular mechanism to targeted strategy. Signal Transduction and Targeted Therapy, 7, 394. https://doi.org/10.1038/s41392-022-01252-z

Zhao, B., Du, F., Xu, P., Shu, C., Sankaran, B., Bell, S. L., Liu, M., Lei, Y., Gao, X., Fu, X., Zhu, F., Liu, Y., Laganowsky, A., Zheng, X., Ji, J. Y., West, A. P., Watson, R. O., & Li, P. (2019). A conserved PLPLRT/SD motif of STING mediates the recruitment and activation of TBK1. *Nature 2019 569:7758*, *569*(7758), 718–722. https://doi.org/10.1038/s41586-019-1228-x

Zhao, T., Chen, D., Chen, Z., Wang, Q., Qing, J., Huang, Q., Zhao, Y., & Zhu, L. (2026). Machine learning-driven prioritization and experimental validation of traditional Chinese medicine-derived STING-inhibitory candidates. *Molecular Diversity*, 1–15. https://doi.org/10.1007/s11030-026-11634-y

Chapter 4

Machine Learning in Chemical Sensors: Fundamentals, Diffusion Theory, and Recent Application

Sibel ÇELİK AÇIKBAŞ[1*], Ali DENİZ[2]

ABSTRACT

Growing concerns over environmental pollution and the increasing release of hazardous volatile organic compounds (VOCs) have accelerated the development of chemical sensors with high sensitivity, selectivity, and reliability for toxic gas detection. Recent developments in sensing materials have significantly improved sensor performance; however, the increasing complexity of sensor responses has highlighted the need for advanced data analysis techniques. In this chapter, the fundamental operating principles of chemical sensors are first introduced, including the structure of sensor systems, sensing mechanisms, and signal transduction processes. Subsequently, the theoretical basis of molecular diffusion is discussed through Fick's First and Second Laws, together with their mathematical formulation for one-dimensional thin-film sensing layers. The early-time approximation of Fickian diffusion is also presented as an effective approach for estimating diffusion coefficients from experimental sensor responses. The chapter then provides an overview of machine learning, covering its fundamental concepts and major learning paradigms, including clustering, classification, and artificial neural networks. Finally, recent studies on the application of machine learning techniques in chemical sensing are reviewed, with particular emphasis on gas identification, sensor calibration, diffusion modeling, response prediction, and intelligent sensor systems. The reviewed literature demonstrates that integrating machine learning algorithms with chemical sensor technologies substantially enhances prediction accuracy, sensor selectivity, and data interpretation, thereby contributing to the development of next-generation intelligent sensing platforms.

Keywords: Chemical sensors; machine learning; artificial neural networks; Fick's laws of diffusion; mathematical modeling.

[1] *Dr. ; Usak University, Department of Mathematics, Faculty of Engineering and Natural Sciences. e_sibel_celik@hotmail.com ORCID No: 0000-0001-8684-1406
corresponding author: Dr. Sibel ÇELİK AÇIKBAŞ (e_sibel_celik@hotmail.com)
[2] Assoc. Prof. Dr.; Usak University, Department of Mathematics, Faculty of Engineering and Natural Sciences. ali.deniz@usak.edu.tr ORCID No: 0000-0002-6514-2320

1. INTRODUCTION

The widespread application of nanotechnology across numerous fields, together with rapid industrial development, has raised concerns regarding its potential adverse effects on human health and associated safety risks (Hsieh et al., 2026). The inhalation of nanoparticles and hazardous volatile organic compounds (VOCs) can result in their deposition in the brain and lungs, leading to various health problems, including oxidative stress, respiratory diseases, skin aging, and inflammation (Paul and Bari, 2022). Consequently, there is an increasing need for rapid and reliable monitoring and control systems, as well as regulatory standards that govern exposure to airborne pollutants, in order to minimize or prevent the resulting health damage. In this context, the development of gas sensors for the detection of hazardous volatile organic compounds has become an essential research priority (Acikbas et al., 2016a; Acikbas et al., 2016b; Acikbas et al., 2017).

In this context, numerous academic studies have been conducted, leading to the development of various organic and inorganic sensors for the detection of hazardous volatile organic compounds in the atmosphere. The accuracy and reliability of the experimental data can be evaluated through theoretical calculations or machine learning approaches. Consequently, the comparison and discussion of experimental and theoretical results become possible, providing a more comprehensive understanding of sensor performance and detection mechanisms.

2. BASIC PRINCIPLES OF CHEMICAL SENSORS

In general, a sensor can be defined as a device that converts the magnitude or state of a physical or chemical property into measurable or observable electrical signals. Today, sensors are being developed for a wide range of applications, including improving human quality of life, preventing environmental pollution, protecting human health, and supporting scientific research. A sensor system typically consists of four main components, as illustrated in Figure 1 below.

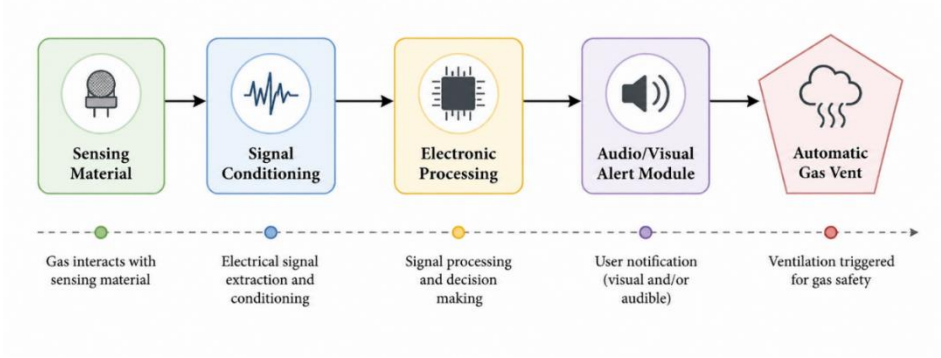

Figure 1. Circuit components of a sensor system.

In a sensor system, the sensing material (receptor) is the component where the sensing mechanism is initiated. The receptor comes into direct contact with the target analyte or surrounding environment. As a result of this interaction, the analyte molecules temporarily interact with the receptor molecules, inducing changes in their physicochemical properties. These changes are subsequently converted into measurable electrical signals by the signal conditioning (transducer) stage. The generated signals are then processed and analyzed by the electronic processing unit, where their magnitude is evaluated and interpreted. Based on the processed signal, the system can display the measurement results on a computer interface or activate an audio/visual alert module when the detected gas concentration exceeds a predefined threshold. In safety-critical applications, the processed signal may also trigger an automatic gas shut-off valve to prevent hazardous gas leakage. The sensing material employed as the receptor is typically composed of organic or inorganic sensitive materials deposited onto the sensor substrate using various coating or fabrication techniques.

3. DIFFUSION THEORY AND MATHEMATICAL FORMULATION FOR CHEMICAL SENSORS

Fick's laws constitute the fundamental principles governing mass transport by diffusion and describe the movement of substances within a medium driven by concentration gradients. Diffusion is a spontaneous transport process in which particles migrate from regions of higher concentration to regions of lower concentration as a result of their random thermal motion, leading to a net transfer of mass until concentration equilibrium is approached.

Fick's First Law describes diffusion under steady-state conditions, where the concentration profile remains constant over time. Under these conditions, the diffusion flux is directly proportional to the concentration gradient and is independent of time. Accordingly, the rate of mass transfer is determined solely by the spatial concentration gradient within the diffusion medium. The mathematical expression of Fick's First Law is given by:

$$J = -D\frac{\partial C(x,t)}{\partial x} \tag{1}$$

where J is the diffusion flux, D is the diffusion coefficient, C denotes the concentration, and x is the spatial coordinate in the direction of diffusion. The negative sign signifies that mass transport proceeds in the direction of decreasing concentration, indicating that diffusion occurs down the concentration gradient.

Although Fick's First Law provides an adequate description of diffusion under steady-state conditions, it cannot account for situations in which the concentration profile evolves with time. In practical diffusion problems, concentration is generally a function of both time and position, requiring a transient diffusion model. Under these circumstances, Fick's Second Law is used to describe the diffusion process by incorporating the principle of mass conservation into Fick's First Law.

According to Fick's Second Law (Crank, 1970), both the concentration of the diffusing species and the diffusion flux vary as functions of time and spatial position. Unlike Fick's First Law, which describes steady-state diffusion, Fick's Second Law provides a mathematical framework for analyzing transient diffusion processes in which the concentration distribution changes with both time and distance. The general form of Fick's Second Law is given in Equation (2).

$$\frac{dC(x,t)}{dt} = -\frac{dJ}{dx} \tag{2}$$

In Equation (2), $C(x,t)$ denotes the concentration of the diffusing species at position x and time t, while D represents the diffusion coefficient of the species within the sensing medium. In chemical sensor studies, diffusion is commonly assumed to occur in a one-dimensional planar sensing film of thickness d, where hazardous gas molecules penetrate from the surface of the sensing layer into its interior. This one-dimensional diffusion assumption simplifies the mathematical description while adequately representing the diffusion behavior of thin-film gas sensors.

Applying a second spatial differentiation to Equation (2), together with the appropriate boundary conditions, results in the governing diffusion equation for the sensing layer.

$$\frac{dJ}{dx} = -D\frac{d^2C(x,t)}{dx^2} \tag{3}$$

is obtained. By substituting the continuity equation into the above expression, Fick's Second Law is obtained in the form presented in Equation (4).

$$-\frac{dC(x,t)}{dt} = D\frac{d^2C(x,t)}{dx^2} \tag{4}$$

The transport of molecules within a sensing medium is governed by diffusion, a process initiated by concentration gradients and sustained through random molecular motion. Consequently, molecules migrate from regions of higher concentration to regions of lower concentration until a state of equilibrium is achieved. In gas sensing studies, the diffusion coefficient (D) is determined from the time-dependent response of organic- and inorganic-based sensing materials exposed to volatile organic compounds (VOCs). The experimental data are interpreted using the mathematical model described by Fick's Second Law of diffusion.

For the thin-film sensing layer, diffusion is assumed to be one-dimensional, occurring only along the x-axis. Accordingly, the spatial domain is defined as $0 < x < d$, where d represents the thickness of the sensing film. This assumption significantly simplifies the mathematical formulation while accurately describing the diffusion process in thin-film chemical sensors.

The diffusion behavior in non-steady-state systems is described by Fick's Second Law. This law explains how the concentration profile evolves over time as a consequence of spatial concentration gradients. Its mathematical formulation is presented in Equation (5).

$$\frac{C(x,t)}{C_o} = \frac{x}{d} + \frac{2}{\pi}\sum_{n=1}^{\infty}\frac{1}{n}sin\left(\frac{n\pi x}{d}\right)e^{-Dn^2\pi^2t/d^2} \tag{5}$$

Here, C_o and C denote the concentrations of the diffusing species at the initial time ($t = 0$) and at time t, respectively. The parameter d represents the initial thickness of the sensing layer, while D is the diffusion coefficient of the diffusing species within the sensing medium. Since the concentration of the diffusing species is directly proportional to its amount in the sensing layer, Equation (5)

can be reformulated in terms of the amount of the diffusing substance, yielding the expression presented in Equation (6).

$$\mathrm{M} = \int_{\mathrm{V}} \mathrm{C}\,\mathrm{dV} \tag{6}$$

Here, M represents the amount of the diffusing species, and V denotes the volume element within the diffusion medium. Substituting Equation (6) into Equation (5) and assuming a constant diffusion coefficient throughout the sensing layer yields the simplified diffusion equation (Erdogan et al., 2008) given in Equation (7).

$$\frac{M_t}{M_\infty} = 1 - \frac{8}{\pi^2}\sum_{n=0}^{\infty}\frac{1}{(2n+1)^2}\,e^{-\frac{(2n+1)^2\pi^2}{4d^2}Dt} \tag{7}$$

In this expression, M_t and M_∞ represent the cumulative amount of the diffusing species absorbed by the sensing layer at time t and at equilibrium ($t \rightarrow \infty$), respectively. The solution of the diffusion equation is governed by the initial and boundary conditions, which depend on the geometry of the diffusion domain. For the case of one-dimensional diffusion in a planar layer, the early-time solution can be approximated by the expression (Erdogan et al., 2010) given in Equation (8).

$$\frac{M_t}{M_\infty} = 4\left(\frac{Dt}{\pi d^2}\right)^{1/2} \tag{8}$$

This simplified expression is commonly referred to as the early-time approximation of Fick's diffusion equation.

4. MACHINE LEARNING AND ITS MAIN TYPES

The volume of data generated worldwide has been increasing continuously. Ubiquitous electronic devices record our choices, decisions, and financial activities. As the amount of available data continues to grow, the proportion of individuals capable of effectively understanding and interpreting these data decreases. The increasing complexity of the modern world further intensifies the challenges associated with analyzing the vast amount of generated data. Consequently, data mining has emerged as an essential approach for uncovering hidden patterns and meaningful relationships within large datasets. Data mining focuses on solving problems by analyzing data stored in databases. Machine

Learning (ML) is a field that combines artificial intelligence and statistical techniques to extract valuable knowledge from large datasets. This knowledge is used to develop predictive models by training computational systems using machine learning algorithms.

Machine learning is a scientific discipline that investigates the design and development of algorithms enabling computers to learn by extracting meaningful information from sensor data. Through these algorithms, intelligent systems are capable of systematically recognizing complex events and objects and making rational, data-driven decisions. According to Arthur Samuel, who introduced one of the earliest machine learning algorithms for the game of checkers, machine learning is "the field of study that gives computers the ability to learn without being explicitly programmed." Data mining learning paradigms have largely evolved from machine learning paradigms, which can be described by three fundamental components: knowledge representation, predictive models, and learning mechanisms. Machine learning originated as a subfield of Artificial Intelligence (AI). While AI is concerned with developing intelligent machines capable of solving problems and reasoning in a human-like manner, machine learning focuses on designing algorithms and computer systems that enable machines to learn from previous experience. Since intelligence cannot be achieved without the ability to learn, machine learning plays a central role in the advancement of artificial intelligence. Based on their functional characteristics, machine learning techniques are generally categorized into three main groups: clustering, association analysis, and classification.

Clustering Analysis

Clustering is one of the most powerful techniques in data mining, aiming to discover and analyze the underlying patterns within a dataset by grouping data points according to their similarities. The fundamental principle of clustering is that data points belonging to the same cluster exhibit high similarity, whereas those assigned to different clusters are expected to be dissimilar Clustering methods consist of four categories: hierarchical methods, partitioning methods, grid-based algorithms, and genetic algorithms.

Classification Techniques

Classification is a supervised machine learning technique that aims to construct a predictive model capable of identifying and distinguishing predefined data classes or concepts. The resulting model is subsequently used to predict the class labels of previously unseen data instances. Model development is based on the analysis of labeled training data, in which the class membership of each data

instance is known. The classification process generally involves defining class categories, identifying discriminative patterns or decision rules, training the model using labeled examples, and assigning new observations to the most appropriate predefined class based on the learned knowledge. As the volume and complexity of datasets continue to increase, the application of machine learning algorithms for learning classification rules and accurately categorizing new data has become both increasingly effective and essential.

Artificial Neural Networks

Artificial Neural Networks (ANNs) are adaptive computational models capable of learning complex input–output relationships directly from data. Inspired by the parallel processing mechanism of the human brain, these models identify hidden patterns by iteratively adjusting the connection weights between interconnected artificial neurons. Unlike conventional analytical approaches, ANNs do not require explicit mathematical descriptions of the underlying system, making them particularly effective for modeling nonlinear processes. Their architecture typically comprises an input layer, one or more hidden layers, and an output layer, where information is processed through distributed computation to produce the final prediction or classification.

5. APPLICATIONS OF MACHINE LEARNING IN CHEMICAL SENSORS

Cıhan et al., (2021) proposed a machine learning–based approach to develop an accurate model for the early prediction of diabetes. In their study, seven classification algorithms were employed, namely Decision Tree (DT), K-Nearest Neighbors (KNN), Support Vector Machine (SVM), Gaussian Naïve Bayes (GNB), Logistic Regression (LR), Artificial Neural Network (ANN) and Random Forest (RF). The predictive performance of these models was assessed using precision, sensitivity, Precision–Recall Curve (PRC), and Receiver Operating Characteristic (ROC) metrics. The experimental results demonstrated that the Logistic Regression model outperformed the other classification algorithms in accurately predicting diabetes.

In a study conducted by Gültepe (2019), various machine learning algorithms were employed to predict air pollution levels in Kastamonu Province using selected meteorological variables. Since machine learning techniques have recently demonstrated promising performance in meteorological and environmental applications, several predictive models were developed based on the Min–Max normalization technique. The evaluated algorithms included Artificial Neural Networks (ANN), Random Forest (RF), K-Nearest Neighbors

(KNN), Logistic Regression (LR), Decision Tree (DT), Linear Regression, and Naïve Bayes (NB). The ANN model achieved a prediction accuracy of 87%, whereas the Random Forest and Decision Tree models yielded the highest accuracy, reaching 99%. In contrast, the Linear Regression model exhibited the weakest performance, with an accuracy of only 30%.

Chauhan and Urooj (2019) proposed an intelligent Metal Oxide Gas Sensor (MOX) model for gas detection applications aimed at preventing industrial accidents. Although MOX sensors exhibit high sensitivity, their performance is often affected by challenges such as environmental interference and limited selectivity. To address these limitations, the authors incorporated an Artificial Neural Network (ANN)–based approach to improve sensor performance. The effectiveness of the proposed model was validated using the MATLAB environment, demonstrating the feasibility of ANN-assisted gas detection systems.

Lamamra and Rechem (2016) developed an Artificial Neural Network (ANN) model for the Metal Oxide Gas Sensor TGS 2610. The TGS 2610 is a thin-film semiconductor gas sensor characterized by high sensitivity to liquefied petroleum gas (LPG), low power consumption, and long operational lifetime. The proposed ANN model was employed to characterize the sensor response to LPG. Comparative analysis between the experimental measurements and ANN predictions demonstrated a high degree of agreement, confirming that the proposed ANN model provides an effective and reliable approach for modeling the LPG sensing characteristics of the TGS 2610 sensor.

Topalović et al. (2019) investigated whether the data generated by individual sensor systems could be calibrated using their own measurements to achieve substantially higher data quality relative to reference instruments. To this end, they performed a comprehensive comparative analysis of univariate Linear Regression, Multivariate Linear Regression, and Artificial Neural Networks (ANNs) for the calibration of low-cost CO and O_3 sensors deployed under field conditions. In addition, three widely used ANN training algorithms were evaluated to determine their effectiveness in improving sensor calibration performance.

Roj (2016) investigated two approaches for implementing dynamic error correction in a gas concentration measurement transducer. The first approach was based on a parametric model describing the transducer's dynamic behavior, whereas the second employed an Artificial Neural Network (ANN). The study examined the dynamic characteristics of gas concentration measurements and led to the development of both a parametric dynamic model and an effective correction algorithm. The results demonstrated that both approaches significantly

reduced the response time of the transducer, thereby improving the dynamic performance of the gas measurement system.

Bahri et al., (2021) investigated the application of graphene-based gas sensors, with particular emphasis on the influence of operating temperature on sensor performance. In their study, a machine learning model was trained using synthetic data generated by a sensor simulation framework. The proposed approach provided valuable insights into the effects of different operating temperatures and training data selection on the predictive performance of machine learning algorithms. Furthermore, the study offered practical guidelines for selecting representative training datasets to improve the robustness and generalization capability of prediction models.

Cruz et al., (2022) employed machine learning techniques to discriminate nitrogen dioxide (NO_2) from other gaseous species by analyzing the mass-loading and elastic response characteristics of CBNm-based sensors. Owing to its compact size, low cost, and satisfactory analytical performance, the proposed sensing system was identified as a promising platform for the on-site detection of NO_2 at sub-ppm concentration levels.

Acikbas et al., (2020) investigated the sensing performance of a deca-pyridine-2-amine functionalized Pillar[5]arene (P5-PA)-based gas sensor toward several hazardous volatile organic vapors. Diffusion coefficients were determined from the experimental gas sensing data using Fick's law of diffusion. To model the sensor response, two deep learning architectures, Nonlinear Autoregressive Neural Network (NARNET) and Long Short-Term Memory (LSTM), were employed due to their effectiveness in handling relatively small datasets. Approximately 83% of the experimental data were used for model training, while the remaining 17% served as the test set for evaluating predictive performance. The predicted responses were subsequently compared with the corresponding experimental measurements. The developed deep learning models achieved correlation coefficients exceeding 0.98 for all investigated vapors, demonstrating excellent predictive capability and strong agreement with the experimental results. Similar studies were studies reported in the literature have demonstrated the successful application of artificial neural network (ANN) models to a wide range of chemical sensing problems, including gas identification, concentration estimation, sensor calibration, response prediction, and diffusion modeling. These studies consistently highlight the capability of ANNs to improve prediction accuracy and effectively capture the nonlinear behavior of sensor responses (Buyukkabasakal et al. (2019); Deniz et al., (2022); Çelik Acikbas et al., (2026)).

Yan et al., (2022) reported an identification accuracy of approximately 90% for mixed ammonia and amine gases at room temperature. Their study demonstrated that integrating molecular design with machine learning techniques significantly enhances the selectivity of sensor arrays. This integrated approach provides a promising strategy for the development of rapid, practical, non-invasive, and cost-effective sensor systems for breath analysis and exhaled gas diagnostics.

To improve the identification of complex gas mixtures, Javed et al., (2022) combined electrochemical sensing with machine learning techniques. Their sensing system consisted of four electrochemical sensors based on metal oxide electrodes and a yttria-stabilized zirconia electrolyte, which produced characteristic voltage signals for different gas compositions. Instead of directly estimating gas concentrations, the proposed methodology first determined the types of gases present through multiclass classification and subsequently quantified the concentration of each identified component. Experimental validation using mixtures containing NO, NO_2, C_3H_8, and NH_3 demonstrated that the framework could accurately characterize both the composition and concentration of mixed gases from a single measurement. Owing to its flexible architecture, the proposed approach can be extended to incorporate additional gases, making it a promising solution for industrial safety, automotive emission control, and environmental monitoring.

To address the problem of mixed-gas quantification, Kanaparthi and Singh (2022) developed an energy-efficient computational strategy based on linear gas sensors. The sensing platform consisted of two ZnS resistive sensors biased at different operating voltages, and the concentrations of NH_3 and CO were determined by exploiting the superposition principle. Recognizing the influence of ambient humidity on sensor performance, the authors incorporated relative humidity into the sensitivity model to compensate for environmental variations. Validation experiments showed that the algorithm maintained a maximum absolute concentration error of nearly 15% over a range of humidity conditions, demonstrating satisfactory performance for practical applications. The combination of low computational demand and reduced power consumption makes this approach particularly attractive for portable gas sensing systems and continuous environmental monitoring.

6. CONCLUSIONS

This chapter has presented a comprehensive overview of the fundamental principles underlying chemical sensing, diffusion theory, and the application of machine learning techniques to chemical sensor systems. The basic architecture

and operating mechanism of chemical sensors were introduced, emphasizing the roles of sensing materials, signal transduction, and electronic processing in converting physicochemical interactions into measurable electrical signals. In addition, the mathematical framework of molecular diffusion based on Fick's First and Second Laws was discussed, highlighting the importance of diffusion modeling for describing mass transport within thin-film sensing materials and for estimating diffusion coefficients from experimental sensor responses.

The chapter also reviewed the fundamental concepts of machine learning and summarized the principal learning paradigms commonly employed in sensor data analysis. Furthermore, recent advances in machine learning applications for chemical sensors were examined, demonstrating that algorithms such as artificial neural networks, deep learning models, support vector machines, random forests, and other classification techniques have significantly improved gas identification, sensor calibration, concentration estimation, and predictive modeling. These approaches effectively compensate for sensor nonlinearity, environmental interference, and cross-sensitivity while enhancing overall sensing performance.

Overall, the integration of advanced sensing materials, diffusion-based mathematical modeling, and machine learning algorithms provides a powerful framework for the development of intelligent chemical sensor systems. As computational methods, sensing technologies, and artificial intelligence continue to evolve, machine learning-assisted chemical sensors are expected to play an increasingly important role in environmental monitoring, industrial process control, healthcare diagnostics, food quality assessment, and public safety. Future research should focus on improving model generalization, explainability, real-time implementation, and the fusion of multimodal sensing data to enable more accurate, robust, and autonomous sensing platforms.

References

Acikbas, Y., Cankaya, N., Capan, R., Erdogan, M., Soykan, C. (2016a). Swelling behavior of the 2-(4-methoxyphenylamino)-2-oxoethyl methacrylate monomer LB thin film exposed to various organic vapors by quartz crystal microbalance technique. *J. Macromol. Sci. Part A*. 53(1), 18-25.

Acikbas, Y., Dogan, G., Erdoğan, M., Çapan, R., Soykan, C. (2016b). Organic vapor sensing properties of copolymer Langmuir-Blodgett thin film sensors, *J. Macromol. Sci. Part A,* 53(8), 470–474.

Acikbas, Y., Bozkurt, S., Halay, E., Capan, R., Guloglu, M.L., Sirit, A., Erdogan, M. (2017). Fabrication and characterization of calix[4]arene LangmuireBlodgett thin film for gas sensing applications, *J. Inc. Phenom. Macrocycl. Chem.* 89, 77-84.

Acikbas, Y., Kursunlu, A. N., Ozmen, M., Capan, R., Erdogan, M., Kucukyildiz, G. (2020). An Aminopyridine Bearing Pillar[5]arene-Based QCM Sensor for Chemical Sensing Applications: Design, Experimental Characterization, Data Modeling, and Prediction, *IEEE Sens. J*., 20 (24), 14732-14739.

Bahri, Y., Schober, S. A., Carbonelli, C., Wille, R. (2021). Temperature Stability Investigations of Neural Network Models for Graphene-Based Gas Sensor Devices", *Eng. Proc.,* 10(1), 19.

Buyukkabasakal, K., Acikbas, S. C., Deniz, A., Acikbas, Y., Capan, R., Erdogan, M. (2019). Chemical Sensor Properties and Mathematical Modeling of Graphene Oxide Langmuir-Blodgett Thin Films. *IEEE Sens. J.,* 19(20), 9097–9104.

Celik Acikbas, S., Buyukkabasakal, K., & Deniz, A. (2026). Data-driven modelling of host–guest interactions and diffusion-induced swelling in pillar[5]arene-based chemosensors. *J. Incl. Phenom. Macrocycl*. https://doi.org/10.1007/s10847-026-01352-1.

Chauhan, N., Urooj (SMIEEE), S. (2019). Model of Smart Gas Sensor with the Application of Neural Network for the detection of Gases in Active Environment*. 2019 International Conference on Computing, Power and Communication Technologies (GUCON) Galgotias University*, Greater *Noida, UP, India. Sep 27-28.*

Cıhan P. *an*d Coşkun H. Performance Comparison of Machine Learning Models for Diabetes Prediction. *2021 29th Signal Processing and Communications Applications Conference (SIU)*, Istanbul, Turkey (2021), 1-4.

Crank. J. (1970). The Mathematics of Diffusion (Second). *Oxford University Press*.

Cruz, C., Matatagui, D., Ramírez, C., Ramirez, I. B., O-Cuevas, E. de la, Saniger, J. M., Horrillo, M. C. (2022). Carbon SH-SAW-Based Electronic Nose to Discriminate and Classify Sub-ppm NO_2, *Sensors*, 22, 1261.

Deniz, A., Celik Acikbas, S., Buyukkabasakal, K., Acikbas, Y., Erdogan, M., & Capan, R. (2022). Mathematical modelling and gas sensing abilities of graphene based optical sensor. *J. Optoelectron. Adv. Mater.*, 24(5–6), 193–200.

Dıker, A., Avci, E., Cömert, Z., Avci, D., Kaçar, E. and Serhatlioğlu, İ. Classification of ECG signal by using machine learning methods. *2018 26th Signal Processing and Communications Applications Conference (SIU)*, Izmir, Turkey (2018), 1-4.

Erdoğan, M., Çapan, İ., Tarimci, Ç., Hassan, A.K. (2008). Modeling of vapor sorption in polymeric film studied by surface plasmon resonance spectroscopy. *J. Colloid Interface Sci*. 323, 235–241.

Erdoğan, M., Çapan, R., Davis, F. (2010). Swelling behaviour of calixarene film exposed to various organic vapours by surface plasmon resonance technique. *Sens. Actuators B Chem.* 145, 66–70.

Gültepe, Y. (2019). Makine Öğrenmesi Algoritmaları ile Hava Kirliliği Tahmini Üzerine Karşılaştırmalı Bir Değerlendirme, *Avrupa Bilim ve Teknoloji Dergisi*, 16, 8-15.

Halay, E., Bozkurt, S., Capan, R., Erdogan, M., Unal, R., Acikbas, Y. (2020). Calix[4]arene-triazine conjugate intermediate: optical properties and gas sensing responses against aromatic hydrocarbons in Langmuir–Blodgett films. *Res. Chem. Intermed*. 46, 4433–4445.

Hsieh, H.C., Su, Y.C., Chen, S.P., Chu, C.H., Tseng, M.H., Lee, K.C., Tseng, P.S., Hsu, P.H., Chang, C.C., Wang, C.H., Wang, J.L. (2026). Comparative Online–offline measurement of airborne toxic VOCs for health risk and source identification in an environmental justice community. *Atmos. Environ.* 372, 121895.

Javed, U., Ramaiyan, K.P., Kreller, C.R., Brosha, E.L., Mukundan, R., Sengupta, A.M., Morozov, A.V. (2022). Quantification of gas concentrations in NO/NO2/C3H8/NH3 mixtures using machine learning, *Sens. Actuators B Chem.*, 359, 131589.

Kanaparthi, S., Singh, S.G. (2022). Simultaneous Detection of CO and NH_3 Gases at Room Temperature with an Array of ZnS Chemiresistive Sensors and the Superposition Principle, *Anal. Chem.*, 4, 11, 4602–4609.

Lamamra, K., Rechem, D. (2016). Artificial neural network modelling of a gas sensor for liquefied petroleum gas detection. *8th International Conference on Modelling, Identification and Control (ICMIC-2016) Algiers*, Algeria-Nov. 15-17.

Paul, S., Bari, M.A. (2022). Elucidating sources of VOCs in the Capital Region of New York State: Implications to secondary transformation and public health exposure. *Chemosphere.* 299, 134407.

Roj, Je. (2016). Correction of Dynamic Errors of a Gas Sensor Based on a Parametric Method and a Neural Network Technique. *Sensors*, 16, 1267.

Topalovićb, D. B., Davidovića, M. D., Jovanovića, M., Bartonovac, A., Ristovskid, Z. Jovašević-Stojanovića, M. (2019). In search of an optimal in-field calibration method of low-cost gas sensors for ambient air pollutants: Comparison of linear, multilinear and artificialneural network approaches. *Atmos. Environ.* 213, 640-658.

Yan, M.Z., Chen, J. M., Wang, B., Xu, W., Cao, H. M., Fu, Y. Y., He, Q. G., Cheng, J. G. (2022). High-sensitivity sensor array base on molecular design and machine learning for amine differentiation in exhaled vapor, *Chin. J. Anal. Chem.,* 50 (3), 100059.

5. Bölüm

Esnek Elektrotların Süperkapasitör Uygulamaları

Aysel AYDIN KOCAEREN[1], Petek TUNÇ[2]

Süperkapasitörler, yüksek güç yoğunluğu, hızlı şarj-deşarj kabiliyeti ve uzun çevrim ömrü ile öne çıkan enerji depolama cihazlarıdır. Bataryalara kıyasla daha kısa sürede enerji sağlayabilmeleri sayesinde, özellikle elektrikli araçlar, taşınabilir elektronikler ve yenilenebilir enerji sistemleri gibi yüksek güç gerektiren uygulamalarda yaygın olarak tercih edilmektedir (Simon & Gogotsi, 2008; Conway, 1999). Bu üstün özellikler, süperkapasitörleri klasik batarya sistemleri ile karşılaştırıldığında daha verimli ve güvenli hale getirmektedir (Özada, Ünal, & Yazıcı, 2023). Süperkapasitörlerin performansı, elektrot malzemesinin yüksek yüzey alanı, iletkenlik, gözenek yapısı ve kimyasal stabilitesi gibi özelliklerine bağlıdır (Zhai vd., 2011; Wang vd., 2012). Bu nedenle, nanoyapılı, iletken polimerli ve hibrit sistemler gibi yenilikçi elektrotlar geliştirmek büyük önem taşımaktadır (Zhang & Zhao, 2009). Süperkapasitörler, yüksek enerji yoğunluğu, hızlı şarj-deşarj süreçleri ve uzun ömürlü kullanım gibi üstün özellikleriyle enerji depolama sistemleri arasında önemli bir yer tutmaktadır (Simon & Gogotsi, 2008). Bununla birlikte, mevcut süperkapasitörler genellikle düşük enerji yoğunluğu ve yüksek maliyet gibi sınırlamalara sahiptir. Bu bağlamda, iletken polimerler ve metal oksitlerin kompozit elektrotlar olarak kullanımı, enerji depolama performansını artırma potansiyeli taşımaktadır (Xi vd., 2025). Polipirol (PPy) ve Polianilin (PANI) gibi iletken polimerler, yüksek elektriksel iletkenlikleri ve kimyasal stabiliteleri nedeniyle süperkapasitörlerde yaygın olarak kullanılmaktadır (Wang vd., 2019; Shimoga vd., 2021). Bununla birlikte, bu polimerlerin tek başlarına kullanıldığında sınırlı kapasitans değerleri ve düşük döngü stabilitesi gibi dezavantajları bulunmaktadır. Metal oksitlerin, özellikle MnO_2'in, enerji depolama performansını iyileştirdiği ve polimerlerle olan sinerjik etkileri nedeniyle bu tür kompozit materyaller daha fazla dikkat çekmektedir (Dülger, 2023).

[1] Doç. Dr, Çanakkale Onsekiz Mart Üniversitesi, Eğitim Fakültesi, Matematik ve Fen Bilimleri Eğitimi Bölümü, Kimya Eğitimi ABD, aysel.kocaeren@comu.edu.tr, ORCID No: 0000-0003-4113-0517.

[2] petektunc973@gmail.com, ORCID No: 0009-0006-3232-9718.

Not: Bu çalışma, "Polipirol Destekli Esnek Elektrotların Süperkapasitör Uygulamaları İçin Tasarımı ve Kapasitif Davranışlarının Elektrokimyasal Yöntemlerle İncelenmesi" başlıklı COMU-BAP FYL-2025-5259 kodlu yüksek lisans tez projesi kapsamında üretilmiştir.

Süperkapasitörler, yüksek güç yoğunluğu, hızlı şarj-deşarj kabiliyeti ve uzun çevrim ömürleri sayesinde günümüzde enerji depolama sistemlerinde önemli bir yere sahiptir. Bu tür kapasitörler, geleneksel kapasitörlerle karşılaştırıldığında daha fazla enerji depolayabilirken pillerden farklı olarak enerjiyi çok kısa sürede sağlayabilirler (Zhang, Gu & Chen, 2023). Enerji depolama mekanizmaları temelde ikiye ayrılır: *i)* elektrostatik yük birikimine dayalı çift tabaka kapasitansı (EDLC) ve *ii)* yüzeyde gerçekleşen hızlı redoks reaksiyonlarına dayalı psödokapasitans (Sharma & Chand, 2023). EDLC'lerde genellikle aktif karbon malzemeler kullanılırken psödokapasitif özellik gösteren süperkapasitörlerde metal oksitler (örneğin MnO_2) ve iletken polimerler (örneğin polipirol) tercih edilmektedir. Bu tür hibrit yapılar, yüksek özgül kapasitans ve daha iyi çevrim stabilitesi sunmaktadır (Low vd., 2019; Chhetri vd., 2020).

Esnek Elektrotlar

Esnek elektrotlar, geleneksel katı elektrotlara göre daha hafif, ince ve esnek olup giyilebilir elektronik ve katlanabilir enerji depolama sistemleri gibi uygulamalar için tercih edilebilir. Bu tür elektrotlar, genellikle polimerler, grafen, karbon nanotüpler (CNT) ve metal oksitler gibi malzemelerle üretilirler. Esnek yapıları, bu elektrotlara yüksek mekanik dayanıklılık, uzun ömürlü performans, yüksek iletkenlik ve yük taşıma kapasitesi kazandırmaktadır (G.S. dos Reis vd., 2021).

İletken Polimerler

İletken polimerler, elektriksel iletkenlik gösterebilen, organik malzemelerdir. Bu polimerler, genellikle metalik bağlar içeren yapılarla, elektronların serbestçe hareket etmesini sağlar. Polipirol (PPy), polianilin (PANI) ve politiyofen (PTh) gibi iletken polimerler, süperkapasitörler ve diğer enerji depolama cihazları gibi birçok uygulamalarda kullanılmaktadır. İletken polimerlerin avantajları arasında esneklikleri, düşük maliyetleri ve kolay işlenebilir olmaları bulunur. Bu polimerler, enerji depolama sistemlerinde yüksek kapasitans değerleri ve iyi döngü stabiliteleri sunarak geleneksel süperkapasitör malzemelerine kıyasla önemli bir performans artışı sağlayabilir. Bununla birlikte, saf iletken polimerlerin sınırlı iletkenlik ve düşük yüzey alanı gibi bazı dezavantajları vardır. Bu nedenle sıklıkla karbon nanotüpler, grafen ve metal oksitler gibi materyallerle kombinasyon halinde kullanılırlar (Namsheer & Rout, 2021; Bezgin Çarbaş, 2016).

Metal Oksitler

Metal oksitler, süperkapasitörler ve diğer enerji depolama cihazlarında yer alan önemli bileşenlerdir. MnO_2, RuO_2, Co_3O_4 gibi metal oksitler, yüksek kapasitans değerleri ve iyi elektrokimyasal özellikleri ile tanınır. Bu oksitler, özellikle iletken polimerlerle veya karbon tabanlı materyallerle kombin edildiğinde, elektriksel iletkenlikleri ve enerji depolama kapasiteleri daha da iyileşir. Metal oksitlerin, polimerler ile sinerjik etkileri, yüksek yüzey alanı ve elektrokimyasal stabilite sağlarken döngüsel kararlılığı artırır ve enerji depolama cihazlarının performansını güçlendirir (An vd., 2019).

Membran

Membran, genellikle bir yüzeyi ayıran, ince, yarı geçirgen bir yapıdır. Elektriksel iletkenlik, iyon iletkenliği, mekanik dayanıklılık gibi özelliklere sahip olan membranlar, enerji depolama sistemlerinde önemli bir rol oynar. Membranlar, genellikle elektrotlar arasındaki iyon akışını kontrol eder ve enerji depolama kapasitesini optimize eder. Bu yapılar, elektrolit ile etkileşime girerek enerji verimliliğini artırır. Süperkapasitörlerde kullanılan membranlar, genellikle yüksek iyon iletkenliği, düşük iç direnç, kimyasal kararlılık ve uzun döngü ömrü gibi özelliklere sahip olmalıdır.

Membran Türleri:

1. Polimerik Membranlar: Polimerik membranlar, süperkapasitörlerde yaygın olarak kullanılmaktadır. Bu membranlar, yüksek mekanik dayanıklılık ve esneklik sağlar, aynı zamanda iyon iletkenliğini optimize eder. Yaygın polimerler arasında polipropilen (PP), polietilen (PE), poliviniliden florür (PVDF) ve poliamid gibi malzemeler yer almaktadır. Polimerik membranlar, kolay üretilebilir ve düşük maliyetli olma avantajına sahiptir. Ayrıca, elektrokimyasal cihazların uzun ömürlü ve güvenilir olmasını sağlar (Szubzda vd., 2014).

2. Seramik Membranlar: Seramik membranlar, yüksek sıcaklık stabilitesine sahip olup, genellikle yüksek performanslı uygulamalar için tercih edilmektedir. Bu membranlar, dayanıklı ve kimyasal olarak inerttir, bu nedenle aşındırıcı ortamlarda bile kullanılabilirler. Yüksek iyon iletkenliği sağlayarak süperkapasitörlerin performansını artırabilirler. Ancak, seramik membranların daha kırılgan ve pahalı olması, kullanım alanlarını sınırlayabilir (Zhang vd., 2018).

3. Biyolojik Membranlar: Son yıllarda, biyolojik membranlar, özellikle çevre dostu ve sürdürülebilir enerji depolama çözümleri için araştırılmaktadır. Bu tür membranlar, doğadan türetilen malzemelerden (örneğin, selüloz, jelatin, kitosan) yapılır. Biyolojik membranlar, polimerik membranlara benzer şekilde işlev görse

de genellikle daha düşük maliyetli ve biyolojik olarak ayrışabilir olmaları nedeniyle çevre dostu bir seçenek sunmaktadır. Bununla birlikte, biyolojik membranların mekanik dayanıklılığı ve elektrokimyasal özellikleri hala geliştirilme aşamasındadır (Penchev vd., 2025).

4. İyonik Sıvı Membranlar: İyonik sıvılar, düşük buharlaşma noktası ve yüksek iyon iletkenliği gibi avantajlar sunan sıvı malzemelerdir. İyonik sıvıların kullanıldığı membranlar, elektrokimyasal kapasiteyi artırabilir ve daha geniş sıcaklık aralıklarında çalışabilir. Ancak, bu tür membranların kullanımı genellikle daha karmaşık ve maliyetli olabilir (Jamil & Debbie, 2022).

5. Kompozit Membranlar: Kompozit membranlar, farklı malzemelerin bir araya getirilerek üretildiği yapılar olup genellikle daha üstün özellikler sunmaktadır. Örneğin, karbon nanotüpler (CNT), grafen, metal oksitler veya polimerlerin birleştirilmesiyle üretilen kompozit membranlar, yüksek iletkenlik ve mekanik dayanıklılığı bir arada sağlar. Bu tür membranlar, enerji depolama sistemlerinin verimliliğini önemli ölçüde artırabilir ve çevresel etkiyi azaltabilir (Akın vd., 2023).

Esnek Membran Elektrotlar

Esnek membran elektrotlar, geleneksel katı elektrotlara kıyasla daha hafif, ince ve bükülebilir yapıları ile enerji depolama cihazlarında önemli bir gelişme sunmaktadır. Bu tür elektrotlar, özellikle giyilebilir elektronik cihazlar, katlanabilir enerji depolama sistemleri, taşıması kolay enerji çözümleri ve mobil cihazlar gibi uygulamalar için uygundur. Esnek membran elektrotlar, elektriksel iletkenlik, kimyasal kararlılık ve mekanik dayanıklılık gibi özelliklere sahiptir, bu nedenle modern enerji depolama sistemlerinde sıklıkla tercih edilmektedir (Zhang vd., 2016; Topçu, 2020).

Esnek membran elektrotlar genellikle üç ana bileşenden oluşur, bunlar; aktif malzeme, destek katmanı ve koruyucu katmandandır.

Kullanılan Malzemeler

• *Polimerler*: Polipirol (PPy), polianilin (PANI) gibi iletken polimerler, esnek membran elektrotların en yaygın malzemeleridir. Bu polimerler, yüksek elektriksel iletkenlikleri ve kolay işlenebilirlikleri ile öne çıkar. Ayrıca, polimerlerin esnek yapıları, elektrotlara mekanik dayanıklılık ve uzun ömür kazandırmaktadır.

• *Grafen ve Karbon Nanotüpler:* Grafen ve karbon nanotüpler (CNT), esnek membran elektrotlar için mükemmel iletkenlik ve dayanıklılık sağlayan malzemelerdir. Bu malzemeler, elektrotların elektriksel performansını artırırken aynı zamanda esnekliğini korumaktadır.

• *Metal Oksitler:* MnO_2, RuO_2 gibi metal oksitler, yüksek enerji yoğunluğu ve kimyasal stabilite sunmaktadır. Metal oksitlerin polimerlerle kombine edilmesi, elektrotların performansını daha da artırabilir (Dülger, 2023).

Avantajlar

• Esneklik ve Bükülme Yeteneği: Esnek membran elektrotlar, katlanabilir ve bükülebilir yapıları sayesinde giyilebilir cihazlar veya portatif enerji depolama sistemleri için idealdir.

• Hafiflik: Bu elektrotlar, geleneksel elektrotlara göre çok daha hafif olup, taşıma ve montaj kolaylığı sağlar.

• Yüksek Elektriksel İletkenlik: Esnek elektrotlar, yüksek iletkenlik sunarak hızlı şarj ve deşarj işlemlerine olanak tanır, bu da enerji depolama verimliliğini artırır.

• Uzun Ömürlü Performans: Esnek yapıları, elektrotların mekanik strese karşı dayanıklı olmasını sağlar. Bu, uzun vadeli kullanımda da yüksek performans sağlar (Hwang vd., 2024; Guan vd., 2021).

Uygulamaları

1. Giyilebilir Elektronikler: Esnek membran elektrotlar, giyilebilir enerji depolama cihazlarında kullanılabilir. Bu tür cihazlar, enerji ihtiyacı olan kişisel cihazlar için verimli enerji depolama çözümleri sunmaktadır (Zhang vd., 2023)

2. Katlanabilir ve Taşınabilir Enerji Depolama Sistemleri: Katlanabilir cihazlar ve taşınabilir enerji depolama çözümleri, esnek elektrotlar sayesinde daha kompakt hale gelir. Bu sistemler, özellikle mobil cihazlar ve robotik uygulamalar için uygundur (Gashaw Hone, Tegegne, & Andoshe, 2021).

Sonuç olarak, esnek membran elektrotlar, modern enerji depolama teknolojilerinde devrim niteliğindedir. Bu tür elektrotlar, daha hafif, esnek, dayanıklı ve yüksek performanslı enerji çözümleri sunarak gelecekteki enerji depolama cihazlarının verimliliğini artırmaktadır.

Süperkapasitör elektrotlar, iletken polimerler ve metal oksitler, yüksek özgül kapasiteleri ve iyi elektrokimyasal performansları sayesinde literatürde oldukça ilgi görmektedir. Bu alanda yapılan birçok çalışma, bu malzemelerin enerji depolama kapasitesini artırmada yenilikçi ve etkili çözümler sunduğunu göstermektedir.

Ma ve arkadaşlarının yaptığı bir çalışmada (2013), PPy/SA nanosferleri sentezlenmiştir. Bu malzeme, 347 $F \cdot g^{-1}$ yüksek bir özgül kapasite göstermiş ve 500 şarj-deşarj döngüsü boyunca iyi elektrokimyasal stabilite sergilemiş ve süperkapasitör uygulamaları için umut verici bulunmuştur (Ma vd., 2013). Fan'ın çalışmasında (2006), yüksek aktif polipirrol elektrotlar, titanyum folyo üzerine

elektrodepozisyon yöntemiyle hazırlanmış ve 1 M KCl çözeltisinde karakterize edilmiştir (Fan vd., 2006). Polipirrolün yüksek gözenekli yapısı, yaklaşık 480 ± 50 F/g gibi yüksek bir özgül kapasite sağlamış, elektrot ise döngü ömrü testlerinde yüksek stabilite göstermiştir. Yan'ın yaptığı başta bir çalışmada (2009), GNS/CNT/PANI kompoziti, PANI'nin katkısıyla yüksek performans göstermiştir (Yan vd., 2009). 6 M KOH çözeltisinde 1035 F/g özgül kapasiteye ulaşırken, saf PANI ve CNT/PANI kompozitlerine göre döngüsel stabiliteyi de iyileştirmiştir. 1000 döngü sonunda kapasite yalnızca %6 azalırken, GNS/PANI ve CNT/PANI kompozitlerinde bu oran sırasıyla %52 ve %67'dir. PANI'nin eklenmesi, iletkenlik ve mekanik gücü artırarak stabiliteyi iyileştirmiştir. Maheswari ve arkadaşının yaptığı çalışmada (2018), CeO_2/PANI nanoyapısı, saf CeO_2'ye kıyasla özgül kapasitansı 1452 F/g'a çıkararak (2 A/g) önemli iyileşme sağlamıştır (Maheswari vd., 2018). Ayrıca, yüksek akımda iyi çevrim kararlılığı ve 75 Wh/kg enerji yoğunluğu sunarak süperkapasitör elektrotu olarak yüksek performans göstermiştir. Altın (2020) çalışmasında karbon nanolif elektrotlar farklı polimerlerle (PEDOT:PSS, PANI) ve grafen katkılarıyla modifiye edilerek süperkapasitör performansı iyileştirilmiştir (Altın vd., 2020). Polimer kaplamalar elektrodun iletkenliğini, özgül kapasitansını (%75'e kadar artış) ve döngüsel stabilitesini belirgin şekilde geliştirmiştir. Gözenekli yapı ve grafen katkılarıyla da yüzey alanı artırılarak toplamda 268 F/g'a kadar özgül kapasitans elde edilmiştir. Yang ve arkadaşlarının yaptığı çalışmada (2014), PEDOT:PSS'in çok katmanlı karbon nanotüplerle (MWCNT) oluşturduğu kompozitlerin süperkapasitör performansına katkısı incelenmiştir (Yang vd., 2014). %5 PEDOT:PSS içeren kompozit en yüksek özgül kapasitansı gösterirken, %50 PEDOT:PSS ise yüksek tarama hızlarında kararlı kapasitif davranış sergilemiştir. Genel olarak PEDOT:PSS, MWCNT elektrotların özgül kapasitansını ve yüksek hızlardaki performansını artırmıştır. Lee'nin yaptığı çalışmada (2017), esnek süperkapasitörler için PEDOT:PSS kaplı MWNT/MnO_2 kompozit elektrot geliştirilmiştir (Lee vd., 2017). Triton X-100, nanotüplerin çözeltide iyi dağılmasını sağlamış, PEDOT:PSS ise iletkenliği ve kararlılığı artırmıştır. MnO_2, yüksek teorik kapasitansı ile özgül kapasitansı yükseltmiştir. Sonuçta, 428.2 F/g kapasitans, 63.8 Wh/kg enerji yoğunluğu ve iyi çevrim ömrü elde edilmiştir. Bu yapı, esnek ve yüksek performanslı enerji depolama için güçlü bir adaydır. Jeong ve ekibi (2019), yarn süperkapasitörlerde yüksek kapasitans ve stabilite sağlamak için MnO_2, karbon nanotüplere (MWNT) yüksek kütle yüklemesiyle kaplanmıştır (Jeong vd., 2019). 60°C'de kaplanan MnO_2/CNTs-60, yüksek areal kapasitans (3.54 F/cm²) ve enerji yoğunluğu (93.8 µWh/cm²) ile üstün performans sergileyerek önceki örneklerden daha verimli olmuştur. Liu'nun yaptığı çalışmada pulse elektrodepozisyon yöntemiyle anilin, H_2SO_4 ve $MnSO_4$ sulu

çözeltisinde polianilin (PANI)/MnO_2 kompoziti sentezlenmiştir (Liu vd., 2025). PANI/MnO_2 kompoziti, saf PANI'ye kıyasla 0.5 A g^{-1} akım yoğunluğunda daha yüksek özgül kapasite (810 F g^{-1}) göstermektedir. Ayrıca, kompozit 1.000 döngü sonrası başlangıç kapasitesinin %86.3'ünü koruyarak mükemmel döngüsel stabiliteye sahiptir. Bu özellikler, PANI/MnO_2 kompozitinin süperkapasitör elektrodu olarak yüksek performans potansiyeline sahip olduğunu göstermektedir. Verilen çalışmalara bakıldığında PANI, PEDOT, PVDF ve MnO_2 gibi iletken polimerler ve metal oksitler, süperkapasitör elektrotlarının performansını önemli ölçüde iyileştiren malzemelerdir. PANI, yüksek özgül kapasite ve döngüsel stabilite sağlarken, PEDOT, karbon nanotüplerle birleştirildiğinde elektrotların kapasitesini ve hızdaki performansını artırmaktadır. MnO_2 ise yüksek teorik kapasitansı ve iyi çevrim kararlılığıyla süperkapasitörlerde enerji yoğunluğunu iyileştirmektedir. Bu malzemeler, süperkapasitörlerin kapasitesini, enerji yoğunluğunu ve döngüsel stabilitesini artırarak, daha verimli ve uzun ömürlü enerji depolama çözümleri sunmaktadır.

Teşekkür

Bu çalışma “Polipirol Destekli Esnek Elektrotların Süperkapasitör Uygulamaları İçin Tasarımı ve Kapasitif Davranışlarının Elektrokimyasal Yöntemlerle İncelenmesi” başlıklı COMU-BAP FYL-2025-5259 kodlu yüksek lisans tez projesi kapsamında desteklenmiş ve üretilmiştir. Desteği için ilgili birime teşekkür ederiz.

Kaynakça

Altın, Y. (2020). Grafen ve iletken polimerler (PEDOT:PSS, PANI) ile modifiye edilmiş karbon nanolif süperkapasitör elektrotların geliştirilmesi ve özelliklerinin incelenmesi (Doktora tezi, Bursa Teknik Üniversitesi, Fen Bilimleri Enstitüsü, Polimer Malzeme Mühendisliği Anabilim Dalı).

An, C., Zhang, Y., Guo, H., & Wang, Y. (2019). Metal oxide-based supercapacitors: Progress and prospectives. Nanoscale Advances, 1(10), 4644–4658. https://doi.org/10.1039/C9NA00543A

Bezgin Çarbaş, B. (2016). İletken Polimerler ve Enerji Uygulamaları. Küresel Mühendislik Çalışmaları Dergisi, 3(1), 46–60. (3. Anadolu Enerji Sempozyumu Özel Sayısı)

Chhetri, K., Tiwari, A. P., Dahal, B., Ojha, G. P., Mukhiya, T., Lee, M., Kim, T., Chae, S. H., Muthurasu, A., & Kim, H. Y. (2020). A ZIF-8-derived nanoporous carbon nanocomposite wrapped with CO_3O_4-polyaniline as an efficient electrode material for an asymmetric supercapacitor. Journal of Electroanalytical Chemistry, 856, 113670. https://doi.org/10.1016/j.jelechem.2019.113670

Conway, B. E. (1999). Electrochemical supercapacitors: Scientific fundamentals and technological applications. Kluwer Academic/Plenum Publishers.

Dülger, Z. (2023). rGO, rGO/MnO_2, rGO/CuO, rGO/MnO_2/PANI, rGO/CuO/PANI ikili ve üçlü nanokompozit sentezleri, süperkapasitör uygulamaları (Yüksek lisans tezi, Tekirdağ Namık Kemal Üniversitesi, Fen Bilimleri Enstitüsü).

dos Reis, G. S., Lima, R. M. A. P., Larsson, S. H., Subramaniyam, C. M., Thyrel, M., & de Oliveira, H. P. (2021). Flexible supercapacitors of biomass-based activated carbon polypyrrole on eggshell membranes. Journal of Environmental Chemical Engineering, 9(5), 106155. https://doi.org/10.1016/j.jece.2021.106155

Fan, L.-Z., & Maier, J. (2006). High-performance polypyrrole electrode materials for redox supercapacitors. Electrochemistry Communications, 8(8), 937–940. https://doi.org/10.1016/j.elecom.2006.03.006

Gashaw Hone, F., Tegegne, N. A., & Andoshe, D. M. (2021). Advanced materials for energy storage devices. In Electrode materials for energy storage and conversion (pp. 77–94). CRC Press. https://doi.org/10.1201/9781003145585-5 Guan, X., Pan, L., & Fan, Z. (2021). Flexible, transparent and highly conductive polymer film electrodes for all-solid-state transparent supercapacitor applications. Membranes, 11(10), 788. https://doi.org/10.3390/membranes11100788

Hwang, C., Hwang, J., Kwak, M.-J., Kim, H.-S., Song, H.-K., & Song, W.-J. (2024). Highly flexible electrodes based on nano/micro-fiber for flexible lithium metal batteries. Advanced Functional Materials, 34(24), 2404649. https://doi.org/10.1002/adfm.202404649

Jamil, R., & Debbie, S. (2022). Ionic liquid gel polymer electrolytes for flexible supercapacitors: Challenges and prospects. Current Opinion in Electrochemistry, 35, 101046. https://doi.org/10.1016/j.coelec.2022.101046 Jeong, J.-H., Park, J., Lee, D., Baughman, R. H., & Kim, S. J. (2019). Electrodeposition of α-MnO_2/γMnO_2 on carbon nanotube for yarn supercapacitor. Scientific Reports, 9, 11271. https://doi.org/10.1038/s41598-019-47744-x

Lee, H. U., Li, J., Park, S. W., & Park, J.-Y. (2017). Preparation and characterization of PEDOT:PSS wrapped carbon nanotubes/MnO_2 composite electrodes for flexible supercapacitors. Synthetic Metals, 228, 84–90. https://doi.org/10.1016/j.synthmet.2017.03.016

Low, W. H., Khiew, P. S., Lim, S. S., Siong, C. W., & Ezeigwe, E. R. (2019). Recent development of mixed transition metal oxide and graphene/mixed transition metal oxide based hybrid nanostructures for advanced supercapacitors. Journal of Alloys and Compounds, 775, 1324–1356. https://doi.org/10.1016/j.jallcom.2018.10.102

Ma, G.-F., Mu, J.-J., Zhang, Z.-G., Sun, K.-J., Peng, H., & Lei, Z.-Q. (2013). Preparation of polypyrrole/sodium alginate nanospheres and their application for high performance supercapacitors. Chinese Journal of Chemistry, 31(10), 1241–1246. https://doi.org/10.1002/cjoc.201300244

Maheswari, N., & Muralidharan, G. (2018). Fabrication of CeO_2/PANI composites for high energy density supercapacitors. Materials Research Bulletin, 106, 357–364. https://doi.org/10.1016/j.materresbull.2018.05.025

Namsheer, K., & Rout, C. S. (2021). Conducting polymers: A comprehensive review on recent advances in synthesis, properties and applications. RSC Advances, 11(9), 5659 5697. https://doi.org/10.1039/D0RA07800J Özada, Ç., Ünal, M., & Yazıcı, M. (2023). Süperkapasitör: Temelleri ve malzemeleri. Gazi Üniversitesi Mühendislik Mimarlık Fakültesi Dergisi, 39(2), 1315–1332. https://doi.org/10.17341/gazimmfd.1141220

Penchev, H., Ivanova, G., Hubenov, V., Boyadzieva, I., Budurova, D., Ublekov, F., Gigova, A., & Stoyanova, A. (2025). Supercapacitor cell performance with bacterial nanocellulose and bacterial nanocellulose/polybenzimidazole impregnated membranes as separator. Membranes, 15(1), 12. https://doi.org/10.3390/membranes15010012

Shimoga, G., Palem, R. R., Choi, D.-S., Shin, E.-J., Ganesh, P.-S., Saratale, G. D., Saratale, R. G., Lee, S.-H., & Kim, S.-Y. (2021). Polypyrrole-based metal nanocomposite electrode materials for high-performance supercapacitors. Metals, 11(6), 905. https://doi.org/10.3390/met11060905

Simon, P., & Gogotsi, Y. (2008). Materials for electrochemical capacitors. Nature Materials, 7(11), 845–854. Szubzda, B., Szmaja, A., Ozimek, M., & Mazurkiewicz, S. (2014). Polymer membranes as separators for supercapacitors. Applied Physics A, 117(3), 1801–1809. https://doi.org/10.1007/s00339-014-8674-y

Topçu, E. (2020). Serbest duran ve esnek MnO_2/grafen kağıt elektrot: Dopamin tayini için yeni tip amperometrik sensör. Gümüşhane Üniversitesi Fen Bilimleri Enstitüsü Dergisi, 10(1), 22–34. https://doi.org/10.17714/gumusfenbil.562555

Wang, G., Zhang, L., & Zhang, J. (2012). A review of electrode materials for electrochemical supercapacitors. Chemical Society Reviews, 41(2), 797–828. Wang, X., Wu, D., Song, X., Du, W., Zhao, X., & Zhang, D. (2019). Review on carbon/polyaniline hybrids: Design and synthesis for supercapacitor. Nanomaterials, 9(6), 849. https://doi.org/10.3390/nano9060849

Xi, S., Qian, X., Cheng, X., Liu, H., Shabanzadeh, H., & Dastan, D. (2025). One-step depositing method of PAni/MnO_2 composites for enhanced supercapacitor performance. iScience, 111774. https://doi.org/10.1002/cjoc.201300244

Yan, J., Wei, T., Fan, Z., Qian, W., Zhang, M., Shen, X., & Wei, F. (2009). Preparation of graphene nanosheet/carbon nanotube/polyaniline composite as electrode material for supercapacitors. Journal of Power Sources, 195(9), 3041–3045. https://doi.org/10.1016/j.jpowsour.2009.11.028

Yang, Q., Pang, S.-K., & Yung, W. K. C. (2014). Study of PEDOT-PSS in carbon nanotube/conducting polymer composites as supercapacitor electrodes in aqueous solution. Journal of Electroanalytical Chemistry, 728, 58–64. https://doi.org/10.1016/j.jelechem.2014.06.033

Zhai, Y., Dou, Y., Zhao, D., Fulvio, P. F., Mayes, R. T., & Dai, S. (2011). Carbon materials for chemical capacitive energy storage. Advanced Materials, 23(42), 4828 4850.

Zhang, J., Gu, M., & Chen, X. (2023). Supercapacitors for renewable energy applications: A review. Micro and Nano Engineering, 100229. https://doi.org/10.1016/j.mne.2023.100229

Zhang, L. L., & Zhao, X. (2009). Carbon-based materials as supercapacitor electrodes. Chemical Society Reviews, 38(9), 2520–2531.

Zhang, M., Halder, A., Hou, C., Ulstrup, J., & Chi, Q. (2016). Free-standing and flexible graphene papers as disposable non-enzymatic electrochemical sensors. Bioelectrochemistry, 109, 87–94.

Zhang, Q., Gao, X.-W., Liu, X., Mu, J.-J., Gu, Q., Liu, Z., & Luo, W.-B. (2023). Flexible wearable energy storage devices: Materials, structures, and applications. Batteries & Technology Energy, 2, 20230061. https://doi.org/10.1002/bte2.20230061

Zhang, X., He, B., Zhao, Y., & Tang, Q. (2018). A porous ceramic membrane tailored high-temperature supercapacitor. Journal of Power Sources, 379, 60–67. https://doi.org/10.1016/j.jpowsour.2018.01.033

6. Bölüm

Zihnin Cebirsel Alışkanlıklarına Pedagojik Bakış

Şahin TOSUN[1], Ali BOZKURT[2]

Özet

Bu bölümde, erken cebir öğretim sürecinde öğrencilerin cebirsel düşünme becerilerini geliştirmek amacıyla geliştirilen Zihnin Cebirsel Alışkanlıkları (ZCA) yaklaşımı pedagojik açıdan ele alınmıştır. Bu çalışma TÜBİTAK destekli bir araştırma projesi (TÜBİTAK 1001 proje no: 223K317) kapsamında yapılmıştır. Yaklaşımın daha iyi anlaşılması için örüntüler, cebirsel ifadeler, eşitlik ve denklemlerle ilgili örnek etkinliklere yer verilmiştir. Ayrıca düşük bilişsel talebe sahip matematik görevlerinin yüksek bilişsel talep gerektiren görevlere dönüştürülmesine dair örnekler verilmiştir. Bu dönüşüme yönelik öğretmenler için uygulamalı öneriler geliştirilmiştir. Çalışma, öğrencilerin zihnin cebirsel alışkanlıkları ve cebirsel muhakeme becerilerini geliştirmeye yönelik kuramsal ve pratik bir zemin oluşturmaktadır.

[1] Dr., dr.sahin.tsn@gmail.com, Nuriye Zekeriya Kına Ortaokulu
Orcid: 0009-0000-2236-7864
[2] Prof. Dr., alibzkrt@gmail.com, Gaziantep Üniversitesi,
Orcid: 0000-0003-4922-7997

Giriş

Cebir, fonksiyonel ilişkileri inceleyen temel bir matematik alanıdır; bu ilişkilerden doğan temsil sistemlerini ve yapıları oluşturup analiz etmeyi içerir. Sayı sistemleri, bilinmeyenler, örüntüler ve denklemler in kurulması ve çözülmesi bu alanın temel parçalarını oluşturur. Cebirsel düşünme, bilinen niceliklerle işlem yapan aritmetik muhakemeden farklıdır; işlemler ile matematiksel yapılardan genellemeler ve kurallar oluşturmayı, bunları sembollerle ifade etmeyi ve bilinmeyenleri tıpkı biliniyormuş gibi işleme dahil edebilmeyi kapsar. Bu doğrultuda süreç, cebirsel işlemlerin, ilişkilerin ve örüntülerin sistematik bir şekilde genellenebilmesine zemin hazırlar. Öğrenciler bu genellemelerden çıkarımlar yapar ve bunları uygun temsillerle ifade eder (Kaput, 1999**;** Bozkurt vd., 2025).

Alanyazın, öğrencilerin cebirsel düşünme becerilerini geliştirme ve gelişim seviyelerini belirleme üzerine yoğunlaşmaktadır (Kaput, 1999; Chimoni vd., 2018; Hart vd., 1998). Bu doğrultuda Kaput'un cebirsel düşünmenin temel bileşenlerine ilişkin çerçevesi, Hart vd.'nin (1998) geliştirdiği cebirsel düşünme düzeyleri modeli ile Chimoni vd.'nin (2018) tanımladığı yapısal bileşenler dikkat çekmektedir. Bu çalışmalar cebirsel düşünmenin çok boyutlu yapısını ortaya koymakta ve kavramsal katkılar sunmaktadır. Söz konusu modeller düşünme biçimlerinin öğretim ortamlarında nasıl inşa edileceğine dair açık yönlendirmeler sunmamaktadır.

Matematiksel içeriğe yönelik faydalı düşünme yolları zihin alışkanlıkları olarak tanımlanır (Cuoco vd., 1996). Bu durum uygulayıcılar için yol gösterici olmaktan uzaktır. Bu nedenle çalışmada kuramsal temel olarak Driscoll (1999)'un çalışmasında yer verilen ZCA yaklaşımı benimsenmiştir. Matematiksel içeriğe yönelik faydalı düşünme yolları zihin alışkanlıkları olarak tanımlanır (Cuoco vd., 1996). Bu yaklaşımdan yola çıkarak cebirsel düşünmenin temelindeki süreçleri kavramsallaştırmak amacıyla Driscoll (1999) tarafından zihnin cebirsel alışkanlıkları çerçevesi geliştirilmiştir. Bu çalışmada kuramsal temel olarak Driscoll (1999)'un çalışmasında yer verilen ZCA yaklaşımı benimsenmiştir. Bu çerçeve cebirsel düşünmeyi yalnızca içerik temelli bir öğrenme süreci olarak görmez. Süreci bilişsel alışkanlıkların dönüşümünü içeren bir gelişim alanı olarak tanımlar. Böylece pedagojik müdahale açısından güçlü bir kuramsal zemin sağlar. Tanımlanan zihinsel alışkanlıklar, öğretim tasarımlarının hangi bilişsel süreçleri harekete geçirmesi gerektiği konusunda sistematik bir yönlendirme sunmaktadır.

Zihnin Cebirsel Alışkanlıkları

Zihnin cebirsel alışkanlıkları cebirle uğraşırken, cebir problemlerini çözerken veya çözümü açıklarken sergilediği davranışlardır. Cebirsel düşünme becerisine sahip olmak, fonksiyonlar ile fonksiyonların işleyiş biçimleri üzerine odaklanmayı gerektirir. Sistemin yapısının hesaplamalar üzerindeki etkisini dikkate almak bu sürecin bir diğer önemli boyutudur. Driscoll (1999), zihin cebirsel alışkanlıklarını üç ana kategoride ele alır (Şekil 1):

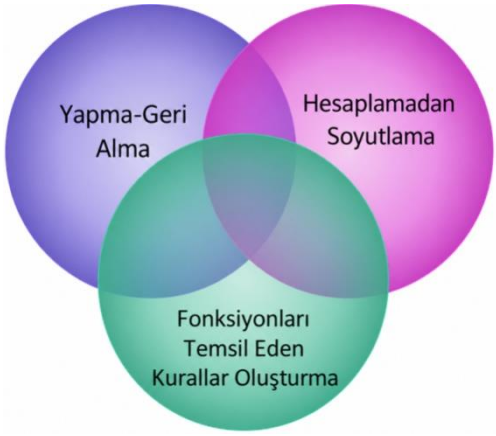

Şekil 1. Zihin cebirsel alışkanlıkları

Yapma – Tersini Yapma

Bu alışkanlık, matematiksel ifadeleri çözmek, yazmak veya yeniden yapılandırmak için kullanılan sembolik manipülasyonları ifade eder. Öğrenciler sadece bir işlemin sonucunu bulmakla kalmaz, sonuçtan yola çıkarak başlangıç noktasına da ulaşır. Bu alışkanlık odağın sadece nihai yanıtta kalmasını önler. Sürecin kendisine yönelik bir yansıtma sağlar (Driscoll, 1999).

Girdiden çıktıya ulaşma: Girdiden çıktı bulma veya bir örüntüde başlangıç değerlerinden istenilen değere ulaşma alışkanlığıdır. Verilen bir ilişki/yapıda girdiyi kullanarak bir istenilen değeri bulur veya bir örüntüde verilen adımları kullanarak istenilen adımdaki değeri bulur. Örneğin x=3 için x^2-5 ün değeri kaçtır? Sorusunda x'in yerine 3 yazarak cevabın 4 olduğunu bulma girdiden çıktıya ulaşma alışkanlığı gerektirir.

Çıktıdan girdiye ulaşma: Verilen bir çıktıdan hareketle, bu çıktıyı oluşturan başlangıç değerini belirlemek amacıyla işlemleri ters sırada ve ters işlem özelliklerini kullanarak bilinmeyen girdiyi bulabilmektir (Driscoll, 1999; Driscoll & Moyer, 2001). Başka bir deyişle bir fonksiyonda veya denklemde sonucun bilinmesi, bilinmeyenin aranması durumudur. Örneğin, x'in hangi değeri için $y = x^2 + 8$ eğrisi grafikte 100 değerine ulaşır? Sorusunda "x, 9 ile

10 arasında bir yerde olduğunda, $y = x^2 + 8$ eğrisi grafikte 100 değerine ulaşır." Cevabına ulaşmak çıktıdan girdiye ulaşma alışkanlığı gerektirir.

Geriye doğru çalışma: Bir problemin çözümüne ulaşırken işlemleri uygulandıkları sıranın tersine izleyerek çözüm sürecini başlangıç noktasına kadar geri takip edebilme stratejisidir (Driscoll, 1999; Driscoll & Moyer, 2001). Başka bir deyişle çok adımlı problemlerde, son adımdan ilk adıma doğru tersine bir işlem zinciri kurmaktır. Örneğin, $\frac{x-11}{3} = 23$ ifadesinde bilinmeyenin kaç olduğunu bulma sürecinde, öğrenci doğrudan tek bir hamle yapamaz; gerçek yaşam durumu problemlerini ya da çok adımlı işlemleri en sondan başlayarak zincirleme şekilde geriye doğru işletir. Önce en dıştaki bölmenin tersi olarak 23' ü 3 ile çarpar (69), ardından çıkarma işleminin tersi olarak 11 ekler ve bilinmeyenin (x) 80 olduğunu adım adım geri sararak bulur.

Fonksiyonları Temsil Eden Kurallar Oluşturma (FTEKO)

FTEKO alışkanlığı büyük ölçüde fonksiyonel ilişkileri arama ve tanımlama becerisiyle ilgilidir. Temsillerle işlemler yapma ve genel kuralı sembollerle ifade etme stratejileri bu kapsamda devreye girer (Driscoll & Moyer, 2001). Bu alışkanlığa dair yedi alt bileşen tanımlanmıştır:

Bilgiyi düzenleme: Probleme ilişkin nicelikleri sistematik biçimde düzenleyerek aralarındaki ilişkilerin görünür hâle gelmesini sağlamaktır. Bu süreçte veriler tablo, liste veya şema gibi uygun temsillerle organize edilir.

Bilgiyi anlamlı parçalara ayırma: Karmaşık bir problem durumunu daha küçük ve yönetilebilir bileşenlere ayırarak nicelikler arasındaki ilişkileri daha kolay analiz etmektir.

Farklı temsiller kullanma: Bu bileşen iki durumda karşımıza çıkmaktadır. Bilgiyi düzenleme sürecinde karşımıza çıktığı gibi ulaşılan matematiksel ilişkiyi/kuralı grafik, şekil, sözel veya cebirsel ifadeler gibi farklı gösterimlerle ifade edebilmeyi de içerir.

Değişimi açıklama: Bir nicelikte meydana gelen değişimin diğer nicelik üzerindeki etkisini açıklayarak değişkenler arasındaki fonksiyonel ilişkiyi ortaya koymaktır

Örüntüleri tahmin etme: Veriler arasındaki düzenliliği belirleyerek örüntünün sonraki adımlarını öngörme ve olası genellemeler geliştirmedir

Kuralı tanımlama: Belirlenen örüntü veya ilişkinin genel yapısını sözel ya da cebirsel biçimde ifade etmektir (Driscoll, 1999; Driscoll & Moyer, 2001).

Kuralı gerekçelendirme: Oluşturulan genel kuralın neden geçerli olduğunu matematiksel gerekçeler ve kanıtlarla açıklamaktır

Örnek 1. Betül'ün incelediği internet tarifesinde giriş ücreti sabit 150 TL'dir. Harcanan her 1 GB internet için bu fiyata 20 TL eklenecektir.

Buna göre;

1- Betül'ün 1 GB, 2 GB ve 3 GB internet harcaması durumunda ödeyeceği toplam tutarları gösteren bir tablo oluşturunuz.
2- Bu tarifede faturayı oluşturan ücretleri sabit ve değişken olarak iki farklı parçaya ayırınız; hangisi sabit, hangisi değişken açıklayınız.
3- Kullanılan internet miktarı arttıkça toplam fatura tutarının nasıl bir değişim gösterdiğini açıklayınız.
4- Betül'ün 4 GB internet harcaması durumunda ödeyeceği tutarı tahmin ediniz.
5- İnternet miktarı ile toplam fatura arasındaki bu ilişkiyi matematiksel sembol kullanmadan, kendi cümlelerinizle sözel olarak tanımlayınız.
6- İnternet miktarı ve toplam faturaya değişkenler atayarak ikisi arasındaki ilişkiyi gösteren bir cebirsel formül yazınız.
7- Yazdığınız formülün, tarifedeki sabit ücret ve GB başı ücret mantığıyla neden tam olarak eşleştiğini gerekçelendiriniz.

Çözüm:

1- 1 GB için 170 TL, 2 GB için 190 TL ve 3 GB için 210 TL ödenir (*bilgiyi düzenleme*)
2- Değişmeyen 150 TL sabit kısımdır, internet kullanımına göre eklenen 20 TL ve katları ise değişken kısımdır. (*Bilgiyi anlamlı parçalara ayırma*)
3- Kullanılan internet miktarı her 1 GB arttığında, toplam fatura bedeli de buna bağlı olarak düzenli şekilde 20 TL artmaktadır. (*Değişimi açıklama*)
4- 3 GB kullanımı 210 TL ise, sabit artış düzenine göre bir sonraki adım olan 4 GB kullanımı 230 TL olur. (*Örüntüleri tahmin etme*)
5- Ödenecek toplam para, harcanan internet miktarının yirmi katı ile başlangıçtaki sabit 150 liranın toplamıdır. (*Kuralı tanımlama*)
6- İnternet miktarı (x) ve toplam fatura (y) arasındaki ilişkiyi gösteren eşitlik $y = 20x + 150$ şeklindedir. (*Farklı temsiller kullanma*)
7- Formüldeki 150 başlangıçtaki GB kullanımına bağlı olmayan giriş ücretini, 20x ise harcanan GB başına ödenen bedeli temsil ettiği için yazılan model tarifenin işleyişini tam olarak doğrular. (Kuralı gerekçelendirme)

Hesaplamadan Soyutlama (HS)

Hesaplamaları, gerçekleştirilen somut işlemlerden bağımsız olarak düşünebilme becerisidir. Bu alışkanlık hesaplamalara yönelik genellemeler

geliştirmeyi sağlayan bir cebirsel yapı anlayışı sunar. Soyutlama bu sürecin temel taşıdır (Lew, 2004). Genellemelere dayalı matematiksel nesne ve ilişkilerin çıkarılmasını içerir (Driscoll & Moyer, 2001). Bu alışkanlığa dair altı alt bileşen tanımlanmıştır:

Hesaplama kısa yolları geliştirme: İşlemleri daha verimli gerçekleştirebilmek amacıyla matematiksel özelliklerden yararlanarak alternatif çözüm stratejileri geliştirmektir.

İşlem yapmadan hesap yapma: Ayrıntılı işlem yapmaya gerek kalmadan, işlemin yapısından hareketle sonucun büyüklüğü, yönü veya niteliği hakkında akıl yürütmektir.

Örneklerin ötesine geçerek genelleme yapma: Belirli örneklerde gözlenen bir matematiksel özelliğin tüm benzer durumlar için geçerli olacağını fark ederek genel bir ilişki oluşturabilmektir.

Eşdeğer ifadeler oluşturma: Aynı matematiksel ilişkiyi farklı ancak eşdeğer cebirsel ifadeler kullanarak gösterebilmektir.

Sembolik ifadeler kullanma: Sayısal örneklerden hareketle genel matematiksel ilişkileri harfler ve cebirsel semboller aracılığıyla ifade edebilmektir.

Kısa yolları gerekçelendirme: Kullanılan zihinsel strateji veya kısa yolun neden matematiksel olarak geçerli olduğunu özellikler, kurallar veya ilişkilerle açıklayabilmektir.

Örnek 2. Bir okul kafeteryası için yan yana dizilen kare masaların etrafına sandalyeler yerleştirilecektir. Bir adet kare masanın etrafına 4 sandalye sığmaktadır. Masalar uç uca eklendiğinde ise birleşen kenarlara sandalye konulamamaktadır.

Buna göre aşağıdaki soruları cevaplayınız.

1- 10 adet kare masa yan yana birleştirildiğinde toplam kaç sandalyeye ihtiyaç duyulacağını, masaları tek tek çizip sandalyeleri saymak yerine, işlemi kolaylaştıracak bir zihinsel yöntemle nasıl hesaplarsınız?
2- Masaları yan yana eklemeye devam ettiğimizi düşünelim. 50 masalık bir düzenek için gereken sandalye sayısının, hiçbir tam hesaplama yapmadan, 100'den büyük mü yoksa küçük mü olacağını masaların ve işlemlerin yapısına bakarak nasıl öngörürsünüz?
3- 1, 2, 3 ve 4 masa için durumları incelediğinizde, masa sayısı ile sandalye sayısı arasında her zaman geçerli olan ortak ilişkiyi nasıl açıklarsınız?
4- Masa sayısını n ile gösterdiğimizde, toplam sandalye sayısını bulmak için üç farklı öğrenci şu ifadeleri yazıyor:
   1. İfade: $2n + 2$
   2. İfade: $6 + 2(n - 2)$

3. İfade: 2(n + 1)

Bu üç ifadeden hangileri birbirine eşdeğerdir ve bu masalar için kurulacak doğru modeli temsil eder?

5- Masaların dizilimindeki genel ilişkiyi temsil etmek üzere, sayılar yerine doğrudan harfleri ve cebirsel sembolleri işe koşarak bu örüntüyü matematiksel olarak nasıl kâğıda dökersiniz?

6- Geliştirdiğiniz bu formülün veya zihinsel kısa yolların, masaların yerleşim düzenindeki matematiksel kurallara neden tam olarak uyduğunu ve neden her zaman doğru sonuç vereceğini nasıl savunursunuz?

Çözüm:

1- İlk masanın sağına ve soluna birer, alt ve üst kenarlarına da birer sandalye yerleştirildiğini düşünebiliriz. Masalar yan yana eklendikçe, aradaki birleşen kenarlar kapanır. Bu durumda her masanın sadece alt ve üst kenarlarına (yani her masa için 2 tane) sandalye gelecektir. En baştaki ve en sondaki iki dış kenara da birer sandalye sabit kalacaktır. Buradan hareketle 10 masa için zihinden 10.2 = 20 hesaplanıp, sabit olan 2 uç sandalye eklenerek 22 sonucuna pratik yoldan ulaşılır. *(Hesaplama kısa yolları geliştirme)*

2- Her masa düzende alt ve üst olmak üzere 2 sandalye taşımaktadır. Sabit olan 2 uç kenar hesaba katılmasa bile, 50 masanın sadece alt ve üst kenarlarına 50.2 = 100 sandalye yerleşir. İki uçtaki sandalyeler de ekleneceği için tam sonucu hesaplamaya gerek kalmadan toplam sandalye sayısının 100'den büyük (102) olacağı yapının karakterinden doğrudan öngörülür. *(Hesaplamadan hesap yapma)*

3- Masalar incelendiğinde; 1 masa için 4, 2 masa için 6, 3 masa için 8, 4 masa için 10 sandalye gerekir. Örneklerdeki masa sayısı ile sandalye sayısı arasındaki ortak ilişki, masa sayısı ne olursa olsun sandalye sayısının her zaman masa sayısının 2 katının 2 fazlası şeklinde ilerlemesidir *(Örneklerin ötesine geçerek genelleme yapma)*.

4- Verilen ifadeleri cebirsel olarak sadeleştirildiğinde; 2(n+1)=2n+2 (dağılma özelliği) ve 6+2n-4=2n+2 (Benzer terimleri toplama-çıkarma) elde edilir. Bu yüzden üç ifade de birbirine tamamen eşdeğerdir. Masalar için kurulacak doğru modeli temsil eder. *(Eşdeğer ifadeler oluşturma)*

5- Masa sayısı olan bağımsız değişken m harfi ile sandalye sayısı olan bağımlı değişken ise s harfi ile sembolize edilebilir. Sayısal denemelerin ötesine geçilerek, bu iki nicelik arasındaki fonksiyonel bağ ve genel ilişki matematiksel olarak s = 2m + 2 eşitliğiyle kâğıda dökülür. *(Sembolik ifadeler kullanma)*

6- Modeldeki “2m” kısmı, dizilimde yan yana duran her masanın alt ve üst kenarlarında mutlaka ikişer adet açık yer bulunmasından kaynaklanır; yani masa sayısı (m) değiştikçe sandalye sayısı ikişer ikişer büyür. Modelin sonundaki “+2” sabit sayısı ise masalar ne kadar uzarsa uzasın sırt sırta veremeyen en baştaki ve en sondaki iki dış uca yerleştirilen değişmez sandalyeleri temsil eder. Geometrik düzenin fiziksel yapısı bu kurallara dayandığı için yazılan formül her zaman doğru sonuç verir *(Kısa yolları gerekçelendirme)*.

ZCA çerçevesine göre Tasarlanmış Etkinlik Örnekleri

Zihin alışkanlıklarının ders kitaplarındaki kazanımlarla nasıl somutlaştığını göstermek adına, çalışma kapsamında geliştirilen özgün etkinlik yapıları doğrudan aşağıda çözümlenmiştir. Bu ZCA senaryoları, öğrencilerin hem işlemsel hem de kavramsal becerilerini eş zamanlı tetikleyen iskele süreçlerini temsil etmektedir.

Kazanım: Bir doğal sayı ile bir cebirsel ifadeyi çarpar.

Etkinlik 1: 3.(x+2) işlemini modelleyerek çözme

Sarı cebir karosu x değişkenini, yeşil cebir karosu +1 sayısını temsil etmektedir. 	ÇÖZÜM	ZCA
Cebir karoları ile 3.(x+2) cebirsel ifadesini modelleyiniz.	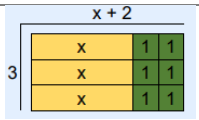	Farklı temsil kullanma
Her bir parçanın alanını veren değerleri toplayın.	3x+6	Cebirsel olarak ifade etme
3.(x+2) = 3x+6 eşitliğinde 3 ile x+2’nin çarpımının eşiti ile 3x+6 arasındaki ilişkiyi tanımlayın.	3 sayısını önce x ile sonra 2 ile çarpıp sonuçları topluyoruz.	Eş değer ifade kullanma
Belirlediğiniz ilişkiye göre bir doğal sayı ile cebirsel ifadenin çarpımına dair genel bir ifade yazınız.	Bir doğal sayı ile bir cebirsel ifade çarpılırken doğal sayı ile cebirsel ifadedeki her bir terim ayrı ayrı çarpılır.	Örneklerin ötesinde genelleme

Etkinlik 2: 2x-4 cebirsel ifadesini bir cebirsel ifade ve bir doğal sayının çarpımı şeklinde yazma

Sarı cebir karosu x değişkenini, mavi cebir karosu -1 sayısını temsil etmektedir. 	ÇÖZÜM	ZCA
2x-4 cebirsel ifade ile bir doğal sayının çarpımı şeklinde yazınız	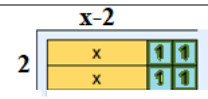	Farklı temsil kullanma
Tüm alanı bulmak için dikdörtgenin alanını hesaplama formülünü kullanın	2(x-2)	Cebirsel olarak ifade etme
2.(x-2) = 2x-4 eşitliğinde 2 ile x-2'nin çarpımının eşiti ile 2x-6 arasındaki ilişkiyi tanımlayın.	Her iki terimde de 2 sayısı ortak olduğu için 2 ortak parantezine alabiliriz	Eş değer ifade kullanma ve
Belirlediğiniz ilişkiye göre bir cebirsel ifadeyi bir doğal sayı (varsa) ile bir cebirsel ifadenin çarpımı şeklinde yazmaya dair genel bir ifade yazınız.	Verilen cebirsel bir ifadedeki her terimde ortak olan sayı ortak parantezine alınabilir	Örneklerin ötesinde genelleme

Bu etkinliklerde, öğrencilerin çarpma işlemini alan ve karo modelleriyle somutlaştırması, ardından süreci tersine işleterek (Yapma-Tersini yapma) çarpanlara ayırma sezgisi kazanması hedeflenir.

Düzenle ve İlişki Ara Aşaması (DO - İleriye Doğru İşlem): Öğrencilere sarı cebir karosunun x değişkenini, yeşil cebir karosunun ise +1 sayısını temsil ettiği bilgisi sunulur. Öğrencilerden 3.(x+2) ifadesini modellemeleri istenir. Öğretmen bu aşamada, her bir parçanın alanını veren değerleri toplayarak bilgileri düzenlemelerini sağlar. *Yönlendirici Soru:* "3.(x+2) = 3x+6 eşitliğinde, çarpanların yapısı ile elde ettiğiniz toplam alan arasındaki ilişkiyi nasıl tanımlarsınız?" Bu soruyla öğrencinin eş değer ifadeleri fark etmesi ve kuralı öngörmesi tetiklenir.

Oluştur Aşaması: Öğrenciler örneklerin ötesine geçerek bir doğal sayı ile cebirsel ifadenin çarpımında katsayının parantez içine nasıl dağıldığını geneller ve cebirsel kuralı kendi cümleleriyle oluşturur.

Kullan aşaması: Alışkanlığı tam anlamıyla yapılandırmak adına süreç tersine çevrilir. Öğrencilere 2x-4 cebirsel ifadesi verilir (Burada mavi karo -1'i temsil eder). Öğrencilerden bu ifadeyi bir doğal sayı ile bir cebirsel ifadenin çarpımı şeklinde yeniden yazmaları istenir. *Pedagojik Hamle:* Öğrenci tüm alanı temsil eden dikdörtgenden yola çıkarak kenar uzunluklarını (girdileri) bulmak için tersine mühendislik yapar ve ifadeyi 2.(x-2) olarak kurar. Böylece odağın yalnızca tek yönlü sonuç bulmada kalması engellenir.

Kazanım: Sayı örüntülerinin kuralını harfle ifade eder. Kuralı verilen örüntünün istenilen terimini bulur.

Etkinlik 3: Nermin Hanım, bahçesine çiçek dikmeye karar veriyor. Nermin Hanım; ilk sıraya 1, ikinci sıraya 3, üçüncü sıraya 5, dördüncü sıraya 7, beşinci sıraya 9 çiçek dikiyor.

Nermin Hanım'ın her bir sıraya diktiği çiçek sayılarının arasındaki ilişkiye dikkat ederek çiçek dikmeye devam etmesi durumunda;

<table>
<tr><th>Yönergeler</th><th>Çözüm</th><th>ZCA</th></tr>
<tr><td>Dokuzuncu sıraya dikeceği çiçek sayısı nasıl bulunabilir? Açıklayınız.</td><td>1,3,5,7,9,11,13,15,17, …
Açıklama: Her adımda bir önceki adım 2 artırılarak 9. Adıma ulaşılabilir.</td><td>Bilgileri düzenle</td></tr>
<tr><td>Adım sayısına göre dikilecek çiçek sayısı gösteren bir tablo oluşturunuz.</td><td><table><tr><td>Adım</td><td>1.</td><td>2.</td><td>3.</td><td>4.</td><td>5.</td><td>6.</td><td>7.</td></tr><tr><td>Çiçek sayısı</td><td>1</td><td>3</td><td>5</td><td>7</td><td>9</td><td>11</td><td>13</td></tr></table></td><td>Farklı temsil kullan</td></tr>
<tr><td>Her bir adımdan diğer adıma geçerken nasıl bir değişim tanımlayabiliriz?</td><td>Her adımda bir önceki adımdaki çiçek sayısından iki tane fazla dikilecek (X Aradığımız kural değil)<table><tr><td>Adım</td><td>1.</td><td>2.</td><td>3.</td><td>4.</td><td>…</td><td>n</td></tr><tr><td>Çiçek sayısı</td><td>1</td><td>3</td><td>5</td><td>7</td><td>…</td><td></td></tr><tr><td>İlişki</td><td>2.1-1</td><td>2.2-1</td><td>2.3-1</td><td>2.4-1</td><td></td><td></td></tr></table>Adım numarası ile o adımda dikilecek çiçek sayısı arasında bir ilişki olduğunu görmemiz.</td><td>Eşdeğer ifade & Değişimi tanımla</td></tr>
</table>

Etkinlik 3: (*Devamı*)

<table>
<tr><td>Herhangi bir adımda dikilecek çiçek sayısını bulmanızı sağlayacak kuralı yazınız.</td><td>Her adımda adım numarasının 2 katının 1 eksiği kadar ağaç dikilecektir.</td><td>Kuralı tanımla</td></tr>
<tr><td>Herhangi adımda dikilecek çiçek sayısını bulmanızı</td><td>n. adımda 2n-1 çiçek dikilecektir.</td><td>Cebirsel olarak ifade et</td></tr>
</table>

sağlayacak kuralı cebirsel olarak ifade ediniz.		
Bu kuraldan hareketle, dokuzuncu sıraya veya yüzüncü sıraya dikilecek çiçek sayısını tek tek saymadan doğrudan nasıl bulabilirsiniz?	2.9-1=18-1=17 2.100-1=200-1=199	İsteneni bul

Bu etkinlikte öğrencilerin uzun uzun aritmetik hesaplamalar yapmaktan uzaklaşarak cebirsel yapıları doğrudan soyutlamaları hedeflenir:

Düzenle Aşaması: Nermin Hanım'ın bahçesine çiçek dikme durumu ele alınır. İlk sıraya 1, ikinci sıraya 3, 3. Sıraya 5, dördüncü sıraya 7 çiçek dikilmektedir. Öğrencilerden ilk olarak adım sayısı ile dikilecek çiçek sayısını gösteren bir tablo oluşturarak bilgileri düzenlemeleri ve farklı temsil sistemlerini kullanmaları istenir.

İlişki Ara Aşaması: Öğrenciler tablodaki ardışık adımlar arasındaki değişimi tanımlar. *Yönlendirici Soru:* "Her bir adımdan diğer adıma geçerken nasıl bir sabit değişim görüyorsunuz? Bu yinelenen parçaları aritmetik toplama yapmadan doğrudan nasıl ifade edebiliriz?" Öğrenciler kuralı sezgisel olarak öngörür.

Oluştur Aşaması: Öğrenciler herhangi bir adımdaki (n. Adım) çiçek sayısını veren genel kuralı 2n-1 şeklinde cebirsel olarak ifade eder. Formülün sadece mekanik olarak ezberlenmediğini göstermek için örneklerin ötesinde bir doğrulama yapılması istenir.

Kullan Aşaması: Soyutlanan kural doğrudan büyük bir adıma uygulanır: "Bu kuraldan hareketle, dokuzuncu sıraya veya yüzüncü sıraya dikilecek çiçek sayısını tek tek saymadan doğrudan nasıl bulabilirsiniz?" Öğrenci genel yapıyı kullanarak sonuca ulaşır.

Kazanım: Eşitliğin korunumu ilkesini anlar ve gerçek hayat durumlarına uygun birinci dereceden bir bilinmeyenli denklem kurar.

Etkinlik 4: PhET yazılımı kullanılarak (https://phet.colorado.edu/tr/simulations/equality-explorer) sol kefesinde mavi bir kutu, sağ kefesinde 5 kg bulunan denge durumundaki terazi modeli elde edilmiştir.

Etkinlik 4: (*Devamı*)

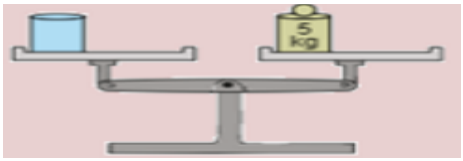

Buna göre teraziye aşağıdaki ağırlıklardan hangisi ya da hangileri konursa terazinin dengesi bozulmaz?

Not: Birkaç sağlayan veya sağlamayan örnek verilerek öğrencilerden örneklerin ötesinde genelleme yapmaları beklenir.

Yönergeler	Çözüm	ZCA
1 tane daha mavi kutu sağ kefeye, 1 tane 5 kg sol kefeye konursa	Bozulmaz.	Bilgileri düzenle Farklı temsil kullan
1 tane daha mavi kutu sol kefeye, 5 tane 1 kg sağ kefeye konursa	Bozulmaz	
Her iki kefede bulunan ağırlıklar 3 katına çıkarılırsa	Bozulmaz	
2 tane daha mavi kutu sol kefeye, 1 mavi kutu ile 5 tane daha 1 kg'lık cisim sağ kefeye konursa	Bozulmaz	
3 tane daha mavi kutu sağ kefeye, 2 mavi kutu ile 2 tane 1 kg sol kefeye konulursa	Bozulur	
Hangi durumlarda terazinin dengesinin bozulduğuna dair ne tür çıkarımlar yapabiliriz. Tartışınız.	Her iki kefede eşit ağırlık yoksa denge bozulur. ….	Değişimi tanımla
Eşit kollu terazinin hangi durumlarda dengesinin bozulmadığına dair bir kural geliştiriniz.	- Her iki kefeye aynı ağırlıkta cisimler eklendiğinde terazinin dengesi bozulmaz. - Her bir kefedeki ağırlıklar 2,3, … veya herhangi bir katına çıkarılırsa terazinin dengesi bozulmaz.	Örneklerin ötesinde genelleme

Etkinlik5: Sol kefede 3 tane mavi kutu, sağ kefede 1 mavi kutu ile bir tane 5 kg, 5 tane daha 1 kg sağ kefeye konulmuş terazi verilmiştir.

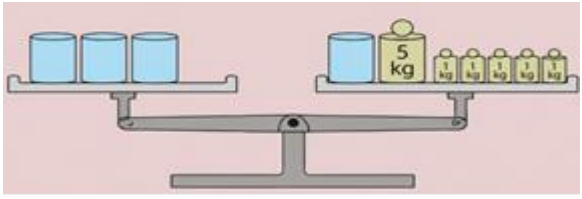

Buna göre teraziye aşağıdaki ağırlıklardan hangisi ya da hangileri konursa terazinin dengesi bozulmaz?

Yönergeler	Çözüm	ZCA
1'er tane mavi kutu her iki kefeden çıkarılırsa	Bozulmaz.	Bilgileri düzenle Farklı temsil kullan
Son durumda her iki kefedeki ağırlıkların yarısı alınırsa	Bozulmaz	

Etkinlik5: (*Devamı*)

2 tane daha mavi kutu sol kefeye, 1 mavi kutu ile 5 tane daha 1 kg'lık cisim sağ kefeye konursa	Bozulmaz	Bilgileri düzenle Farlı temsil kullan (*devamı*)
3 tane daha mavi kutu sağ kefeye, 2 mavi kutu ile 2 tane 1 kg sol kefeye konulursa	Bozulur	
Hangi durumlarda terazinin dengesinin bozulduğuna dair ne tür çıkarımlar yapabiliriz. Tartışınız.	Her iki kefede eşit ağırlık yoksa denge bozulur. ….	Değişimi tanımla
Eşit kollu terazinin hangi durumlarda dengesinin bozulmadığına dair bir kural geliştiriniz.	Her iki kefeden aynı ağırlıkta cisimler çıkarıldığında terazinin dengesi bozulmaz. Her bir kefedeki ağırlıklar yarıya 3'te birine veya herhangi bir oranına indirilirse terazinin dengesi bozulmaz.	Örneklerin ötesinde genelleme

Etkinlik6: Terazi etkinliklerindeki denge durumu "eşitlik" yani "=" sembolünü kullanabiliriz. Bu durumda etkinlik 2 deki kuralları (örneklerin ötesinde genelleme) kullanarak aşağıdaki eşitliklerin bozulmaması için şekiller yerine gelecek sayıları bulunuz.

Yönergeler	Çözüm	ZCA
$\mathbf{7 + 2 = \Delta - 3}$	7 + 2+3 = Δ-3 +3 (Her iki tarafa 3 ekle) 12 = Δ	Kuralı kullan
$\mathbf{4 + 2 = \square \cdot 3}$	6 = □·3 (Her iki tarafı 3 e böl) □=2	
$\mathbf{3 + 5 = \frac{\blacklozenge}{2}}$	8 = ♦/2 (Her iki tarafı 2 ile çarp) ♦=16	
$\mathbf{3 + 2 = 3 - \Theta}$	$3 + 2 + \Theta = 3 - \Theta + \Theta$ (Her iki tarafa Θ ekle)$5 + \Theta = 3$ (Her iki taraftan 5 $çıkar$) $5 + \Theta - 5 = 3 - 5$ $\Theta = -2$	

Etkinlik7: "*Deniz'in parası, Gülcan'ın parasının 4 katının 4 fazlası kadardır. Deniz'in 60 TL parası olduğuna göre, Gülcan'ın kaç TL parası vardır?'' ifadesine uygun bir denklem yazınız." p*roblemini çözmek için aşağıdaki yönergelerde istenilenleri yapalım:

Yönergeler	Çözüm	ZCA
Gülcan'ın parasına x diyelim. Bu durumda Deniz'in parasını veren cebirsel ifadeyi yazalım	4x+4	Bilgileri düzenle
Deniz'in parası 60 TL olduğuna göre cebirsel ifade ile Deniz'in parasının eşitliğini cebirsel olarak gösterelim.	4x+4=60	Farklı temsil kullan
Denklemi oluşturmak için ne yaptığımızı tartışınız.	Değişken tanımladık, Cebirsel ifade yazdık. Bu cebirsel ifadenin eşit olduğu değeri yazdık ve denklemi oluşturduk.	Değişimi tanımla /Kuralı öngör
Gerçek hayat durumlarına uygun birinci dereceden bir bilinmeyenli denklem kurmak için hangi adımları takip etmeliyiz?	Gerçek hayat durumlarına uygun bir denklem yazılırken 1.Adım. Önce bilinmeyenin yerine bir harf belirlenir. 2.Adım. İfadede bilinmeyenin; - Fazlası deniyorsa toplama, - Eksiği deniyorsa çıkarma, - Katı deniyorsa çarpma, - Oranı veya bölümü deniyorsa bölme işlemi yapılır. 3.Adım. Denklem yani bilinmeyen içeren eşitlik elde edilir.	Örneklerin ötesinde genelleme

Bu etkinliklerde, terazideki denge durumunu "Eşitlik" yani "=" sembolüyle ilişkilendirerek matematiksel yapıları gerekçelendirmeyi içerir.

Düzenle ve İlişki Ara Aşaması**:** Dijital bir terazi simülasyonunda, sol kefede bir mavi kutu (x), sağ kefede ise 5 kg'lık bir ağırlık dengededir. Teraziye her iki tarafa aynı ağırlıklar eklendiğinde (Örn: her iki tarafa 5 kg eklenmesi veya her iki tarafın 3 katına çıkarılması) dengenin bozulmadığı, farklı işlemler yapıldığında ise dengenin bozulduğu durumlar listelenerek bilgiler düzenlenir.

Oluştur Aşaması: Öğrenciler bu denemelerden yola çıkarak "hem eşitliğin her iki tarafına aynı sayının eklenmesi veya çıkarılması hem de eşitliğin her iki tarafının aynı sayıyla çarpılması veya bölünmesi durumunda eşitlik korunur" (Kieran, 2018; Tanışlı & Köse, 2020) genellemesine ulaşır. Bu kuralı oluşturduktan sonra, gerçek hayat durumlarına taşırlar: "Deniz'in parası, Gülcan'ın parasının 4 katının 4 fazlasıdır. Deniz'in 60 TL'si olduğuna göre Gülcan'ın parasını veren eşitliği yazınız." Öğrenci sözel durumu 4x+4=60 şeklinde yapılandırarak denklemi kurar ve doğrular.

Matematiksel Görev Dönüşümleri

Erken cebir öğretiminde, ders kitaplarında yer alan standart ve düşük bilişsel talebe sahip işlemsel görevlerin, öğrencilerin cebirsel düşünme becerilerini ve matematiksel zihin alışkanlıklarını geliştirecek nitelikte yeniden yapılandırılması mümkündür. Alan yazınında, matematiksel görevlerin bilişsel talebinin yalnızca görevin kendisine değil, öğretmenin görevi nasıl düzenlediğine, sunduğuna ve sınıf içinde nasıl yönettiğine bağlı olduğu vurgulanmaktadır (Smith & Stein, 1998; Stein et al., 2000). Erken cebir yaklaşımı da öğretmenlerin rutin hesaplama etkinliklerini; örüntüleri fark etme, genelleme yapma, matematiksel ilişkileri açıklama, değişkenleri anlamlandırma, eşitlik kavramını ilişki temelli ele alma ve matematiksel muhakemeyi destekleme fırsatlarına dönüştürebileceklerini ortaya koymaktadır (Kaput, 2008; Blanton & Kaput, 2011; Kieran, 2007). Bu doğrultuda görev dönüşümü; işlemsel soruların öğrencileri neden-sonuç ilişkileri kurmaya yönlendirecek şekilde yeniden düzenlenmesi, birden fazla çözüm yoluna olanak tanınması, öğrencilerden çözümlerini gerekçelendirmelerinin istenmesi, örüntü ve fonksiyonel ilişkiler üzerinden genelleme yapmalarının teşvik edilmesi, çoklu temsil biçimlerinin kullanılması, açık uçlu sorulara yer verilmesi ve sınıf içi matematiksel tartışmaların desteklenmesi gibi stratejilerle gerçekleştirilebilir (Stein et al., 2000; Smith & Stein, 2011). Bu tür görevler, öğrencilerin yalnızca doğru sonuca ulaşmalarını değil; matematiksel ilişkileri keşfetmelerini, genellemeler oluşturmalarını ve cebirsel düşünmenin temelini oluşturan matematiksel zihin alışkanlıklarını geliştirmelerini desteklemektedir (Kaput,

2008; Blanton & Kaput, 2011). Tablo 2'de düşük bilişsel talep içeren görevlerin yüksek bilişsel talep içeren görevlere dönüşüm örnekleri verilmiştir:

Tablo 2.
Düşük bilişsel talep içeren görevlerin yüksek bilişsel talep içeren görevlere dönüşüm örnekleri

Düşük bilişsel talep içeren görev	*Yüksek bilişsel talep içeren görev*
Bilinen kuralı kullanma: Kısa kenarı 5 cm, uzun kenarı 10 cm olan dikdörtgenin alan formülünü kullanarak alanını hesaplayınız.	Kural keşfi ve doğrulama: Çevresi 30 cm olan farklı dikdörtgenler oluşturunuz. Bu dikdörtgenlerin kenar uzunlukları ile alanları arasındaki ilişkiyi düzenleyerek alanı en büyük olan dikdörtgenin yapısına dair genel bir kural oluşturup gerekçelendiriniz
Yöntemsel akıl yürütme: $4x - 8 = 6 + 2x$ denklemini çözünüz.	Yapma-tersini yapma ve Farklı temsil kullanma: Çözüm kümesi $x = 7$ olan iki farklı doğrusal denklem sistemi oluşturunuz. Oluşturduğunuz denklemlerin katsayıları arasındaki ilişkileri düzenleyerek sistemin yapısını grafiksel ve cebirsel temsillerle açıklayınız.
Hesaplama: 3, 7, 11, 15, ... şeklinde devam eden sayı örüntünün 8.terimini bulunuz.	Yapısal ilişkileri inceleme ve kural keşfi: Bir örüntünün 4. adımı 15, 7. adımı 27 olarak veriliyor. Bu örüntünün büyüme ilişkisini gösteren geometrik bir model tasarlayınız. Tasarladığınız modelden yola çıkarak örüntünün herhangi bir adımı ile o adımdaki eleman sayısı arasındaki zemin ilişkisini açıklayınız. Oluşturduğunuz genel kuralın neden her adım için geçerli olduğunu mantıksal olarak gerekçelendiriniz.
Hesaplama: Genel terimi 3n–1 olan sayı örüntüsünün ilk 4 adımını yazınız.	Değişmeyen özellikleri fark etme ve hesaplamadan soyutlama: Genel terimi 3n-1 olan örüntünün adımları arasındaki büyüme hızını değiştirmeden, sadece başlangıç miktarını değiştirerek yeni bir örüntü oluşturunuz. İki örüntünün 100. adımları arasındaki farkı hesaplamadan, kuralların yapısındaki değişim üzerinden bu farkı tahmin ediniz ve düşünme sürecinizi açıklayınız.

Sonuç

Matematiksel zihin alışkanlıkları, müfredat kazanımları görev yapılarına birlikte işlenmelidir. Bu bütünlük, öğrencilerin işlemsel bilgi ile kavramsal anlamayı bir arada geliştirmesini sağlar (Kaput, 2008).Erken cebir yaklaşımında süreç sadece doğru sonuca ulaşmaktan ibaret değildir. Öğrencilerin matematiksel ilişkileri fark etmesi, genellemeler yapması ve değişmez özellikleri belirlemesi önceliklidir. Farklı temsil biçimleri arasında bağ kurmak ve düşünceleri gerekçelerle savunmak bu sürecin zeminini oluşturur (Blanton & Kaput, 2003; Kieran, 2007). Bu doğrultuda öğretmen hazır bilgiyi aktaran kişi konumundan uzaklaşır. Öğretmenin rolü, cebirsel düşünmeyi ortaya çıkaracak ortamları tasarlamak ve öğrencilere rehberlik etmektir.

Görevlerin bilişsel talebini artırmak sadece soruların şeklini değiştirmek anlamına gelmez. Öğrencilerin yapıları incelemesi, ilişkileri keşfetmesi ve farklı çözümleri karşılaştırması hedeflenir. Genellemeleri test etmek ve sonuçları mantıksal gerekçelerle savunmak kalıcı öğrenme deneyimleri yaratır. Yüksek bilişsel talebe sahip görevlerin sınıftaki başarısı doğrudan öğretmenin uygulamalarına bağlıdır (Stein et al., 2000; Smith & Stein, 2011). Öğretmenin soruları yönlendirme biçimi, düşünceleri görünür kılması ve tartışma yönetimi bu başarıyı belirler. Süreç boyunca görevin niteliğini korumak temel bir adımdır. Bu rehberdeki dönüşüm örnekleri, ders kitaplarındaki rutin etkinlikleri zengin öğrenme fırsatlarına dönüştürmek için pratik bir yol haritası sunar. Görevler zihin alışkanlıkları ekseninde yeniden yapılandırıldığında, öğrenciler sadece işlem yapan kişiler olmaktan çıkar. Matematiksel ilişkileri araştıran, varsayımlar kurup test eden ve düşüncesini gerekçelendiren aktif bireylere dönüşürler. Tasarlanan görevler, müfredat kazanımlarını gerçekleştiren sıradan araçlar değildir. Bu görevler, erken cebirsel düşünmenin ve üst düzey muhakemenin sistemli şekilde geliştiği birer öğrenme zeminidir (Kaput, 2008; Blanton & Kaput, 2011; Kieran, 2007; Stein et al., 2000).

Öğretmenlerin görevleri analiz etmesi ve cebirsel potansiyeli değerlendirmesi öğretim kalitesini ve akademik başarıyı doğrudan artırır (Tosun vd., 2026). Gerekli durumlarda uygun stratejilerle dönüşüm yapmak değerli bir mesleki beceridir. Bu yaklaşım, öğrencilerin ileride ihtiyaç duyacağı problem çözme, modelleme ve akıl yürütme becerilerine güçlü bir bağ oluşturur.

KAYNAKLAR

Blanton, M. L. & Kaput, J. J. (2003). *Developing elementary teachers' algebra eyes and ears*. *Teaching Children Mathematics, 10*(2), 70–77. https://doi.org/10.5951/TCM.10.2.0070

Blanton, M. L. & Kaput, J. J. (2011). Functional thinking as a route into algebra in the elementary grades. In J. Cai & E. Knuth (Eds.), *Early algebraization: A global dialogue from multiple perspectives* (pp. 5–23). Springer. https://doi.org/10.1007/978-3-642-17735-4_2

Bozkurt, A., Özmantar, M. F. & Şimşekler Dizman, T. H. (2025). Utilization of algebraic habits of mind according to types of algebraic demands. *The Eurasia Proceedings of Educational and Social Sciences*, 47, 231-237. https://doi.org/10.55549/epess.996

Chimoni, M., Pitta-Pantazi, D. & Christou, C. (2018). Examining early algebraic thinking: Insights from empirical data. *Educational Studies in Mathematics, 98*(1), 57–76. https://doi.org/10.1007/s10649-018-9803-x

Cuoco, A. A., Goldenberg, E. P. & Mark, J. (1996). Habits of mind: An organizing principle for mathematics curricula. *Journal of Mathematical Behavior, 15*(4), 375–402. https://doi.org/10.1016/S0732-3123(96)90023-1

Driscoll, M. (1999). *Fostering algebraic thinking: A guide for teachers, Grades 6–10*. Heinemann.

Driscoll, M. & Moyer, J. C. (2001). Using students' work as a lens on algebraic thinking. *Mathematics Teaching in the Middle School, 6*(5), 282–287.

Hart, K. M., Brown, M. L., Kerslake, D., Küchemann, D. E., Ruddock, G. & McCartney, M. (1998). *Children's understanding of mathematics: 11–16*. John Murray.

Kaput, J. J. (1999). Teaching and learning a new algebra with understanding. In E. Fennema & T. A. Romberg (Eds.), *Mathematics classrooms that promote understanding* (pp. 133–155). Lawrence Erlbaum Associates.

Kaput, J. J. (2008). What is algebra? What is algebraic reasoning? In J. J. Kaput, D. W. Carraher, & M. L. Blanton (Eds.), *Algebra in the early grades* (pp. 5–17). Lawrence Erlbaum Associates.

Kieran, C. (2007). Learning and teaching algebra at the middle school through college levels: Building meaning for symbols and their manipulation. In F. K. Lester Jr. (Ed.), *Second handbook of research on mathematics teaching and learning* (pp. 707–762). Information Age Publishing.

Kieran, C. (2018). *The learning and teaching of algebra: Ideas, insights and activities*. Routledge.

Lew, H. C. (2004). Developing algebraic thinking in early grades: Case study of Korean elementary school mathematics. *The Mathematics Educator, 8*(1), 88–106.

Smith, M. S. & Stein, M. K. (1998). Selecting and creating mathematical tasks: From research to practice. *Mathematics Teaching in the Middle School, 3*(5), 344–350.

Smith, M. S. & Stein, M. K. (2011). *5 practices for orchestrating productive mathematics discussions*. National Council of Teachers of Mathematics.

Stein, M. K., Smith, M. S., Henningsen, M. A. & Silver, E. A. (2000). *Implementing standards-based mathematics instruction: A casebook for professional development*. Teachers College Press.

Tanışlı, D. & Köse, N. Y. (2020). Ortaokul öğrencilerinin aritmetikten cebire geçiş sürecindeki cebirsel düşünme becerilerinin incelenmesi. Ege Eğitim Dergisi, 21(1), 45-63. https://doi.org/10.37217/egeegtm.573934

Tosun, Ş., Bozkurt, A. & Özmantar, M. F. (2026). The effect of professional development-supported instructional practices on students' algebra achievement. *International e-Journal of Educational Studies, 10*, e2026208. https://doi.org/10.31458/iejes.1810576